Fabrication and Characterization of Graphene Induced Metal Semiconductor Metal (MSM) Structure for Detection and Sensing Applications

MS Thesis

Submitted by: **Engr. Shoaib Alam**

Registration No: **391-FET/MSEE/F14**

Supervised by: **Prof. Dr. Ahmed Shuja Syed**

Session 2014 - 2017

Department of Electronic Engineering

Faculty of Engineering and Technology

International Islamic University Islamabad Pakistan

Accession No. Th 18953

MS
620.11
SHF

بسم الله الرحمن الرحيم

Certificate of Approval

Title of Thesis: "Fabrication and Characterization of Graphene Induced Metal Semiconductor Metal (MSM) Structure for Detection and Sensing Applications"

Name of Student: Eng. Shoaib Alam

Registration No.: 391-FET/MSEE/F14

Accepted by the Faculty of Engineering and Technology, INTERNATIONAL ISLAMIC UNIVERSITY, in partial fulfillment of the requirement for the Master of Philosophy Degree in Electronic Engineering.

Viva Voce Committee

Dean
Prof. Dr. Muhammad Amir
FET, IIUI.

Chairman
Dr. Suheel Abdullah
DEE, FET, IIUI.

External Examiner
Dr. Salman Iqbal
Principal Dr. A. Q. Khan Institute of Computer Sciences and Information Technology (KICSIT)

Internal Examiner
Prof. Dr Muhammad Amir
DEE, FET, IIUI.

Supervisor
Prof. Dr. Ahmed Shuja Syed
Executive Director CAEPE, IIUI.

This thesis, titled, "Fabrication and Characterization of Graphene Induced Metal Semiconductor Metal (MSM) Structure for Detection and Sensing Applications", is submitted by Shoaib Alam, Registration No.: 391-FET/MSEE/F14; to the Faculty of Engineering and Technology (FET), International Islamic University Islamabad (IIUI), in partial fulfillment of the requirements for the degree of MS Electronics.

This Thesis is

DEDICATED TO

My Beloved Parents,

Wife, Daughter

& Friends

ABSTRACT

As the semiconductor electronics technology is moving towards even smaller scales to surmount the barriers of pbysical dimensions imposed on us by the nature, new materials and devices with such potential are realized and studied upon. This gives the world a new hope to realize the More than Moore's approach owing to the even tougher requirements posed by International Technology Road Map of Semiconductor (ITRS). For the realization of next generation semiconductor devices giants like INTEL, IBM, Fujitsu etc bave already given the world the new perspective about systems with different domain devices integrated together on higb end assembly line. This integration has evoked a debate to find and research new device structures from inter disciplinary domains for their potential embedment with the already available marketed systems and well established fabrication routine line. New structures that can provide ease of manufacturing and flexibility in design are investigated using altogether new approach. Another paradigm of research industry is to fabricate these devices using new and improved material with good electrical properties, so that they can come up with the solution that can be taken up by the semiconductor industry. Nearly all possible design and structures are been reinvestigated and studied upon. Metal Semiconductor Metal structure is one of such structure that can provide the industry with pertinent qualities that may be utilized to gain better device systems for future electronics.

ACKNOWLEDGEMENTS

In the name of Allah (SWT), the most merciful and the greatest benefactor, I am thankful to Allah Almighty for giving me the courage and showing me the path so that I can complete my research.

I am truly indebted to my worthy supervisor Prof. Dr. Ahmed Shuja Syed, for his guidance, constant support, and knowledge feedback that gave me the hope and pathway to complete my research phase. His level of commitment towards research and wisdom has been an inspiration for myself and others.

I would like to extend my gratitude to the Centre of Advanced Electronics & Photo-Voltaic Engineering, its research associate and supporting staff especially Engr. Muhammad Ali, for his profound cooperation and help throughout my research phase.

(Engr. Shoaib Alam)

TABLE OF CONTENTS

Abstract -------- iv
Acknowledgements -------- v
Table of Contents -------- vi
List of Figures -------- viii
List of Tables -------- xi
Chapter 1 Introduction -------- 1
1.1 Scaling in Nano Electronics/ Need of new approaches -------- 1
1.2 Introduction to the Metal-Semiconductor-Metal (MSM) Structure --- 5
1.2.1 Working Principal -------- 6
1.2.2 Applications -------- 7
1.3 Introduction to the Graphene -------- 7
1.3.1 Electrical properties of Graphene -------- 8
1.3.2 Applications and Devices -------- 9
1.4 Motivation of This work -------- 11
1.5 Problem, Methodology and their outline -------- 13
Chapter 2 Literature Review -------- 16
2.1 Introduction -------- 16
2.2 Graphene and MSM in the Literature : A Survey -------- 20
Chapter 3 Sample Preparation and Synthesis -------- 24
3.1 Wafer Cleaning/Starting Wafer -------- 24
3.1.1 RCA Clean -------- 24
3.2 Oxide Growth -------- 25
3.2.1 Chemical Vapour Deposition (CVD) -------- 26
3.3 Metallization of Nickel -------- 26
3.3.1 Atomistic Layer Deposition System -------- 26
3.4 CVD of Graphene on Nickel -------- 28
3.5 Fabrication of MSM Structure -------- 28
3.5.1 Routine 1 - All graphene/Ni MSM -------- 28
3.5.2 Routine 2 - Graphene/Ni/Rough Al MSM -------- 29
3.5.3 Routine 3 - Graphene/Ni/Al MSM -------- 30
3.5.4 Routine 4 - All Aluminium MSM -------- 31
Chapter 4 Experimental Techniques -------- 32
4.1 Hall Effect System -------- 32
4.1.1 Van Der Pauw Technique -------- 34
4.1.2 Resistivity Analysis -------- 35
4.2 ASMEC -------- 35
Chapter 5 Experimentation, Results and Discussion -------- 37
5.1 Result and analysis of device all graphene/Ni MSM (Routine 1) -------- 38
5.2 Result and analysis of device graphene/Ni/Rough Al MSM (Routine 2) - 49
5.3 Result and analysis of device graphene/Ni/Al MSM (Routine 3)-------- 55
5.4 Result and analysis of device All Aluminium MSM (Routine 4)-------- 65
5.5 Comparison of the fabricated devices -------- 69

Chapter 6 Conclusion and Future Work ---------- 77
6.1 Conclusion ---------- 77
6.2 Future Work ---------- 78
References ---------- 79

LIST OF FIGURES

Fig 1.1: Future approach for Nano-electronics devices by Intel 1
Fig 1.2: Technology nodes of the Si- CMOS Transitory 2
Fig 1.3: Scaling issues with CMOS 3
Fig 1.4: More than Moore Illustration 3
Fig 1.5: Beyond CMOS devices 4
Fig 1.6: Schematic of Metal semiconductor metal photo diode (MSM-PD) 5
Fig 1.7: Schematic of Aluminium/silicon based Metal semiconductor metal photo detector (MSM-PD) 6
Fig 1.8: Transport mechanism in the Metal Semiconductor Metal Structure 7
Fig 1.9: Layer of graphene atoms in honeycomb arrangement 8
Fig 1.10: illustration of a graphene channel field effect transistor 10
Fig 1.11: Graphene as an interface between the two materials for better thermal stability 10
Fig 1.12: Schematic illustration of graphene based SBSC 10
Fig 1.13: Graphene based flexible membrane 11
Fig 1.14: Intel abandoning the conventional CMOS electronics to search for new paradigms 12
Fig 1.15: The device matrix for our proposed research 14
Fig 3.1: Ingot cutting and slicing to form raw silicon wafers 24
Fig. 3.2: wafer polished to get the desired smooth reflecting surface 24
Fig. 3.3: Basis Chemical Vapour Deposition reactor assembly 26
Fig. 3.4: Atomistic Layer Deposition System assembly 27
Fig. 3.5: Layer structure of the sample 28
Fig. 3.6: Cross-sectional view of the sample prepared using the process routine 1 29
Fig. 3.7: Cross-sectional view of the sample prepared using the process routine 2 30
Fig. 3.8: Cross-sectional view of the sample prepared using the process routine 3 31
Fig. 3.9: Cross-sectional view of the sample prepared using the process routine 4 31
Fig. 4.1: Basic schematic of Hall Effect 33
Fig. 4.2: Van der pauw technique possible sample geometries 34
Fig. 4.3: Van der pauw setup for the resistances R_A and R_B 35
Fig. 5.1: Flowchart of the experimentation performed 37
Fig. 5.2: AFM image of the trench engraved in the sample prepared by the routine 1 39
Fig. 5.3: 50nm AFM of the graphene MSM structure 39
Fig. 5.4: (a) Line profile analysis of the graphene sample surface, (b) Average thickness profiling of the first line scan between two points, (c) Average thickness profiling of the second line scan between two points 40

Fig. 5.5: I-V Dark and Light Curves of the Graphene induced MSM at different temperatures 41
Fig. 5.6: I - V dark and light scan on the temperature 300 k 42
Fig. 5.7: I - V dark and light scan on the temperature 310 k 42
Fig. 5.8: I - V dark and light scan on the temperature 320 k 43
Fig. 5.9: I - V dark and light scan on the temperature 330 k 43
Fig. 5.10: I - V dark and light scan on the temperature 340 k 44
Fig. 5.11: Photo-stimulated current scan w.r.t time on multiple constant applied voltages 45
Fig. 5.12: Photo-stimulated voltage scan w.r.t time on multiple constant applied voltages 46
Fig. 5.13: Dark and Light Electric current measurements w.r.t time 47
Fig. 5.14: I-V Dark and Light Curves of MSM device Prepared form Routine 2 at different temperatures 48
Fig. 5.15: I - V dark and light scan on the temperature 293 k for the device fabricated using the routine 2 49
Fig. 5.16: I - V dark and light scan on the temperature 300 k for the device fabricated using the routine 2 49
Fig. 5.17: I - V dark and light scan on the temperature 310 k for the device fabricated using the routine 2 50
Fig. 5.18: I - V dark and light scan on the temperature 320 k for the device fabricated using the routine 2 50
Fig. 5.19: I - V dark and light scan on the temperature 330 k for the device fabricated using the routine 2 51
Fig. 5.20: I - V dark and light scan on the temperature 340 k for the device fabricated using the routine 2 51
Fig. 5.21: Photo-stimulated current scan w.r.t time on multiple constant applied voltages on the device prepared by the Routine 2 52
Fig. 5.22: Photo-stimulated voltage scan w.r.t time on multiple constant applied voltages on the device prepared by Routine 2 53
Fig. 5.23: Dark and Light Electric current measurements w.r.t time for the device fabricated using the routine 2 54
Fig. 5.24: Dark and Light I-V scans of the sample fabricated using the routine 3 at different temperatures 55
Fig. 5.25: I-V Dark and Light Curves of MSM device Prepared form Routine 3 at different temperatures 56
Fig. 5.26: I - V dark and light scan on the temperature 290 k for the device fabricated using the routine 3 57
Fig. 5.27: I - V dark and light scan on the temperature 300 k for the device fabricated using the routine 3 57
Fig. 5.28: I - V dark and light scan on the temperature 310 k for the device fabricated using the routine 3 58

Fig. 5.29: I - V dark and light scan on the temperature 320 k for the device fabricated using the routine 3 58
Fig. 5.30: I - V dark and light scan on the temperature 330 k for the device fabricated using the routine 3 59
Fig. 5.31: I - V dark and light scan on the temperature 340 k for the device fabricated using the routine 3 59
Fig. 5.32: I - V dark and light scan on the temperature 350 k for the device fabricated using the routine 3 60
Fig. 5.33: I - V dark and light scan on the temperature 360 k for the device fabricated using the routine 3 60
Fig. 5.34: I - V dark and light scan on the temperature 370 k for the device fabricated using the routine 3 61
Fig. 5.35: Photo-stimulated current scan w.r.t time on multiple constant applied voltages on the device prepared by the Routine 3 62
Fig. 5.36: Photo-stimulated voltage scan w.r.t time on multiple constant applied voltages on the device prepared by Routine 3 63
Fig. 5.37: Dark and Light Electric current measurements w.r.t time for the device fabricated using the routine 3 63
Fig. 5.38: Dark and Light I-V scans of the sample fabricated using the routine 4 65
Fig. 5.39: Photo-stimulated current scan w.r.t time on multiple constant applied light intensities on the device prepared by the Routine 4 66
Fig. 5.40: Photo-stimulated voltage scan w.r.t time on multiple constant applied light intensities on the device prepared by Routine 4 67
Fig. 5.41: Dark and Light Electric current measurements w.r.t time for the device fabricated using the routine 4 68
Fig. 5.42: Dark and Light transient behaviour comparison of the devices at 0v . 70
Fig. 5.43: Dark and Light transient behaviour comparison of the devices at 1v . 71
Fig. 5.44: Dark and Light transient behaviour comparison of the devices at 2v . 72
Fig. 5.45: Dark and Light transient behaviour comparison of the devices at 3v . 72
Fig. 5.46: Dark and Light transient behaviour comparison of the devices at 4v . 73
Fig. 5.47: Dark and Light transient behaviour comparison of the devices at 5v . 74

LIST OF TABLES

Table 1.1: ITRS roadmap for current and future technology 11
Table 4.1: ASMEC specifications and operational range 36
Table 4.2: ASMEC measurable quantities 36
Table 5.1: Hall Effect measurements of the device fabricated through Routine 1 38
Table 5.2: Hall Effect measurements of the device fabricated using the routine 2 55
Table 5.3: Hall effect results of All Aluminium Metal Semiconductor Metal Structure 64
Table 5.4: Comparative Hall effect results of the devices fabricated 69

Chapter 1

Introduction

1.1 Scaling in Nano Electronics/Need of new approaches

As the semiconductor electronics technology is moving towards even smaller scales to surmount the barriers of physical dimensions imposed on us by the nature, new approaches in the form of improved and strengthen materials, new structure and other sucb potential routines are realized and studied upon. This gives the world a new hope to realize the More than Moore's approach owing to the even tougher requirements posed by International Technology Road Map of Semiconductor (ITRS). Researches all around the world alongside the international organizations have predicted and defined the road map of scaling. Intel back in 2005 predicted and defined their company product trend with empbasis on two dimensional material as the future of nano-electronics semiconductor industry. An illustration of which can be seen on the figure 1.1 below [1]:

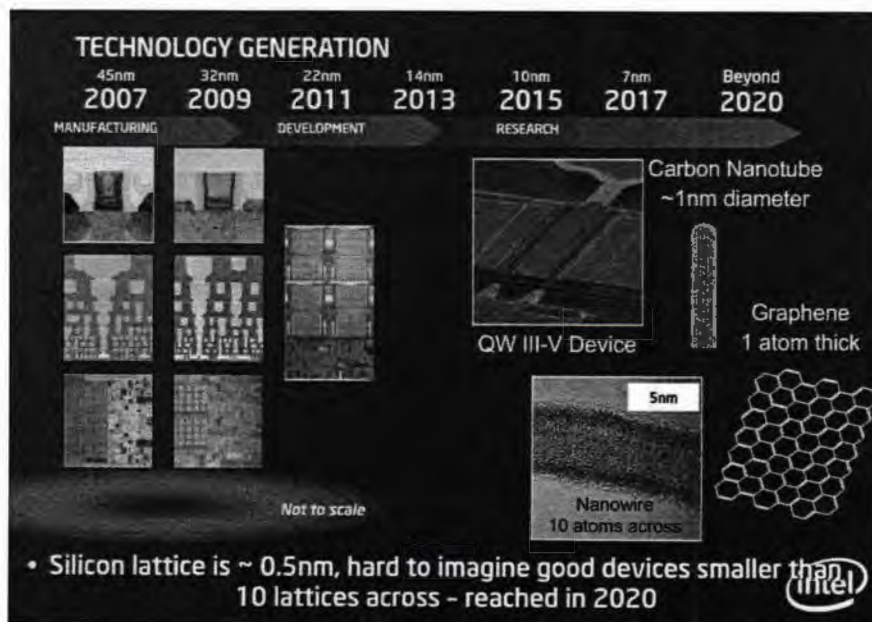

Fig 1.1: Future approacb for Nano-electronics devices by Intel [1]

So far CMOS is the major working horse of the semiconductor industry and that too has gone through a constant scaling down cycle in order to realize the Moore's law. This can be seen with the figure 1.2 below [2]:

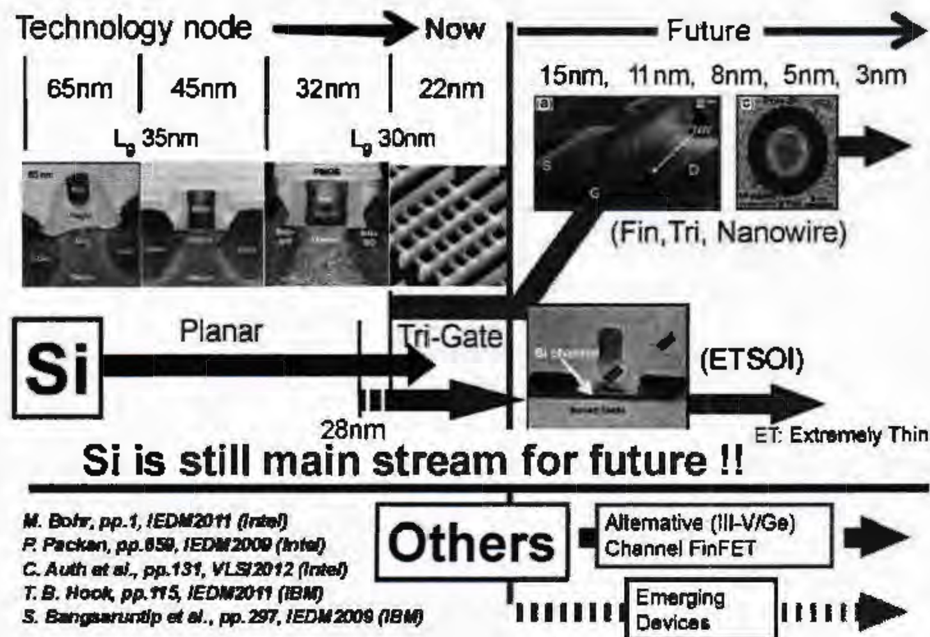

Fig 1.2: Technology nodes of the Si- CMOS Transitory [2]

Even though the CMOS scaling is going gradually, the structural limitation imposed by the scaling itself are becoming more and more reality. This is presumed that the scaling of the CMOS will suffer some major setback when this does happen. Even now it is becoming very difficult to follow the miniaturization trend in these devices. One of such difficulty is the quantum effects that came in to play as we move towards the atomic and sub atomic regimes. The scaling options along with their outcomes are shown in the figure 1.3 below [3]:

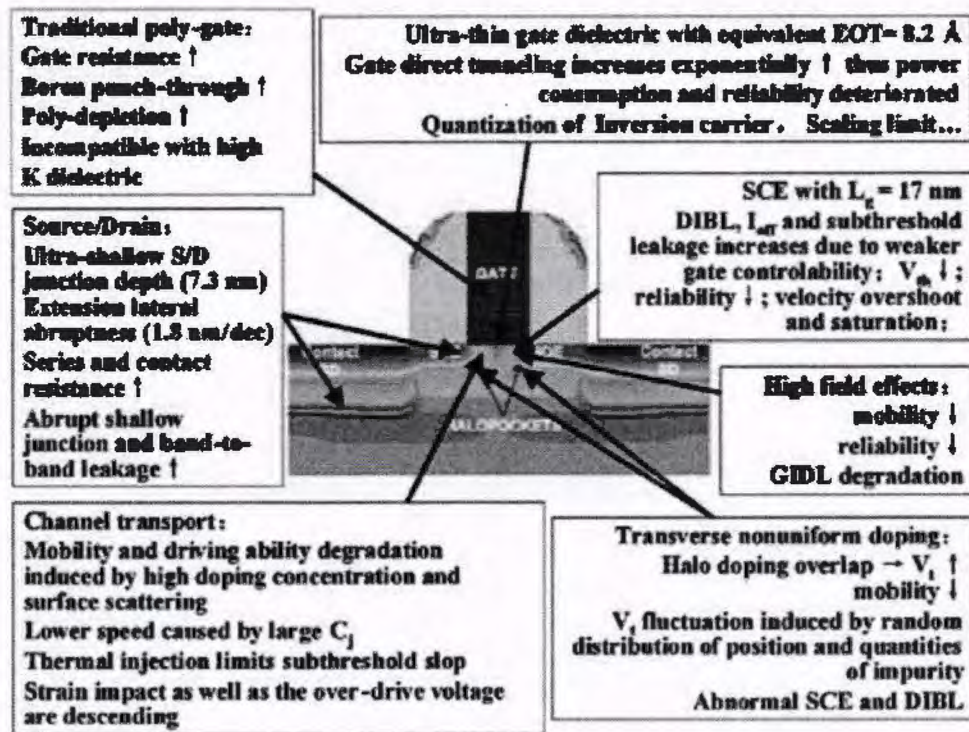

Fig 1.3: Scaling issues with CMOS [3]

International Technology Roadmap of Semiconductor coins the term more than Moore [4], in order to meet the demands of the consumer market, thriving towards more faster and robust devices. The approach required new understanding of the potential possibilities to achieve such goals. A beyond CMOS approach was needed as shown in the figure 1.4 [4]:

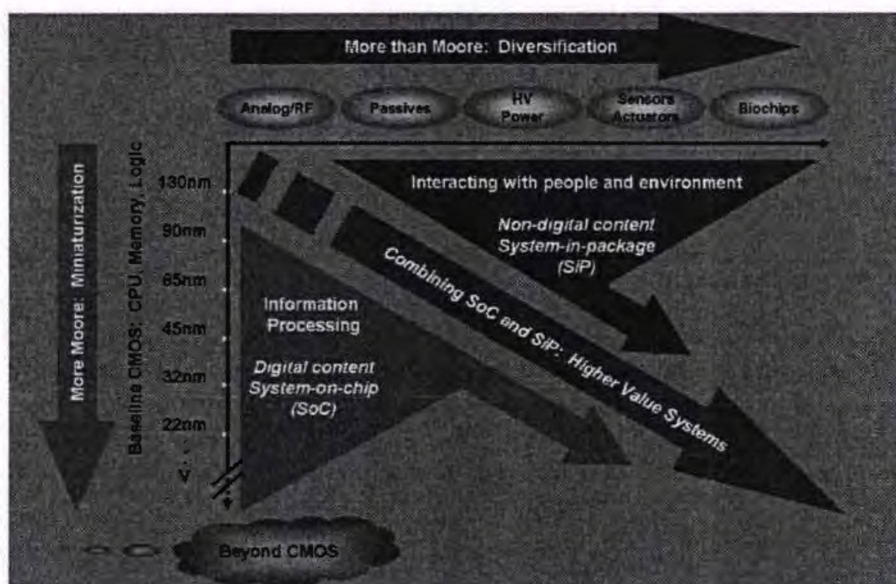

Fig 1.4: More than Moore Illustration [4]

This change in the trend of the semiconductor industry bring about new manufacturing techniques like the Heterogeneous Integration [5] of the devices, new and improved materials like the High K [6] and the altogether new structure devices [7]. One of such device structure in Metal Semiconductor Metal structure (MSM).

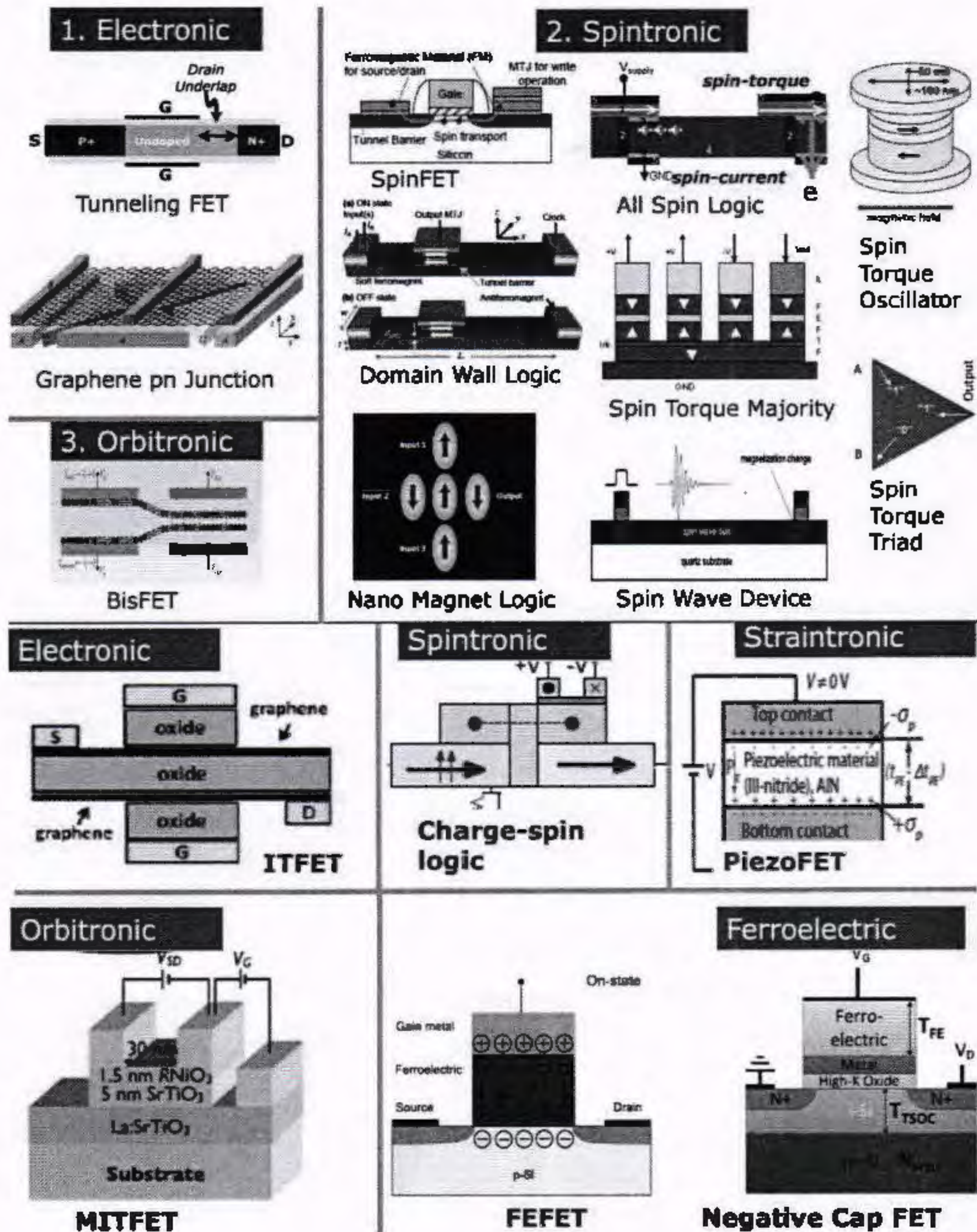

Fig 1.5: Beyond CMOS devices [8]

1.2 Introduction to the Metal-Semiconductor-Metal (MSM) Structure

Metal-Semiconductor-Metal (MSM) is a novel structure and has a noticeable application in optical telecommunication industry driven devices, switching circuitry and sensors [9]. As the semiconductor industry is focused on the miniaturization, the metal semiconductor metal (MSM) matrix has boosted up a great interest and area of research for next generation specific devices. The stable structure and the choice of the shape of MSM gives rise to many new photo detectors based on the MSM structure. The structure mainly consists of two same or different metals with a sandwiched semiconductor in between:

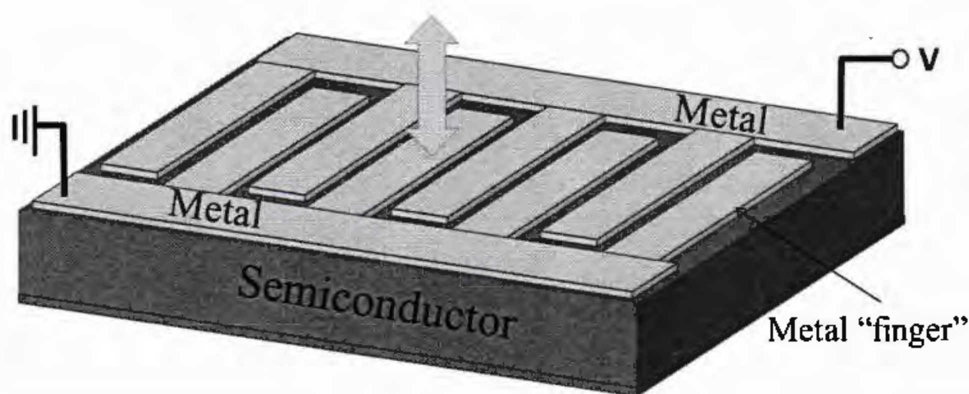

Fig 1.6: Schematic of Metal semiconductor metal photo diode (MSM-PD) [9]

The simplicity of the design and the fabrication makes the MSM structure gain much interest in the semiconductor industry. An active grating aluminum-silicon MSM based photo detector is represented here for better insight:

Fig 1.7: Schematic of Aluminum/silicon based Metal semiconductor metal photo detector (MSM-PD) [10]

1.2.1 Working Principal

When the semiconductor is sandwiched in between the two same or different metals and potential difference is applied to the metals, upon the exposure of flux on to the whole structure, the carriers in the doped semiconductors gain enough energy to form a channel. This channel based on the applied biased forces the carriers to travel in between the metal electrodes [11]. The magnitude of the output current and the sensitivity of the device depends on the applied biased and the structure morphology.

Or in other words when a uniformly doped semiconductor is thin enough that it can be completely depleted before avalanche breakdown occurs, the structure can exhibit many novel transport behaviours. Two outstanding features of the structure are that (1) a wide range of high-level injection of minority carriers can be achieved by varying the barrier heights of the two contacts and (2) the critical voltage at which the minority carrier injection increases rapidly can be varied by varying the semiconductor doping and thickness [12].

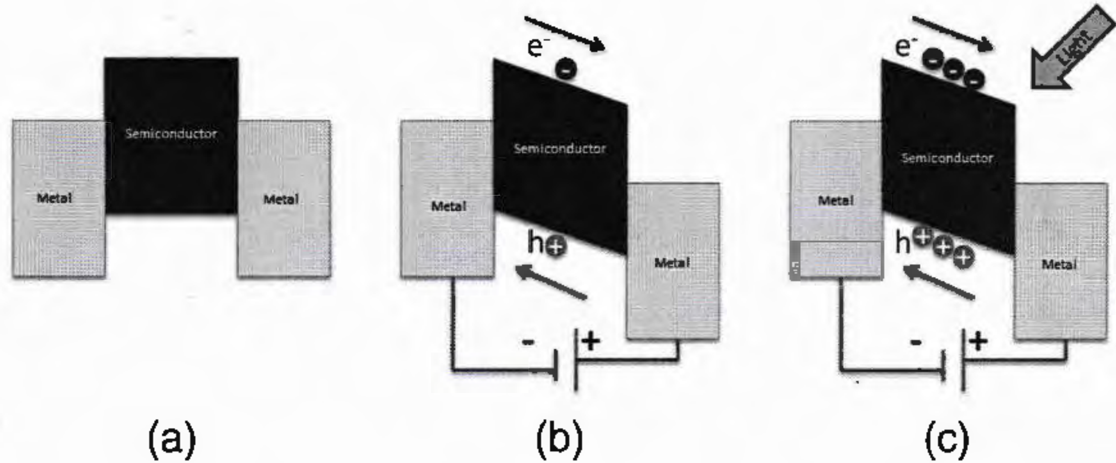

Fig 1.8: Transport mechanism in the Metal Semiconductor Metal Structure

1.2.2 Applications

- They are used in the high speed optical communications [9].
- The Metal Semiconductor Meta have noticeable application in the optical detection [10].
- The MSM is primarily used for UV detection [13].
- The structure is used in the making of waveguide [14].
- Due to its fast and accurate thinking it is used in combination with micro electromechanical systems to make pressure sensors [15].
- Due to the toughness of the structure design MSM structures are used in high temperature applications [16].

1.3 Introduction to the Graphene

Graphene an allotropic form of carbon was first discovered by P.R Wallace in 1947. He was the first person who exploited the mystery of this phenomenal material, theoretically by understanding the Graphite 3D electrical properties through the massless fermi Dirac equation [17].

G. Ruess in 1948 gave the world the first ever TEM image of few layers of Graphene [18]. Couple of years later Electron Microscopy was implied to see the single layer

Graphene. In 1990 up till 2004 scientist were successful to mechanically exfoliate the graphene thin films flakes [19]. They were close to have 50 to 70 layers thick Graphite flakes. In 2004 monoatomic layers of grapheme was extracted from bulk Graphite by two scientist named Andre Geim and Kostya Novoselov at the University of Manchester [20]. They then successfully transferred these monolayers of Graphene onto SiO2 /Si substrate using the micromechanical cleavage also known as the scotch tape method. Using this method of transfer, quantum Hall effect of these Graphene layers was observed, providing the evidence of massless Dirac fermions theoretically predicted.

Graphene a 2-D material classified as one of the world's smallest material has shown excellent conductive and intrinsic behavior that the use of such a material in the device is forthcoming. The global market for such a new material has already reached over 20 million USD [21]. The material graphene layer thickness was found to be 0.345 nm. It is 200 times stronger than steel and has a honey comb atomic structure [22]. As shown:

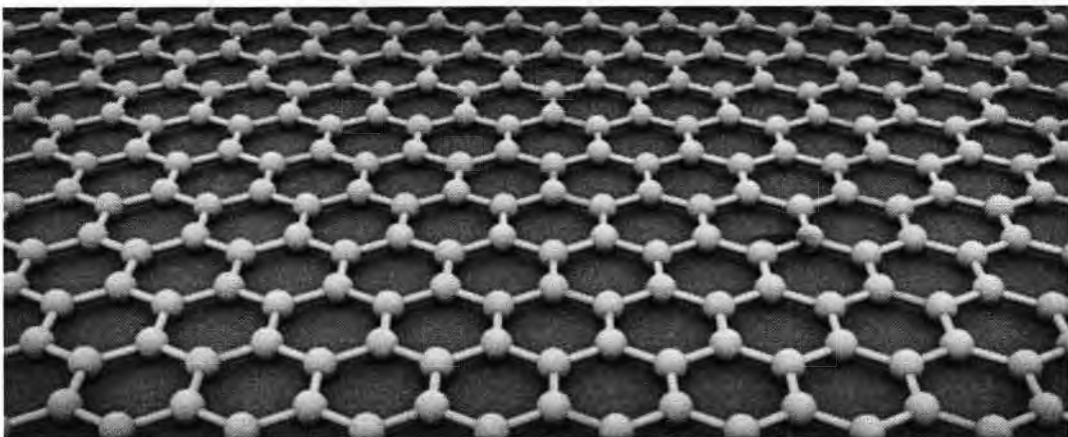

Fig 1.9: Layer of graphene atoms in honeycomb arrangement [22]

1.3.1 Electrical properties of Graphene

Before the synthesis of graphene in 2004, the mathematical theory lead to a belief that due to temperature in-stability, for two dimensional compounds, to be in a stable

condition at room temperature is entirely impossible. However graphene monolayer from bulk graphite disapproves this theoretical formation and a single atomic 2D layer of carbon was found to be stable at room temperature. The research study suggest this can only be possible due to the strong bonding in between the carbon atoms, preventing the layer from destabilizing.

Graphene act as a semi-metal with zero overlapped band gap, meaning electron and holes both act as charge carriers. Since graphene has a hexagonal structure with six carbon atoms arranged in the hexagon, each atom contributes a free electron for charge transportation. The electron mobility of suspended graphene is found to be 15,000 cm^2 /V. S and remain unchanged with in the temperature span of 10K to 100K. Theoretically predicted electron mobility of graphene is found out to be 2×10^5 cm^2 /V. S at room temperature which is 10×10^6 times higher than that of copper. Sheet resistance of graphene is in the order of 10^{-6} Ω cm less than silver [23]. The most significant and possibly the most important electrical property of graphene is that an electron, at room temperature, on the graphene layer can cover distance of micrometer without any collision, this phenomenon is called the ballistic transport of charge carriers. Graphene also holds the potential to be doped externally to attain the desired band gap for specific application.

1.3.2 Applications and Devices

- Based on the excellent intrinsic properties of the material graphene, and its capability to be doped as per application requirements, its use in the next generation transistors and detectors has already gain influence and multiple structures are being investigated and reported in the literature, most important of them is the graphene field effect transistor where the nanomaterial graphene is used as a channel material to enhance the performance of the device [24 - 26].

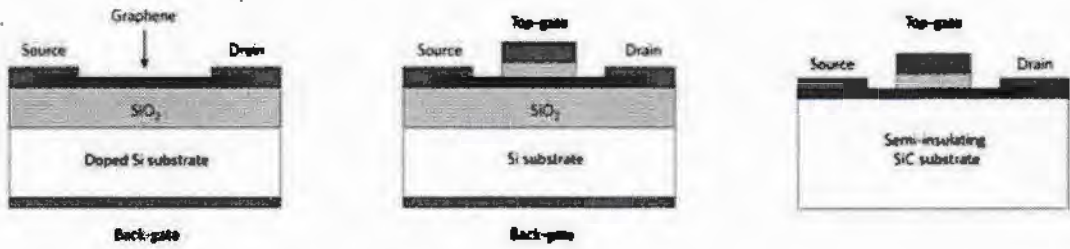

Fig 1.10: illustration of a graphene channel field effect transistor [24-26]

- Graphene has been investigate to be used as a thermal interface in between the materials for exhibiting better thermal conductivity [27].

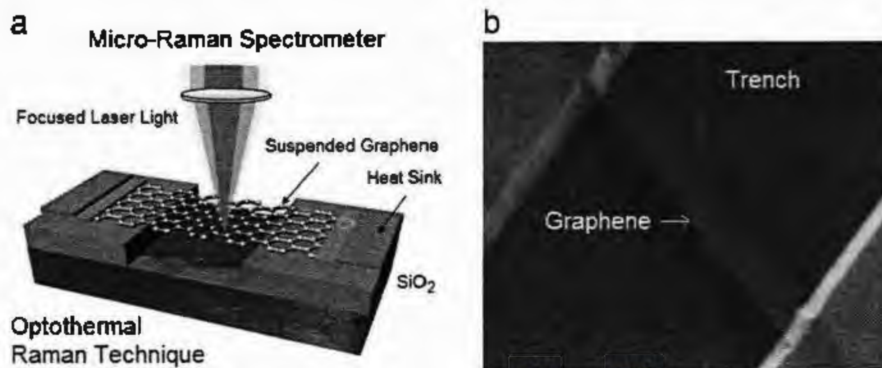

Fig 1.11: Graphene as an interface between the two materials for better thermal stability [27]

- Graphene has been used for the making of solar cells and is utilized in structure where the need of high conductivity is needed. Couple of study have been carried out to exploit this possibility and have turned out to be very forthcoming [28].

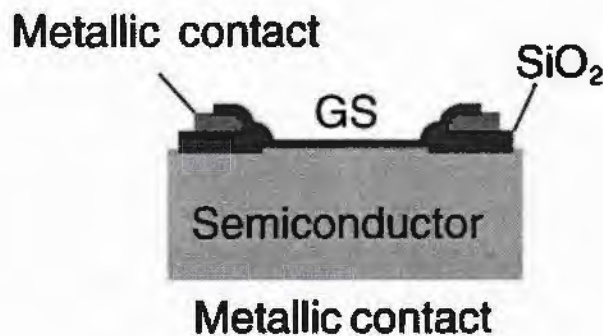

Fig 1.12: Schematic illustration of graphene based SBSC [28]

- Another great area of research for the material graphene is it can be used for the making of super capacitors that can be used for the next generation energy storage devices, which can store huge amount of data quickly and efficiently [29].
- Since graphene is known as the strongest material in the world and exists stably in 2D form, it is greatly investigated in the making of flexible displays and other devices. Research has revealed that such flexible devices are not only possible but some are even in the production right now [30].

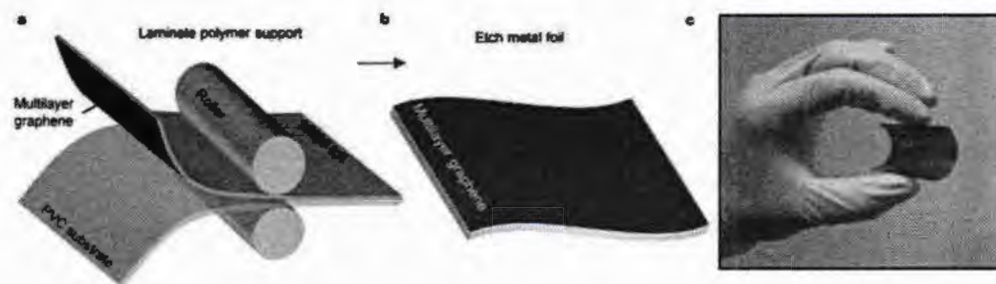

Fig 1.13: Graphene based flexible membrane [30]

1.4 Motivation of This work

The semiconductor industry is moving toward even smaller scales to meet up with the ITRS technology requirements. In 2013 ITRS gave us the road map for the future devices with the technology nodes as follows [31]:

Table 1.1: ITRS roadmap for current and future technology

Year	Node	Year	Node	Year	Node
1971	10 μm	1995	350 nm	2010	32 nm
1974	6 μm	1997	250 nm	2012	22 nm
1977	3 μm	1999	180 nm	2014-15	14 nm
1982	1.5 μm	2001	130 nm	2016-17	10 nm
1985	1 μm	2004	90 nm	2018-19	7 nm
1989	800 nm	2006	65 nm	2020-21	5 nm
1994	600nm	2008	45nm		

The concept of internet of things or big data, meaning everything is connected to everything was evolved. In 2015 at ITRS-RC Workshop, W. R. Bottoms gave a presentation [32]. The presentation was about the industry response to the ITRS nodes. He pointed out that the industry is now working on the heterogeneous integration of devices, where multiple different structural devices are assembled together to form a system. This approach requires new researched data about other nonconventional methods that can be utilized along with the existing process routine to achieve better systems.

Intel, one of the biggest manufacturer of the semiconductor devices in the world is also looking to explore new architecture design for their future products, which include new materials, all together new structures and other fabrication technologies. One of such option is photonics to replace the conventional CMOS electronics alongside graphene.

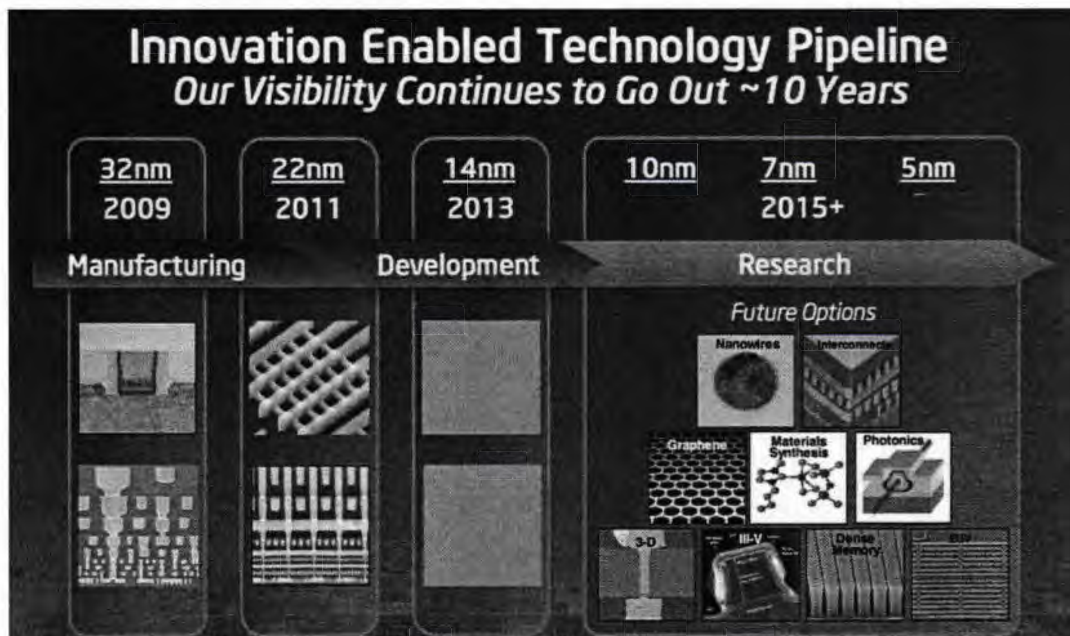

Fig 1.14: Intel abandoning the conventional CMOS electronics to search for new paradigms [32]

The Metal Semiconductor Metal (MSM) structure is unique and has a precise use in optical detection and next generation sensory based devices. The matrix itself is a

detector on its own. The structure can be tailored to desired requirements and provides a window of easy architecture design and miniaturization. On the contrary Graphene being the strongest and the smallest known material in the universe, with excellent electrical and thermal properties being induced in to the MSM structural morphology will open up new possibilities and studies.

1.5 Problem, Methodology and their outline

- **Problem Statement**

To experiment and investigate the possibility to fabricate a workable MSM structure with integrated graphene with lesser fabrication process steps while exploiting the outcome of the process to further utilize the scheme into transistors or sensors.

- **Methodology and their outline**

- A comprehensive study will be undertaken to understand the basic about the metal semiconductor metal (MSM) structure its functionality, fabrication process routine, application and the integration in the next generation electronic devices.
- The metal semiconductor metal (MSM) device with graphene induced will be fabricated in the advanced electronics lab using the available graphene layer matrix and keeping in mind the end application (Detection and sensing), a thorough study will be conducted on this new MSM device structure to find the specifics electrical properties of this device using Nano chip reliability grade Hall Effect system. For the broader spectrum research point of view and deep down analysis of this device an even hypersensitive electrical characterization tool Automatic System of Material Electro-Physical Characterization (ASMEC).
- The resulted raw data for the machines will be analyzed and compared to get the salient parameters of the fabricated device to extend and conclude the device

potential compatibility or applicability with the future sensors and detectors fabrication schemes.

One of the base device layer structure that will be researched upon has following parameters:

Wafer size =100 mm

Growth technique =high pressure chemical vapor deposition (HP-CVD)

Graphene film thickness=1 to 10 layer

Wafer orientation of silicon= (110)

Wafer thickness =500 um

SiO_2 layer thickness =500 nm

Ni thickness =300 nm

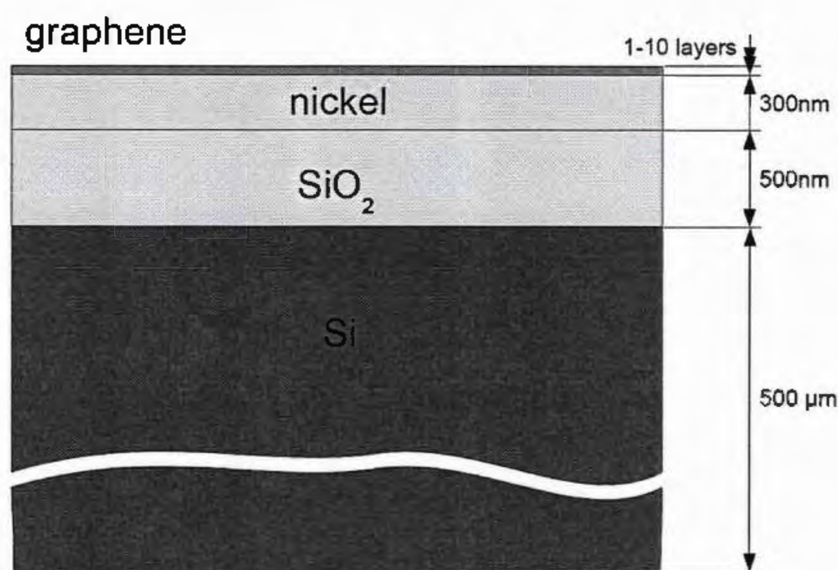

Fig 1.15: The device matrix for our proposed research

The matrix presented here is a transistor main structure hierarchy and is capable to be utilized in fabricating the graphene based Metal Semiconductor Metal (MSM) devices. The graphene growth on the transition metal like nickel (Ni) is subjugated such that the material graphene can be integrated and utilized for the next generation 2-D phase devices. The detailed electrical and optical study of the subject Metal Semiconductor

Metal (MSM) structure will give the insight to this customized layer stack for its use in the transistor and detector fabrication.

The problem is to tailor this design in to a workable MSM structure with integrated graphene in it and then to exploit its potential in to the transistor fabrication with lesser fabrication process steps.

Chapter 2

Literature Review

2.1 Introduction

In this chapter we will be reviewing some of the important and relevant research topics about our research, which include the general MSM devices structure and routines that the people of our time have fabricated, simulated and experimented upon to find the respective outcome related to their research problem. In the second part we will he reviewing the dedicated studies where close to our graphene induced MSM structure have been fabricated and investigated. The review is as follows:

A. Karar along with others simulated the silver (Au) and gold (Ag) comb contact MSM structure with Gallium Arsenide (GaAs) substrate using the finite-difference time domain (FDTD) method to extrapolate the light absorption capability of the GaAs metal-semiconductor metal photo-detector (MSM-PD). They imply the Surface Plasmon Polaritons (SPPs) on to the device surface to enhance the sensitivity of the deviec. Doing so they were able to increase the sensitivity of the MSM by 10 times the original structure [33]. S. V. Averine and N. V. Alkeev simulated the gallium arsenide based MSM pin diode to fine the impulse response of the device for communication applications. Their study was to map the movement of the electron and hole pair inside the active region of the device. This way they were able to retrieve the detector response to the incoming light [34]. In the similar study a group fabricated the aluminum gallium nitride (AlGaN) and silver/nickel (Au/Ni) as a contact metal for a MSM structure with sapphire as a substrate using metal organic chemical vapor deposition technique (MOCVD). They investigated the dark current analysis of the fabricated device by Optical transmission spectroscopy (OTS) and Cathodo-luminescenec (CL) spectrum

for its use in the high temperature regime. The device fabricated was designed in such a way that the regular sunlight may not affect its performance output parameters, so that when device is used in the high temperature environment the efficiency or the detection accuracy remains error free [35]. S. Singh prepared an Aluminum doped zinc oxide (ZnO) MSM ultra violet sensor on silicon substrate using RF sputtering technique and did the laminating and dark current response analysis. He then prepare the same structure with 5 nm SiO_2 layer sandwiched in between the ZnO and silicon substrate and compare the two in order to substantiate the use of his matrix in the optoelectronics devices [36]. A. M. Selmana and Z. Hassana reported silicon photo diode with titanium dioxide (TiO2) nano-rods as a mesh for the MSM. The layer of TiO_2 is synthesized using radio frequency (RF) reactive magnetron sputtering and then the chemical bath deposition is used of the growth of the TiO_2 Nano rod on top of the silicon. The silicon wafer was of p-type with (1 1 1) planer orientation. They measure the current and voltage characteristics of the device as it operates in the Ultraviolet (UV) region [37]. Researchers at Institute of Radio-engineering and Electronics of Russian Academy of Sciences investigated multiple hetero-structure based on MSM routine to find the UV spectral responsively of the devices. They investigated the ZnCdS/ZnMgS/GaP, ZnCdS/ZnS/GaP hetero-structures for a wide band gap material. Photo luminesce and current analysis was reported of these devices [38]. Nickel and Gold were used as the electrodes for the MSM. Tertiary compound based MSM was worked upon by M. E. Besseghi and others. They simulated the indium gallium arsenide (InGaAs) based MSM structure for higher wavelength photo-detection [39]. The parameters found were dark current, the photocurrent, the capacity, and the cut-off frequency of the photo-detector as a function of applied voltage and the inter-electrode spacing. Their study was based on the application of the MSM in the fast communication devices. The structure was

designed and tested on the wavelengths up to 1.55 μm. A. D. Zebentouta along with his colleague developed and fabricated a GaAs based MSM as a schottky micro-wave optical switch. The basic research was to develop a planer MSM photo detector circuitry with calculated contact spacing that shows better On/Off ratio, to be used as an optical microwave switch [40]. V. E. Babicheva investigated a wave guide been built out of MSM hierarchy of an InGaAsP-based and few more active material layers. They investigated the switching characteristics of these wave guide according to their efficiency and material intrinsic properties. Plasmonics were used as a gain material to enhance the sensing capability of the active layer. The design of the device was made compact to harness the phenomenon of the wave guide [41]. A. M. Selman and Z. Hassan fabricated the high quality nano rods of ZnO MSM structure for fast detection on different substrate and then characterize it by looking in to the surface and layer morphology. They also investigated the light and optical behaviour of the MSM structure. ZnO was used for its better optical properties and wide band gap tailoring [42]. The transport properties of the material graphene nano ribbons with multiple type semiconductor material were investigated by the researchers to find the metallic behavior of the graphene ribbons. They applied the tight-binding model and the non-equilibrium Green's function method for developing their model to justify the transfer properties of the material graphene, when came in contact with another metal [43]. Another study on the material graphene investigated the methods to reduce the graphene oxide to a workable graphene material on semiconductor. They used the thin layers of tungsten oxide and titanium dioxide to transfer the electron to the graphene layer. This was they were able to reduce the graphene oxide layer. They also worked on the different techniques to grow graphene on top of semiconductor for study [44]. Researchers have already devised a spectro-meter based on the MSM concept. The

device had a wave guide and an MSM contact hierarchy. The device was designed in such a way so that it can be compatible with CMOS. This approach is necessary for the next generation heterogeneous integration of devices where multiple devices are connected on to a same substrate [45]. D. Geum fabricated a MSM 2-DEG varactor diode structure for extremely high cut off frequency and investigated its I-V, C-V and high frequency behaviour. The gate length and the gate spacing was different for all samples. [46]. Xin Li et al, fabricated a flexible metal semiconductor metal structure device on the wafer scale using the hexagonal Boron nitride grown by the method of metal-organic vapour phase epitaxy . The hexagonal boron nitride was induced due its intrinsic properties close to that of graphene. The structure was characterized to find the dark current and photoconductivity behaviour for its potential application in the deep ultra violet photo detection [47]. A thin, compact metal semiconductor metal wave guide based on the plasmonics was fabricated by E. Viktoriia along with some others people [48]. They used Indium Phosphate as the base material for their device design. This approach help them to find the widow of operation of the device according to the end application. The compact design of the device was chosen so that the structure can be integrated in to the optoelectronics circuitry easily. The analytical calculation were based on both the two dimension modelling as well as the conventional 3D approach. Diamond thin films were also used to make the MSM structure [49]. The electrodes were made from the metal aluminium and the layer of thin diamond was placed in between them. The structure was tested for the photo detection of the shorter wavelength, primarily because of the large band gap of the diamond. Shaivalini Singh et al, grow ZnO nano rods on top of the silicon substrate using the hydro thermal two steps process. Palladium electrode are placed in the comb configuration on top of these rods and the whole structure was tested for UV application and detection [50]. J. D.

Hwang et al, using the metal semiconductor metal structure fabricated the photo detectors with low leakage current. They imply oxygen-plasma treatment on $Mg_xZn_{1-x}O$ surface for this output goal. They find out the I-V characteristics and the responsively of the device for both the UV and real region [51]. Another study uses the same $Mg_xZn_{1-x}O$ material, grown on the sapphire substrate, to fabricate a laser device [52]. The structure was found out to be emitting the random lasers with the wavelength ranging in between 320nm to 340nm. The idea was to use these results for the fabrication of Deep Ultra Violet photo detector. Y. Ding et al, studied the use of the metal semiconductor metal structure cascaded with the waveguide. They find out that doing so, photo generated carriers are efficiently swept out by applying voltage bias, and carrier lifetime shortens [53]. Researchers at the Peking University Shenzhen Graduate School fabricated AIGaN/GaN based Metal semiconductor metal structure compatible with the high electron mobility transistor. They calculated the effect on the capacitance of the device with the variation in the size and width of the comb arms of the MSM structure. A fixed applied voltage of 6V was maintained throughout the experimentation and the results were calculated based on the equivalent circuit of the device [54]. X. X. Gong et al, used lead tellurium nanowires to fabricate the infrared Photo detector. The MSM structure was employed with gold used as the electrode material and the PbTe was deposited on top of the SiO_2. The detail characterization of the fabricated structure results in low dark current, better response time and fast operation speed [55]

2.2 Graphene and MSM in the Literature: A Survey

From graphene point of view, A graphene induced MSM with copper metal mesh contacts were fabricated and studied by the Y. An and few more people. They successfully fabricated the MSM device by transferring the graphene on to the silicon

substrate using PMMA after growing the graphene on top of the copper layer. Their study was to find the potential usage of graphene in the existing silicon technologies as a schottky contact junction [56]. M. Kumara along with his team worked on fabricating a multi-layer graphene induced gallium/zinc oxide (Ga/ZnO) substrate and copper and silver metal mesh. They also discussed the process routine for transferring graphene on the substrate silicon (Si). Calculations were made to find the spectral range of the matrix [57]. C. J. Lee et al, used graphene layers on top of the GaN layer to fabricate a MSM structure acting as a UV sensor. The fabricated graphene electrodes GaN MSM UV sensor was tested for maximum photo responsivety with minimum applied bias and a response to the noise in visible regime. They devised a treatment for improving the device photoelectrical parameters which include Buffer Oxide Etch process [58]. J. Hicks et al, fabricated the metal semiconductor metal structure entirely out of material graphene [59]. The graphene is grown on top of the Silicon carbide substrate which was etched earlier to exhibit a pattern shape of steps. This approach helped them to get the accurate sized very thin graphene strips, which are spread over the SiC substrate. The structure pave way for new techniques to surpass the limitation of the lithography. The device was then tested to find the energy gap of 0.5 electron volt. S. Rathi et al, used graphene in conjugate with few layers MoS_2 to create a hetro-structure device. Gold electrodes were used and graphene – MoS_2 layer was sandwiched in between the electrodes. Silicon was used as a substrate. The fabricated device is then characterized to get the current – voltage spectra at different applied bias. The device was also tested for frequency response [60]. A deep UV photo detector was fabricated by Wei-Yu Kong along with its colleagues [61]. They grow the graphene layers separately and then transfer them to N - type Ga_2O_3 substrate. Gold electrodes were used to electrically read out the data on the graphene side and silver chromium alloy electrode was used on the

Ga_2O_3 side. The structure output parameters reveal very good detection in the deep UV range of 254 nm wavelength, with peak wavelength of 220 nm to 280 nm in UV. I-V characteristics were extracted to get the better picture of the operation window of the device functionality. Feng-Xia Liang et al, used graphene on top of the TiO_2 Nano rods, that were grown on top of the fluorine doped tin oxide by hydro thermal process. Before transferring graphene on top of TiO_2, wet chemistry was used to remove any defects and impurity from the TiO_2 nano rods. I-V curves and responsitivity of the fabricated structure was thoroughly investigated to find the efficiency of the device [62]. Another study fabricated metal semiconductor metal structure by patterning Graphene oxide layer on top of the TiO_2 layer. Gold comb structure is used as an electrode and quartz is used as substrate. The device is tested for noise ratio, responsitivity and output voltage [63]. F. Yang et al, fabricated MSM structure with graphene where few layer graphene was placed of germanium. The germanium layer was grown on top of the SiO_2 and Si. Ni/Au alloy was used as the electrode material. The hybrid structure was tested to find the responsitivity and detection [64]. Another study uses graphene to make a position sensing detector based on the Metal semiconductor metal morphology. They used reduced graphene oxide papers with different concentration of oxygen and graphene and devised a method to get thick GO layer. Ag electrodes were placed on the layer. The structure is then exposed to the laser, which was moved over the layer. Based on the movement, output parameters such as photo response and quantum efficiency. Photo voltage was found to vary over the layer when the laser was moved from position to position [65]. J. H. Seol et al, fabricated an AlGaN/GaN metal semiconductor metal structure with graphene integrated on the surface of the device. Ni electrodes in comb hierarchy are placed on the device and are used as sensing element. Responsitivity and I-V characteristics of the structure is measured to find the operation window of the

device [66]. Another study uses graphene as an electrode material on GaN to make a MSM device with sapphire as a substrate for UV detection application. The device undergo electrical and electro-optical characterization to get the I-V and the responsitivity of the device [67]. Graphene is used in another study, in conjugate with the silicon structure to get the desired MSM photo detector. This type of device was designed with the goal of scalability and ease of manufacturing [68]. The structure responsitivity and running characteristics are reported.

Chapter 3

Sample Preparation and Synthesis

In this chapter step by step fabrication of the device Metal Semiconductor Metal is represented for subsequent characterization and experimentation.

3.1 Wafer Cleaning/ Starting wafer

A P-type silicon wafer of 500 um thick and 100 mm in diameter has been prepared using the czochralski process. The wafer is then went through the cutting, dicing and polishing phase to acquire the smooth and defect free surface for the fabrication of the semiconductor device. The process is illustrated below [69]:

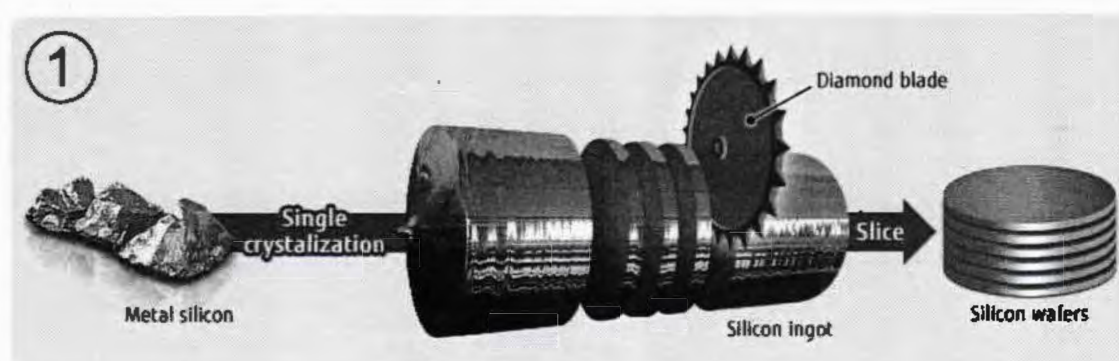

Fig 3.1: Ingot cutting and slicing to form raw silicon wafers [69]

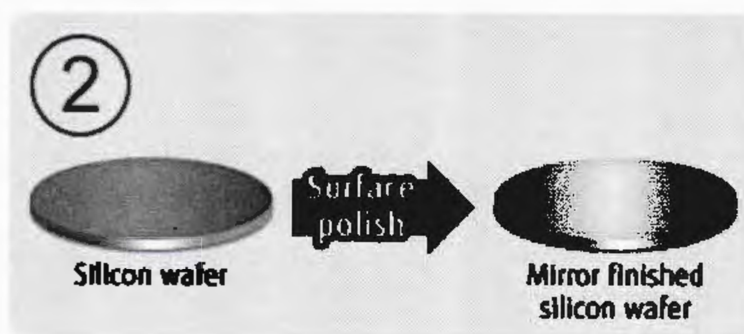

Fig. 3.2: wafer polished to get the desired smooth reflecting surface [69]

3.1.1 RCA Clean

Before any fabrication of the device the wafer went through the Fab-Driven RCA clean protocol. The RCA cleaning technique is used to further clean the sample smooth

surface so that any residue or impurity or most importantly any unwanted layer like SiO_2 layer that may have grown on top of the wafer when it came in contact with the air may be removed. This process is implied to ensure the efficiency of the next coming processes, whatever they may be [70]. RCA cleaning routine vary from material to material in our case the following routine is used:

Since the starting material in our case is Silicon there might be a chance that a thin layer of SiO_2 may have grown on some part of the wafer.

1. To remove the SiO_2 layer 20:1 H_2O: HF solution was prepared in a petri disc.
2. The wafer was dipped in to the chemical
3. Using the Swab the surface of the wafer was rubbed so that any residue may be lifted of the surface.
4. After thorough rubbing the wafer is taken out of the chemical and is washed with distilled water to remove any chemical and particles.
5. The wafer is then blow dried by Nitrogen blast until all the water particles are removed.
6. The wafer is then placed in airtight container so that environment cannot interact with the clean surface.

Following the process of cleaning the wafer is taken for the subsequent process step for the fabrication of the device.

3.2 Oxide Growth

The layer of SiO_2 is then required to be grown on the wafer. To achieve a fine and calculated thickness of 500 nm SiO_2 layer. The technique of Chemical Vapour Deposition is used to achieve this process step [71].

3.2.1 Chemical Vapour Deposition

Chemical Vapour Deposition (CVD) is one of many methods used to grow different material layers in the fabrication process. The technique gives ease of batch operation and good repeatability however to achieve better and much finer layers, the tcehnique has its limitation.

The main principal of CVD is, in a controlled environment, the sample on which the layers have to be grown is placed and gasses are flown in to the chamber. Upon contact the gasses react and form a solid layer on top of the sample. Different catalyst are also used to speed up the reaction and a sample can travel in multiple heating zones. Parameters such as temperature, pressure, gases flow rate, angle of the impact, sample position and rotation etc are controlled by the user from outside. A diagrammatical representation of the CVD is given below [72, 73]:

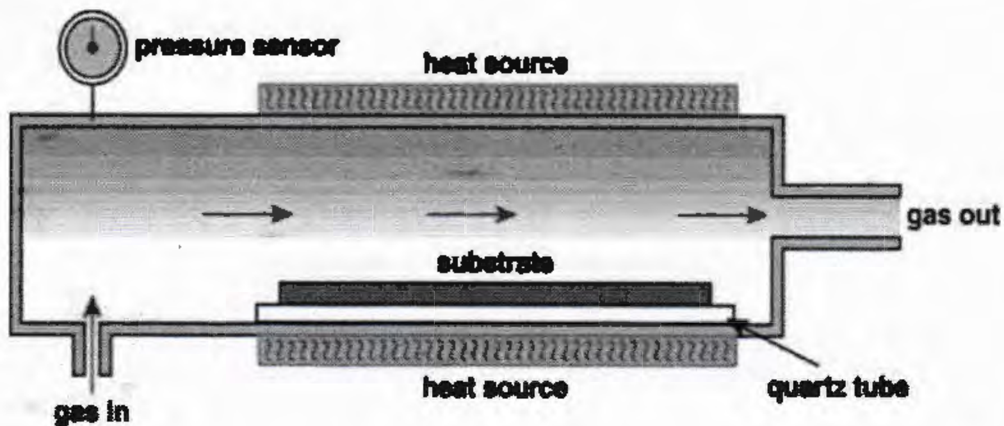

Fig. 3.3: Basis Chemical Vapour Deposition reactor assembly [72, 73]

3.3 Metallization of Nickel

After the growth of oxide layer a 300 nm thick layer of Nickel is deposited on to the device surface using the hyper fine process technique of Atomistic Layer Deposition.

3.3.1 Atomistic Layer Deposition System

Atomistic Layer Deposition System is a highly controlled process used to grow metals and other organic layers on the sample surfaces. The technique implies the basics of

physical vapour deposition process but retune it to get extremely uniform and bomogeneous layers from scale as low as the few atomic layers to sub-micron.

The process works by placing the target material (the material which is required to be deposited) in a carrier or boat. The boat comes in many sizes and shape and is made up of materials whicb have high melting temperatures. The sample is mounted on the top of the whole assembly facing downwards towards the boat carrying the target material. The whole process is carried out in the vacuum environment. As shown in the figure below:

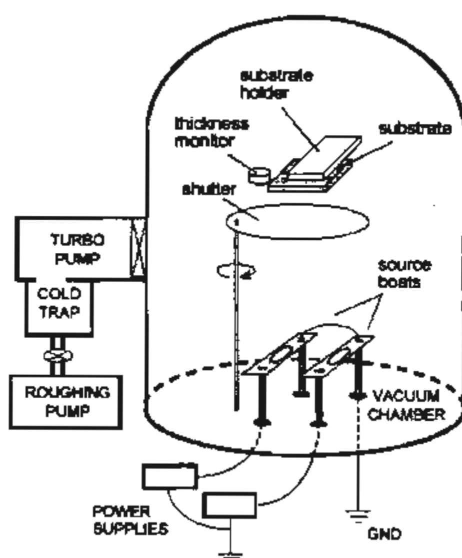

Fig. 3.4: Atomistic Layer Deposition System assembly [74]

The system works by supplying high current to the boats. This causes the temperature of the target material inside the boat to rise and eventually it meltdown. Upon melting the atoms of the target material fly towards the substrate suspended above and settle down on to the surface of the substrate after condensing. The sample holder/mounting assembly is capable of rotating in one direction for the uniform deposition. A thickness monitor is installed aside the substrate to note the thickness of the growing layer accurately [74].

3.4 CVD of Graphene on Nickel

The technique of Chemical vapour deposition of graphene on Nickel is used in our process to synthesis monolayers of graphene [75]. This hierarchy is implied based on the fact that lattice mismatch of graphene and Nickel is very little and the process routine yields better stickiness of graphene on Nickel [75].

3.5 Fabrication of MSM Structure

Three process routines are used to create the Metal Semiconductor Metal device structure for experimentation. Each process routine is different from the other. This approach was used so that detailed measurements can be done later to get the result, pointing directly toward the window of operation and implication of such process routine in next generation electronics. So far the sample layer structure looks like this:

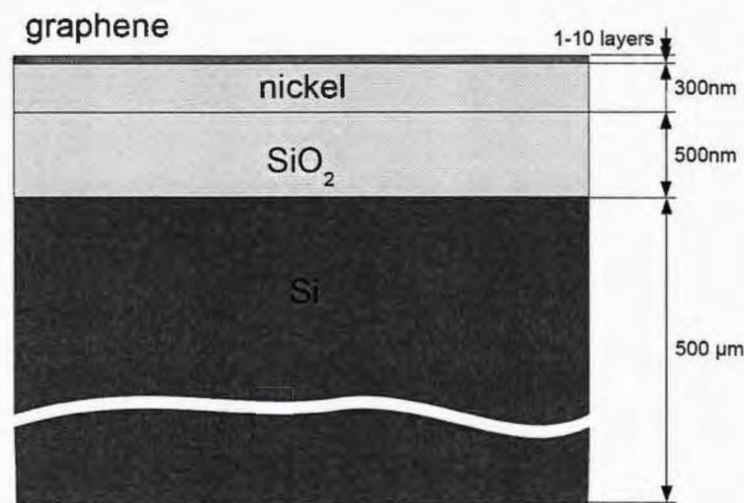

Fig. 3.5: Layer structure of the sample

3.5.1 Routine 1 – All Graphene/Ni MSM

3.5.1.1 Mechanical Engraving

The first set of sample was prepared by mechanically engraving the trench in the middle of the sample. This was consider in to account that the trench is deep enough to expose the silicon semiconductor underneath the metal Nickel and the dielectric SiO_2. The

Mechanical Scriber was mounted on to a stand directly above the sample and sample was placed on the alignment stage that could move in all X, Y, Z direction. Using microscope and control movement the sample was engraved until the silicon as exposed. The sample was then blasted with dry nitrogen so that the residue precipitates can be removed. The end result of the device fabricated is shown in figure below:

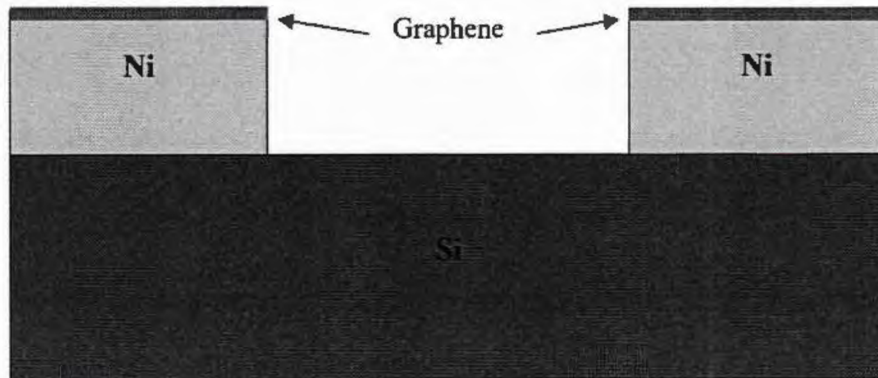

Fig. 3.6: Cross-sectional view of the sample prepared using the process routine 1

TH:18953

3.5.2 Routine 2 – Graphene/Ni/ Rough Al MSM

In routine 2 one side of the electrode Ni/Graphene was replaced by Aluminium. The Ni/Graphene electrode was ripped of the silicon surface with the solution of Ferrous-tri-Chloride ($FeCl_3$). 1:3 solution of $FeCl_3$ and water was prepared for the etching [76]. The sample was half dipped in to the solution until Nickel completely etch away. After the etching the sample is rinsed with distilled water and blasted with nitrogen for drying. The sample is then capped with the mask covering all the Ni/Graphene electrode side and some of the silicon which will later play the part of the device channel path.

Aluminium as the electrode material is then deposited on the silicon using the Atomistic layer deposition system. A 300 nm layer of Aluminium is deposited considering the layer thickness and atomic mass of Ni/Graphene electrode to balance the resistance induce on the electron as it moves through the electrodes. The sample holder assembly was rotated slowly throughout the process of deposition. The vacuum pressure inside

the chamber was noted to be 10^{-6} Torr and the deposition rate of the range 0.5 to 1 nm was maintained. The whole process took 5 hours followed by one day cool down time. The sample device prepared looks like this:

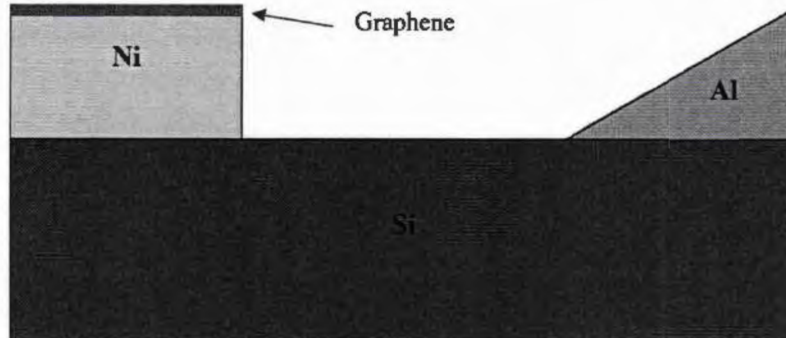

Fig. 3.7: Cross-sectional view of the sample prepared using the process routine 2

The structure electrode part was grown uneven on purpose so that the impact of the surface roughness on the device measurements/operation can be seen. This was also necessary to map so that when the device is put in to operation in the real circuitry the degradation of the electrode might occur, in short the reliability of the device may affected by it.

3.5.3 Routine 3 – Graphene/Ni/Al MSM

In the routine 3 the sample was prepared exactly the same as routine 2 up to the point of etching of Nickel but after that sample was masked for deposition and instead of the deposition the sample is first cleaned again to remove the dielectric layers if any from the sample surface. The process of deposition was again initiated but this time the rotation of the sample was controlled with the etching rate and pressure. The sample after the deposition process was cool down for the day to let the new deposited material layers settle down properly and completely. The prepared device structure is as follows:

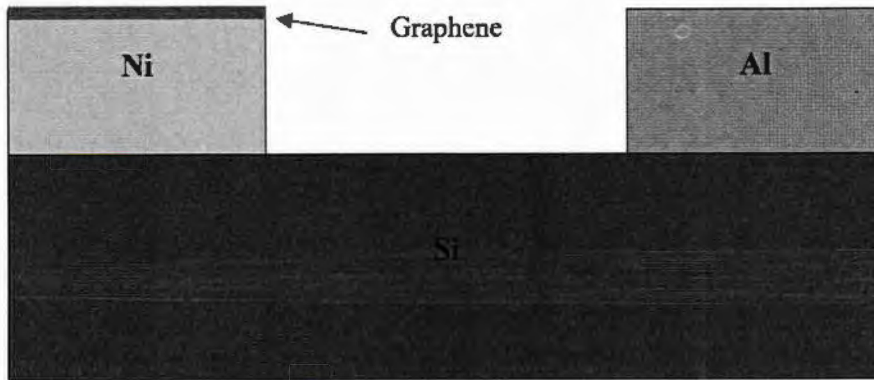

Fig. 3.8: Cross-sectional view of the sample prepared using the process routine 3

3.5.4 Routine 4 – All Aluminium MSM

The routine 4 was used so that Aluminium alone electrode sample device matrix can be prepared and tested. For the sample went through the etchant solution same as the previous routines to remove the Ni/Graphene electrodes, followed by the RCA cleaning. The device matrix is then capped and masked and went through the deposition of the electrode process. This was put in to consideration that electrodes grown are uniform and homogeneous. A steady pressure and growth rate was maintained throughout the process. The resulted device matrix looks like this:

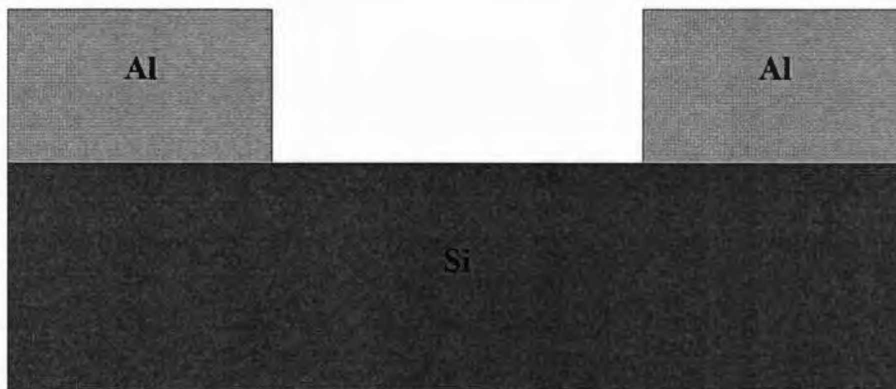

Fig. 3.9: Cross-sectional view of the sample prepared using the process routine 4

Chapter 4

Experimental Techniques

This chapter focusses on the experimental techniques that are used in this study to quantify and generate the quality results of the devices that were fabricated using routine specified in the previous chapter.

4.1 Hall Effect System

In 1879 a scientist named Edwin Herbert Hall discovered the Hall Effect [77]. The whole principle of Hall Effect was fundamentally derived from the physical principle of Lorentz force. The Lorentz force consist of two components forces which are the electric and the magnetic force. The effect is described as to when a conductor is placed parallel in a magnetic field and the current is passed through it a force is generated inside the conductor which is perpendicular to the applied current and magnetic field. This force is governed by Lorentz principal denoted hy the following equation 1 [77]:

$$\mathbf{F = - q\,(E + v \times B)} \quad \text{..} \quad (1)$$

Where

$q = (1.602 \times 10^{-19}\ C)$ = charge on electron,

E= Electric field,

V = Velocity of the charge carrier and

B = Magnetic field.

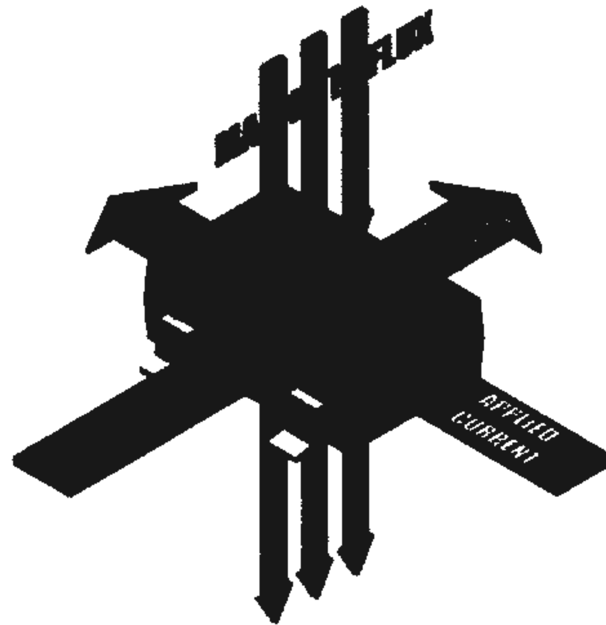

Fig. 4.1: Basic schematic of Hall Effect [77]

Assuming the uniform magnetic flux is in the direction of the z-axis and the current applied in the direction of the x-axis, perpendicular to the magnetic flux, the electrons move in the third y-axis direction. This causes their number to increase on the one side of the sample. This access of charge carriers produces a voltage called Hall voltage given by the equation 2 [77]:

$$\mathbf{V_H = IB/and} \quad \text{...} \quad \mathbf{(2)}$$

Where

d = sample thickness

B = magnetic field strength

q = charge on elementary particle

n = bulk density

I = current

For a two dimension sheet measurements, sheet density term is used (n_s = nd) instead of bulk density changing the equation 2 in to the expression 3 [77]:

$$\mathbf{n_s = IB/q|V_H|} \quad \text{...} \quad \mathbf{(3)}$$

Based on the expression to calculate the "n_S" sheet density Hall voltage must be known or calculated. The hall voltage gives out a value with a charge pointing towards the type of the semiconductor (n type or p type). Normally Van der pauw technique is used to find the Sheet resistance. This is discussed in the next topic.

To find sheet resistance value one must know the values of electron mobility and sheet density. The equation for mobility is [77]:

$$\mu = |V_H|/R_S IB = 1/(qn_S R_S) \quad \ldots\ldots (4)$$

Knowing the thickness of the measuring sheet one can then calculate the resistivity and the density of the change carriers easily.

4.1.1 Van Der Pauw Technique

The Van der pauw method was first proposed by L.S. Van der pauw in 1958 [78]. This method is used to find the key parameters of Hall Effect like resistivity and Hall coefficient. The technique is applied on the selected samples that satisfy the process condition. The sample must be flat and perfect square with homogeneous surface and uniform thickness. Possible geometries are:

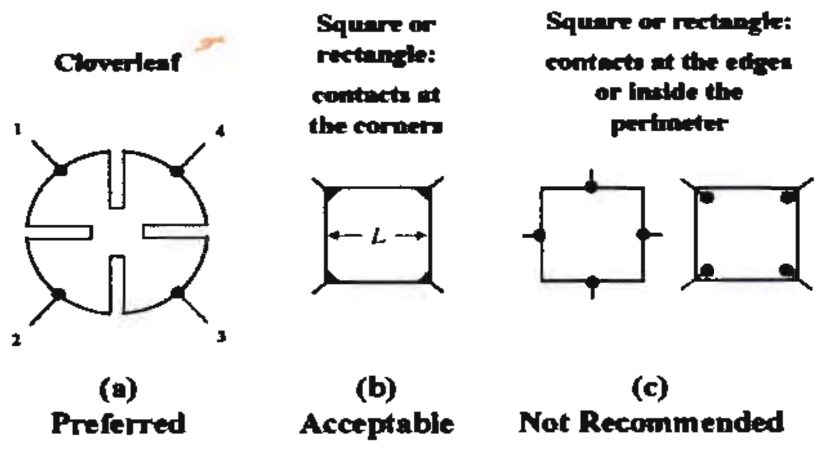

Fig. 4.2: Van der pauw technique possible sample geometries [78]

4.1.2 Resistivity Analysis

For resistivity measurements we use Van der pauw technique. Basically we have two resistances known as the R_A and R_B as shown in figure 4.3. The equations for the resistances R_A and R_B according to the van der pauw are given as follows:

$$\mathbf{Exp}\ (-\pi R_A/R_S) + \exp(-\pi R_B/R_S) = 1 \quad \ldots\ldots (5)$$

And to extract Sheet resistance we get:

$$R_S = -\Pi/\ln\ (1/\exp(R_A) + \exp(R_B)\ ) \quad \ldots\ldots (6)$$

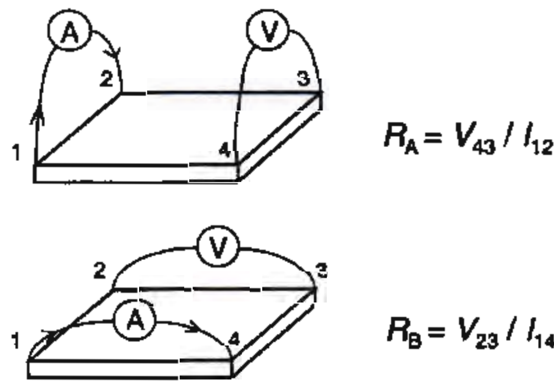

Fig. 4.3: Van der pauw setup for the resistances R_A and R_B

4.2 ASMEC

ASMEC stand for Automatic System of Material Electro-Physical Characterization. This system is capable of inducing multiple environments on to the sample and give the insitu results. The system specification as mentioned on the International Islamic University Islamabad website is as follows:

Table 4.1: ASMEC specifications and operational range

Current Sensitivity	• 1pA
Charge Sensitivity	• 5 E- 16C
Range of Bias Voltage	• -13.5V to +13.5V
Range of Rate window	• 10μs-200s
Temperature	• **72K-500K (Extendable)**
Interface	• Probe-station /External Acquisition
Deep level concentration sensitivity	• 5 E -7

The system can be tailored to perform many calculations one of which is the study of the effect of the light on to the sample/device operation.

This makes it a good machine to quantify the quality of the sensor and its output parameters. Apart from that the system is also capable of calculating following electro-physical quantities:

Table 4.2: ASMEC measurable quantities

▪ Ultra low ampere resolution current application ▪ Kinetics of free and trapping charges. ▪ C-V Characterization (Pulse and line scanned) ▪ I-V characteristic ▪ J-V Characteristic ▪ Charge-DLTS ▪ Photo-stimulated Internal Field Transient Spectroscopy (PIFTS) ▪ Electrical Excitation ▪ Optical Excitation ▪ Iph(t) ▪ Vph(t)	▪ Q(t) ▪ ΔQ(t) ▪ I(t) ▪ Emission/Recombination Rate ▪ Minority Carrier Concentration ▪ Minority carrier Life time ▪ Built-in Voltage ▪ Resistivity/Conductivity ▪ Trapping center concentration ▪ Arrhenius Analysis/Activation Energy ▪ Capture cross-section ▪ Concentration of non-compensated donors and acceptors	▪ Dielectric constant ▪ Charge Analysis ▪ Carrier Concentration/Deep Level concentration ▪ Failure mode Analysis ▪ Process Protocols Characterization of diverse devices such as Photo-detectors, Electro-luminescent devices, diodes etc. ▪ and much more..

Chapter 5

Experimentation, Results and Discussion

This chapter demonstrates the findings and the outcomes of the experimentation performed by myself, to investigate the possible case scenario for the workable graphene induced metal semiconductor metal structure, for its potential application in the next generation electronics. The heretical flow of the findings in the form of graphs that are represented here can be seen through the following flowchart for better understanding:

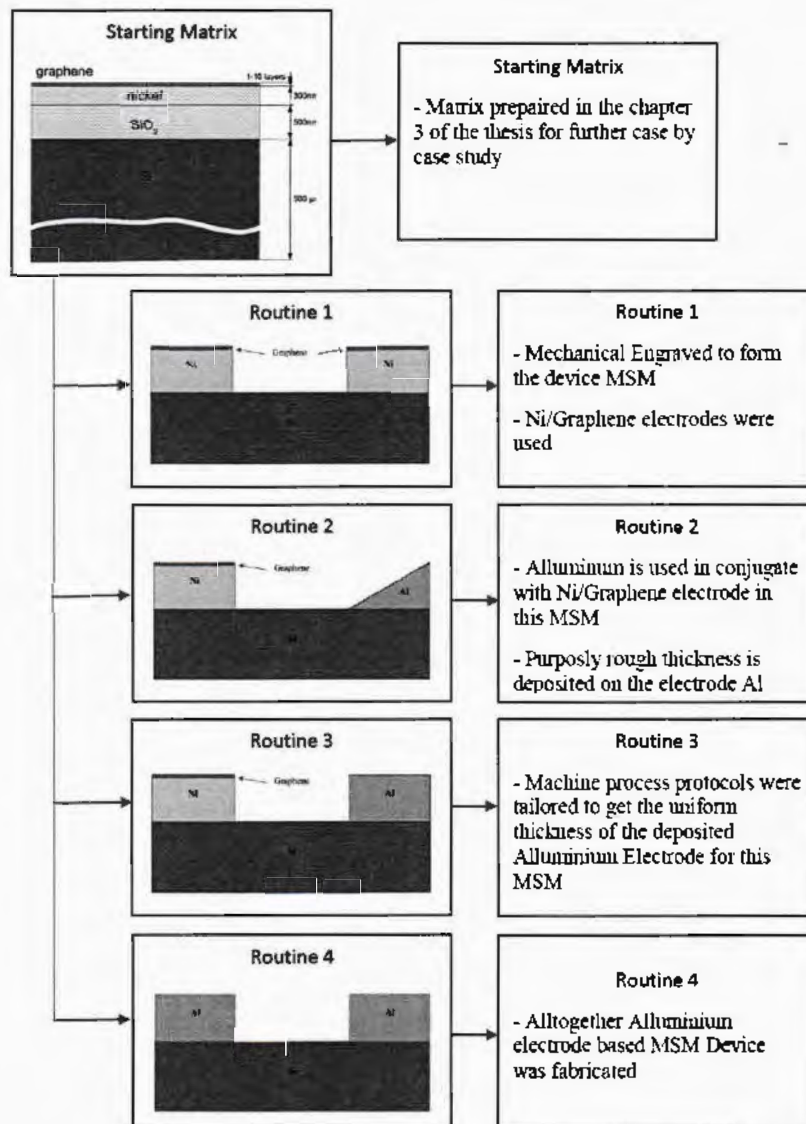

Fig. 5.1: Flowchart of the experimentation performed

From the literature review [56 – 68], the salient features/behaviour of the MSM structure are noted. Based on these any MSM device structure can be quantified and judged. It is noted that for a good MSM structure the current and the voltage produced by the device wben placed in the illuminated environment is very important to judge its quality. Also the ranges of the current produces by the device is also as much important as device itself. Other feature to quantify the MSM device is the delta different of the current produced by the device when placed in the light to the current produced by the device when no light is exposed on it. This difference should be sufficient enough so that the read out electronics can differentiate between either the device is detecting or not. For a good MSM the current output should be constant when the light is shined on to it, meaning the value of the current produced should be constant throughout the time the device is exposed to the light environment. These qualities must be exhibited by the structure to be called a Metal Semiconductor Metal Device [56 - 68].

5.1 Result and analysis of device all graphene/Ni MSM (Routine 1)

The device fabricated by the routine 1 had the structure of MSM where the two electrodes are made of the Graphene\Ni and the semiconductor is Silicon. The structure went through the mechanical scribing and the end fabricated device is first tested on the Hall Effect system to quantify whether the device is actually fabricated or not. The Four point probe system was used to get the accurate data of the device under study. Based on the results the device will be tested on the advanced electrical characterization modules. The results of the Hall Effect are shown in the table 5.1 below:

Table 5.1: Hall Effect measurements of the device fabricated through Routine 1

Sample	Metal Thickness	Rs (ohm/sq)	Rho (ohm-cm)	Con (1/ohm-cm)	Ns ($/cm^2$)	Ns ($/cm^3$)	µs (cm^2/Vs)

Graphene MSM Prepared through Routine 1	401.23nm: 401.23nm/ 500μm Si	2.61 E+03	1.30 E+02	7.67 E-03	-3.32 E+13	-6.63 E+14	7.24 E+01

The sheet resistance of the device was found out to be 2.61 E+03 which is a clear indication that the device is fabricated and the channel Metal semiconductor Metal is formed. As the value of the resistance is quite greater than the value of the resistance obtained from the graphene alone, as reported by us in our paper earlier, titled "**Effect of metal contact and rapid thermal annealing on the electrical characteristics of 2D graphene matrix**" [79].

Another qualification of the device was conducted with the help of imaging equipment. Atomic force Microscopy was used on this sample to get the image and the depth of the trench that was engraved in the making of the device. As shown:

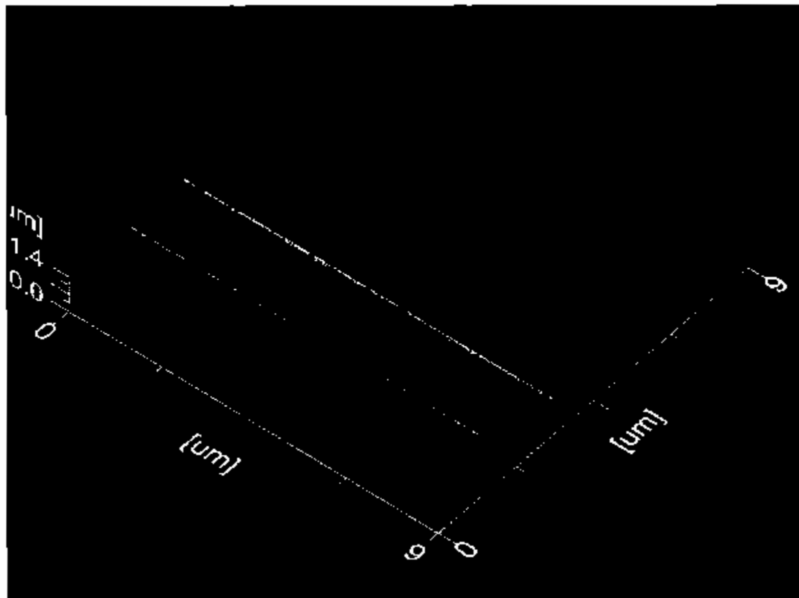

Fig. 5.2: AFM image of the trench engraved in the sample prepared by the routine 1

The depth of the trench was found out to be 1.4 micron which is the depth at which the substrate part of the device or the initial matrix of silicon is present. As described in the chapter 3, the layer hierarchy of the initial device matrix contain 1-10 layers of graphene followed by 300nm Nickel, then 500nm SiO_2 and the substrate is Silicon (100). The

presence of graphene was confirmed with the park systems AFM model NX-10. The scan show the 50 nm areal image with the surface roughness of 2.899nm:

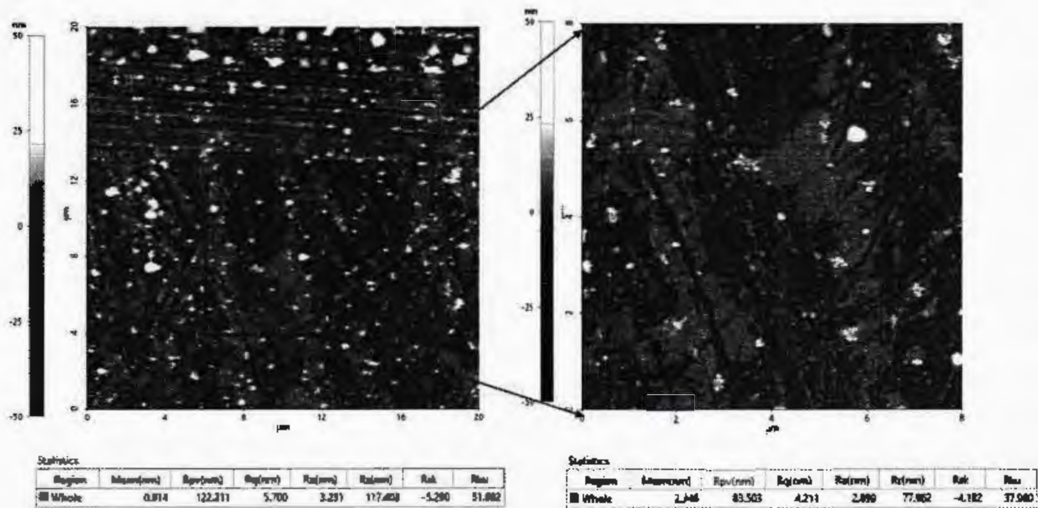

Roughness:
Ra=3.23nm

Roughness:
Ra=2.899nm

Fig. 5.3: 50nm AFM of the graphene MSM structure

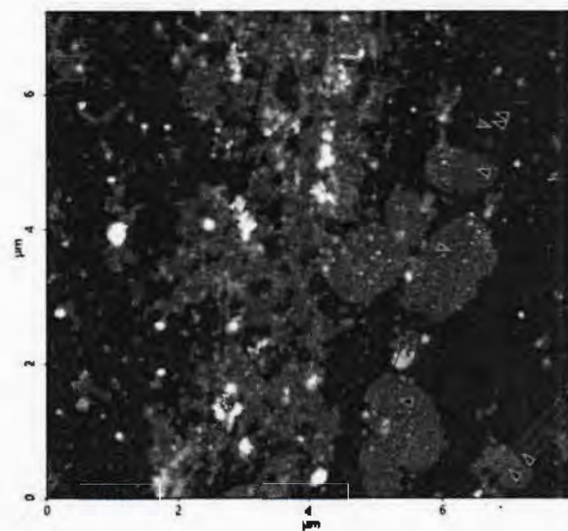

(a)

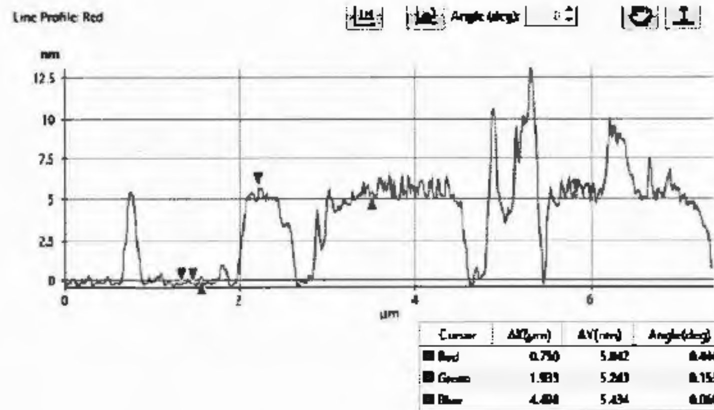

(b)

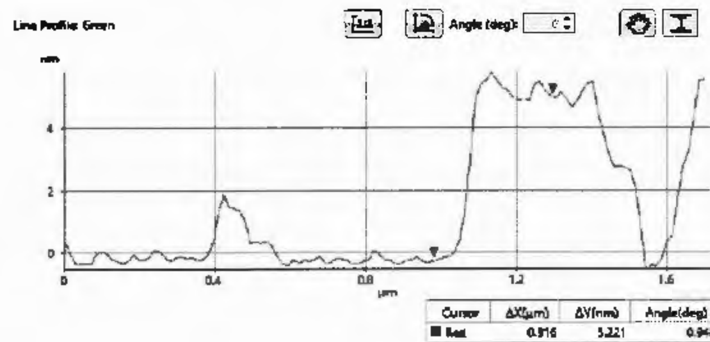

(c)

Fig. 5.4: (a) Line profile analysis of the graphene sample surface, (b) Average thickness profiling of the first line scan between two points, (c) Average thickness profiling of the second line scan between two points

The thickness of graphene was found out to be in the range of 5.2-5.8nm. The graphene was also found to be distributed randomly on to the device surface. After the initial confirmation about the channel formation in the device and the presence of graphene on top of the sample, the device was tested for the quality parameters to substantiate our argument of this research.

The device was tested for the standard parameters that are necessary to judge not only the reliability of the fabricated device but also to compare it with the already reported devices present in the market [56 - 68].

The advanced characterizations were performed on ASMEC system placed at Centre of Advanced Electronics & Photovoltaic Engineering, International Islamic university Islamabad. The resulted scan for the device fabricated through Routine 1 are as follows:

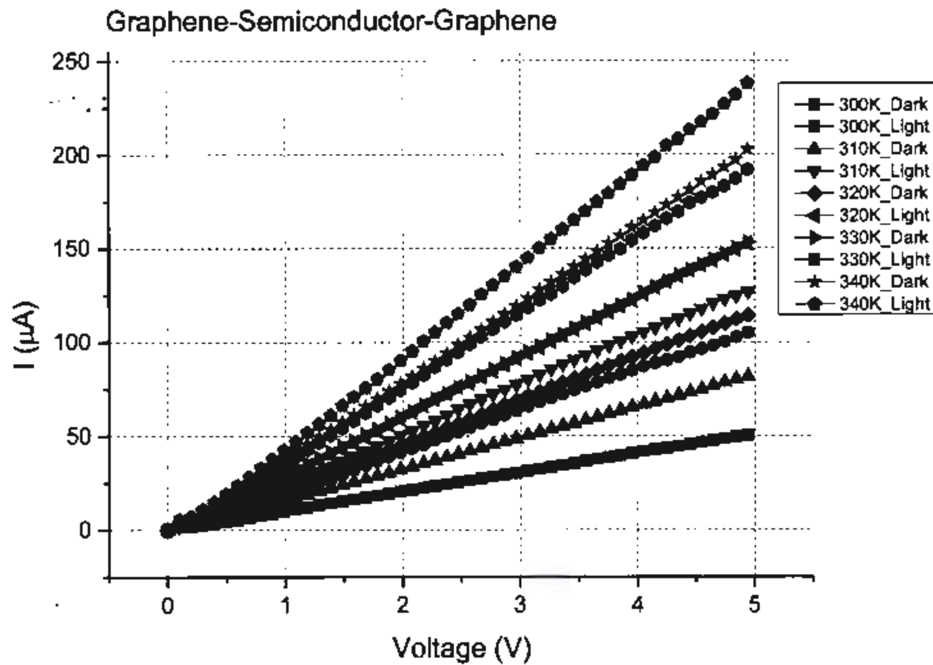

Fig. 5.5: I-V Dark and Light Curves of the Graphene induced MSM at different temperatures

The current-voltage scan is taken at different temperatures in both luminosity and darkness. The scan gives us the idea about the leakage current present in the device when no light is present and also the difference in the magnitude of the output voltage of the device when exposed to the light and when not exposed. The difference also known as Delta can be used to correctly judge the operating range of the device.

For more clear view the figure 5.5 is broken down in to small intervals based on the temperature. Since the data is taken on many temperatures it was necessary to see the change on the device parameters when exposed to different temperatures:

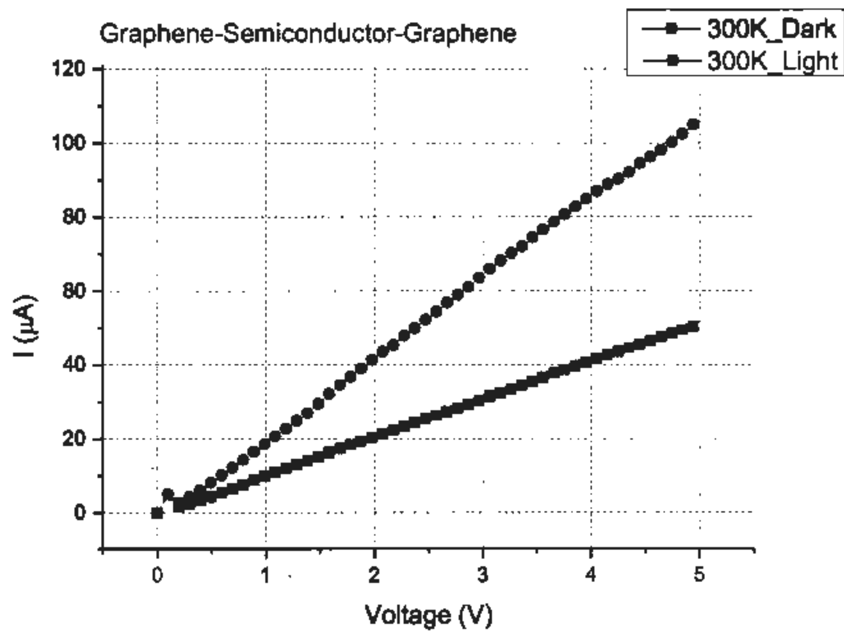

Fig. 5.6: I - V dark and light scan on the temperature 300 k

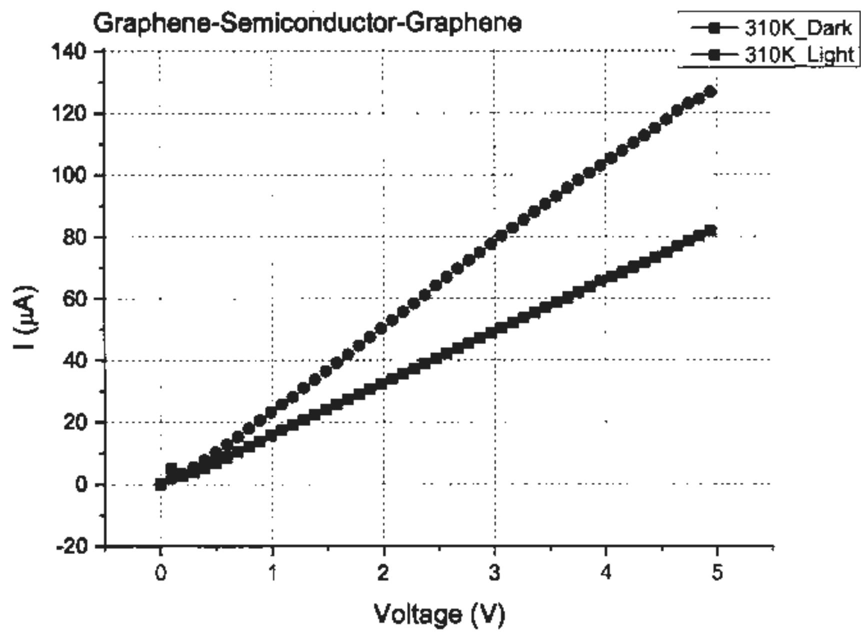

Fig. 5.7: I - V dark and light scan on the temperature 310 k

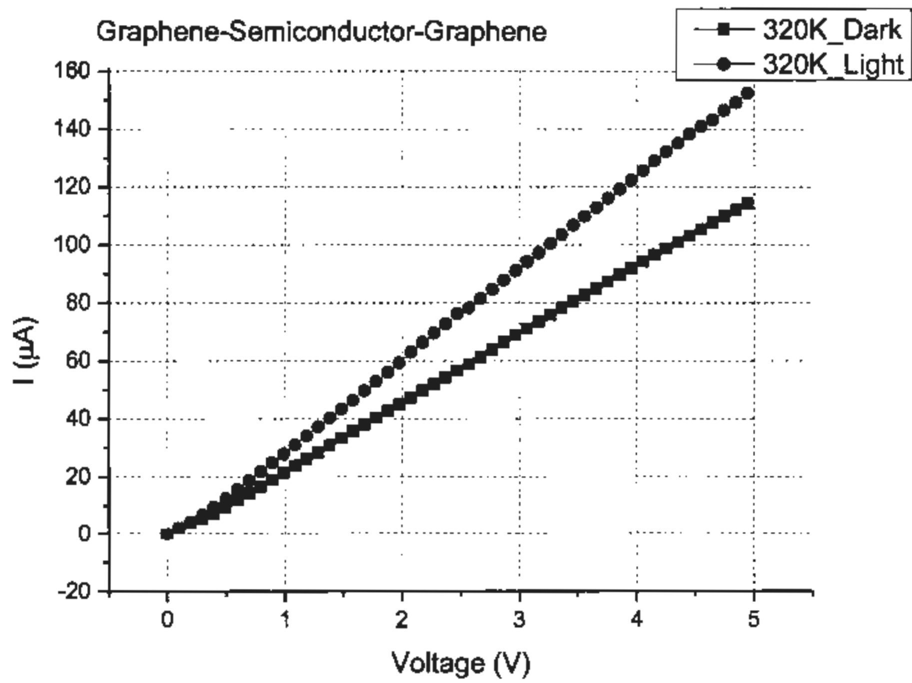

Fig. 5.8: I - V dark and light scan on the temperature 320 k

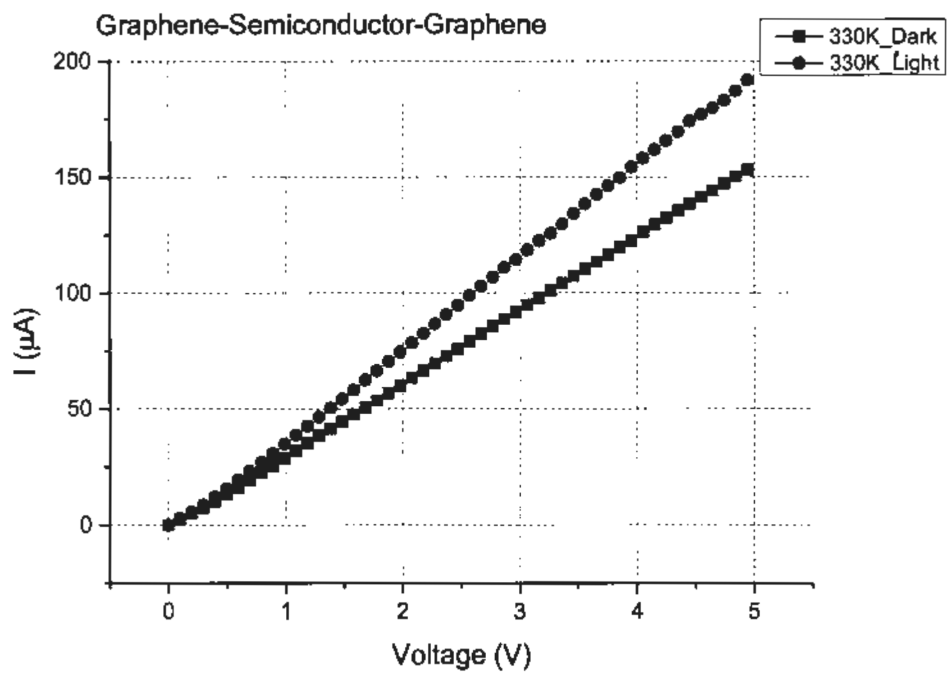

Fig. 5.9: I - V dark and light scan on the temperature 330 k

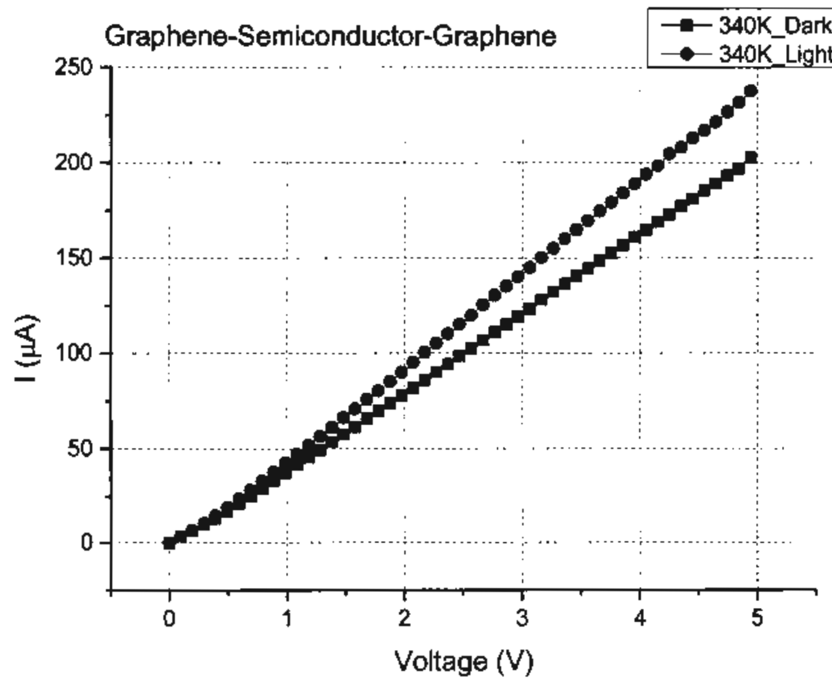

Fig. 5.10: I - V dark and light scan on the temperature 340 k

This can be seen from the graph that as the temperature is increased the difference between the light and dark spectra reduces, meaning the impact of light on to the device is diminishing. This gave rise to the thought that the device has very little window of operation and not prone to the impact of temperature. Also reduction in the delta part means that the device is no more than a detector.

We also test the device for photo-generated current on multiple voltages ranging from 0 to 5 volts. The temperature was kept at the 295k (room temperature) for these measurements. The voltages were applied to the device keeping in view the conventional electronics system circuitry, where every component is needed some voltage for operation. The scan is as follows:

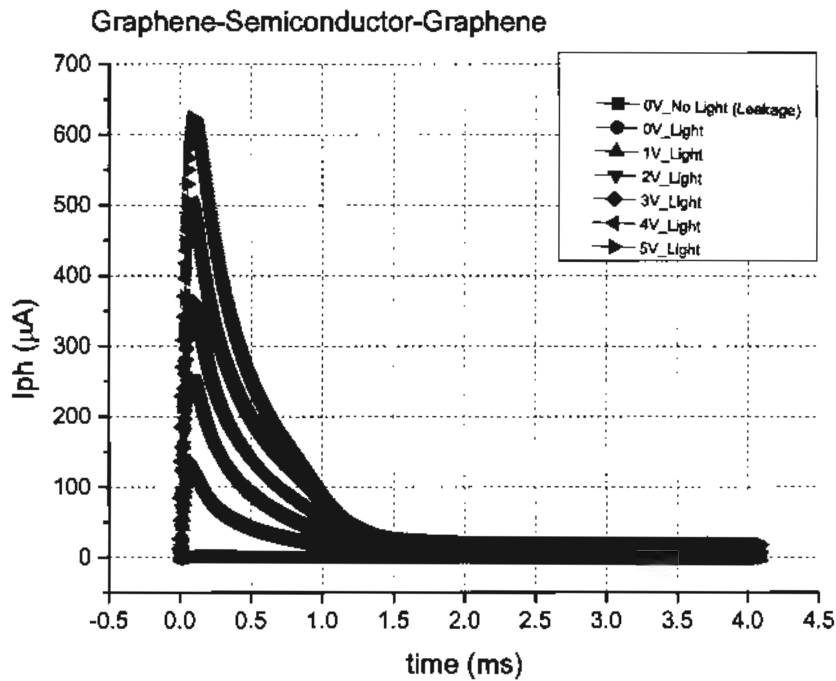

Fig. 5.11: Photo-stimulated current scan w.r.t time on multiple constant applied voltages

It can be seen that the device behaves very abruptly to the applied voltage and in the mere milliseconds comes to its rest position. This points toward the idea that the device of this structural hierarchy may be used for fast switching. The values of the current produced by the device are also in significant ranges with the highest value of 0.06 mA. Also a condition of no light applied is taken here so that leakage current can be mapped. A graph showing the photo-stimulated voltages with respect to time is shown in the figure below:

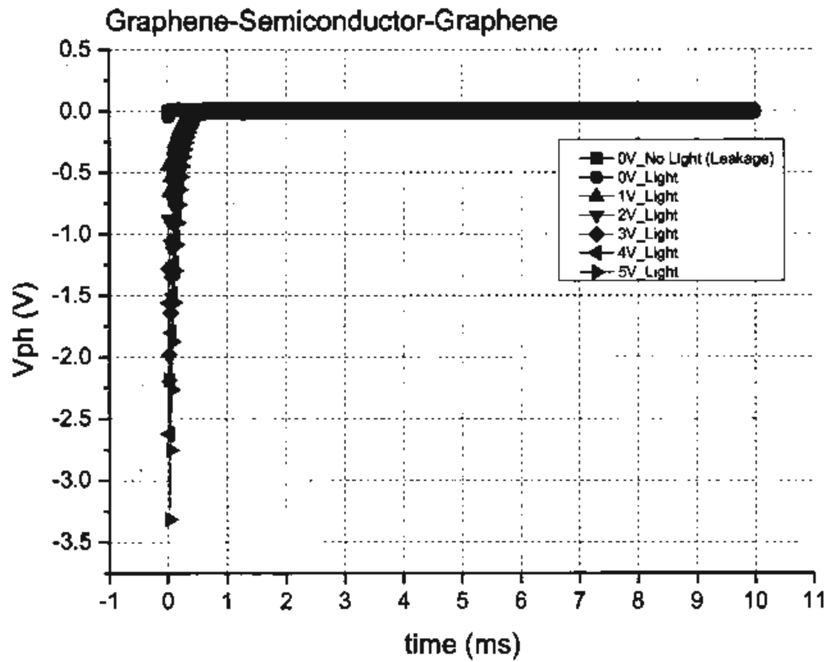

Fig. 5.12: Photo-stimulated voltage scan w.r.t time on multiple constant applied voltages

For any device to be made workable in the conventional electronics, it must satisfy the voltage range of the real world electronics. The scan taken in the figure 5.12 in based on that. The graph shows the generation of the voltage for very less time before they reach zero. Meaning the device does not hold the voltages for sufficient time. In other words this point out towards the possibility of leakage in the device, which is verified in the next scan:

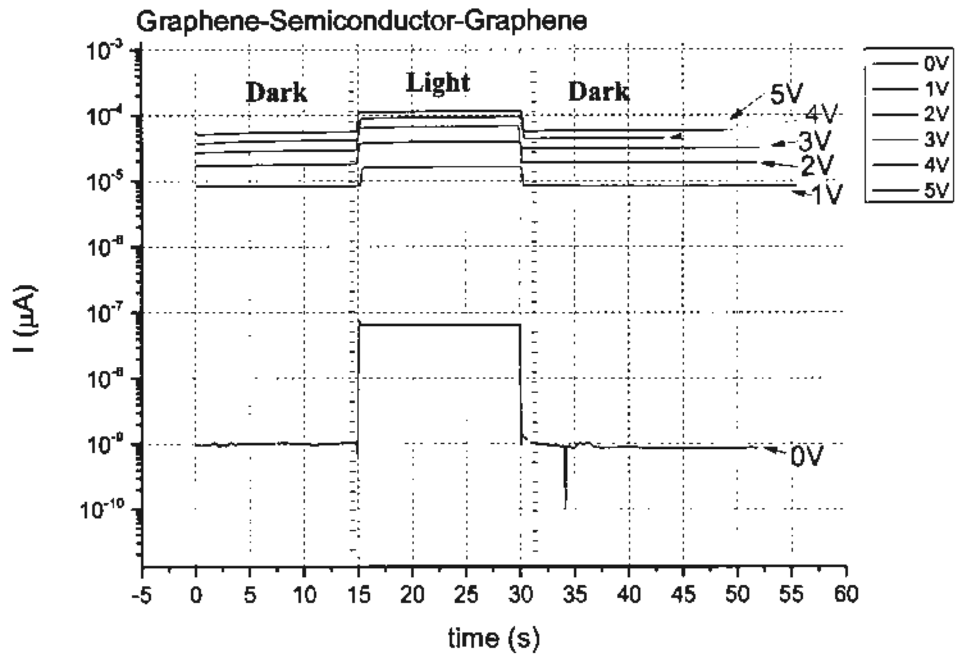

Fig. 5.13: Dark and Light Electric current measurements w.r.t time

This graph represents the characteristics of the device when it is placed in a constant time of 15 seconds in dark and light environment with applied voltage. The idea is to get the readings for the current of the device when exposed to longer durations of light ambience. On 0 applied voltage the device show the dark current of 10^{-9} uA, which rises up to 10^{-7} uA when the light is incident on to the device. The device hold the value over the time of applied light and then return back to its initial value of 10^{-9} uA. Same rise and fall can be seen in all other case of applied voltage however the values of dark current with respect to when the light is applied on to the device is not that much of a change in value. This much increase in the dark current directly points out towards the leakage in the device. Even though the current ranges of the device are in the operation zone of the workable electronics but the leakage is high and the device does not hold the voltage for too long.

5.2 Result and analysis of device graphene/Ni/Rough Al MSM (Routine 2)

The sample prepared by routine 2 had one electrode of the Metal semiconductor metal device made of Graphene/Ni and the other electrode was made from unevenly grown aluminium. The uneven growth of the Aluminium sample was introduced on purpose so that the impact of the electrode quality can be mapped on the device operation. Current- voltage analysis for this sample is shown in the figure 5.14 below:

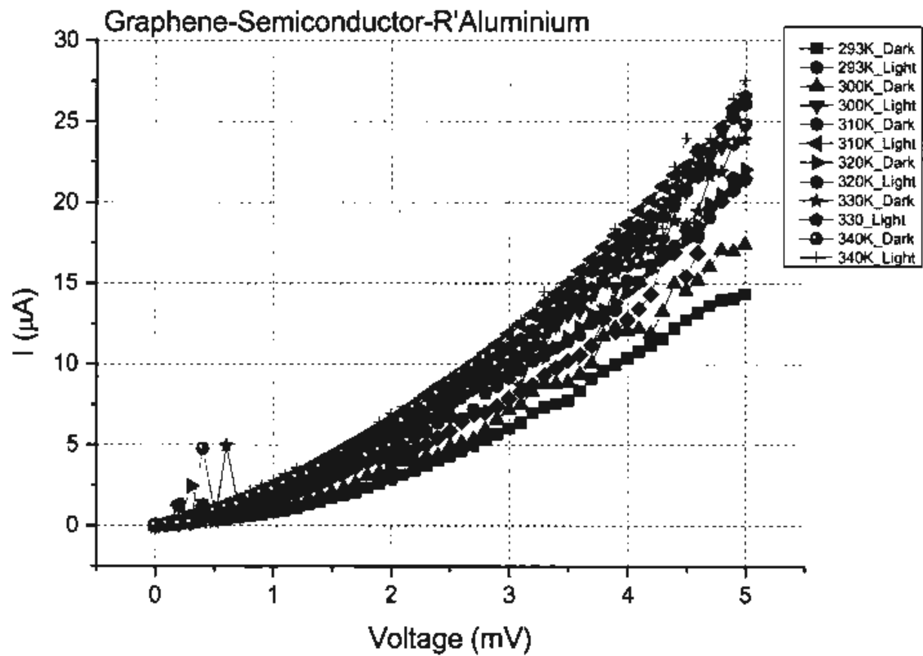

Fig. 5.14: I-V Dark and Light Curves of MSM device Prepared form Routine 2 at different temperatures

The same temperature range implied on the device prepared from routine 1 was used to get the scan for this device. The measurement parameters and operating conditions of the machine were same for this case. It can be seen from the graph that the measurements taken at all the temperature, both in the light and dark show very less change in value. The spectra in figure 5.14 is broken down in to intervals of dark and light on individual temperature below for clear picture.

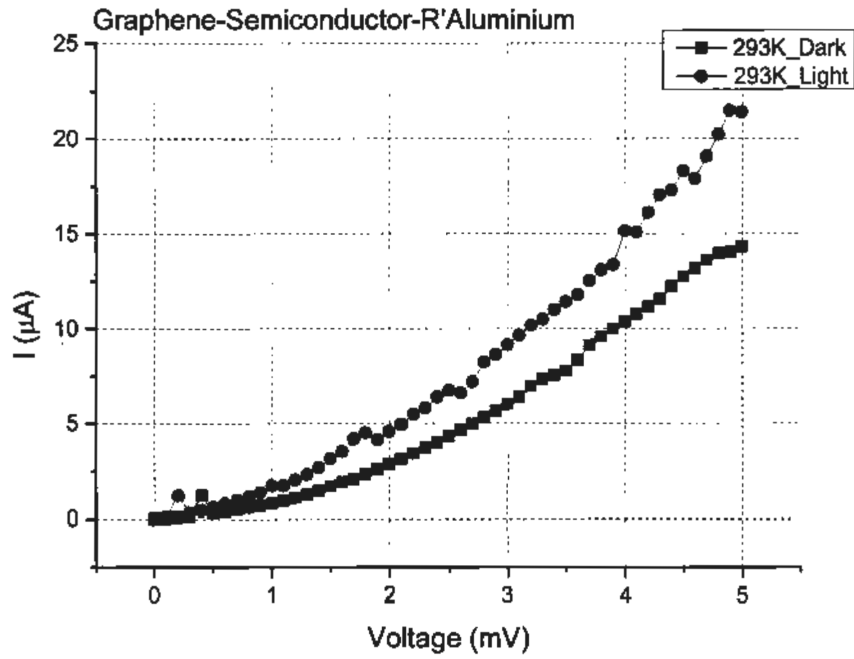

Fig. 5.15: I - V dark and light scan on the temperature 293 k for the device fabricated using the routine 2

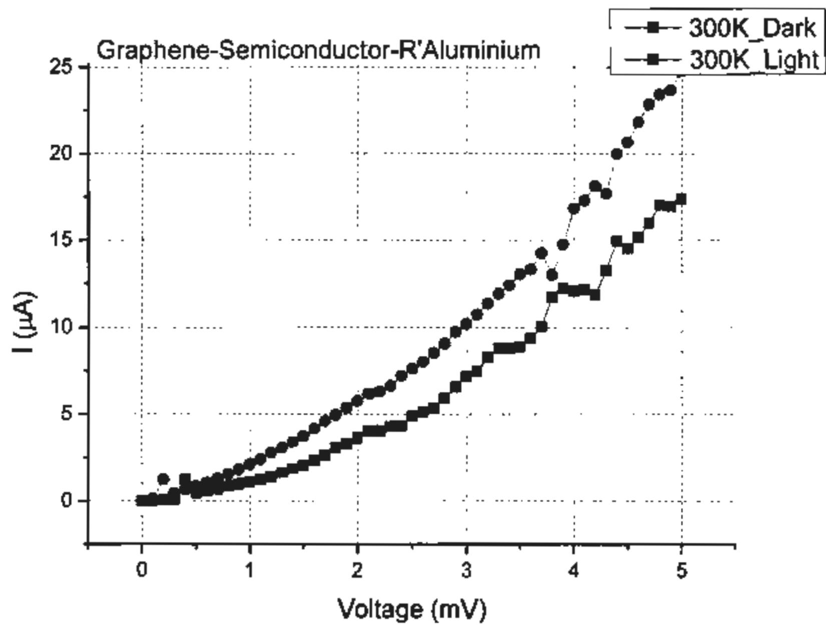

Fig. 5.16: I - V dark and light scan on the temperature 300 k for the device fabricated using the routine 2

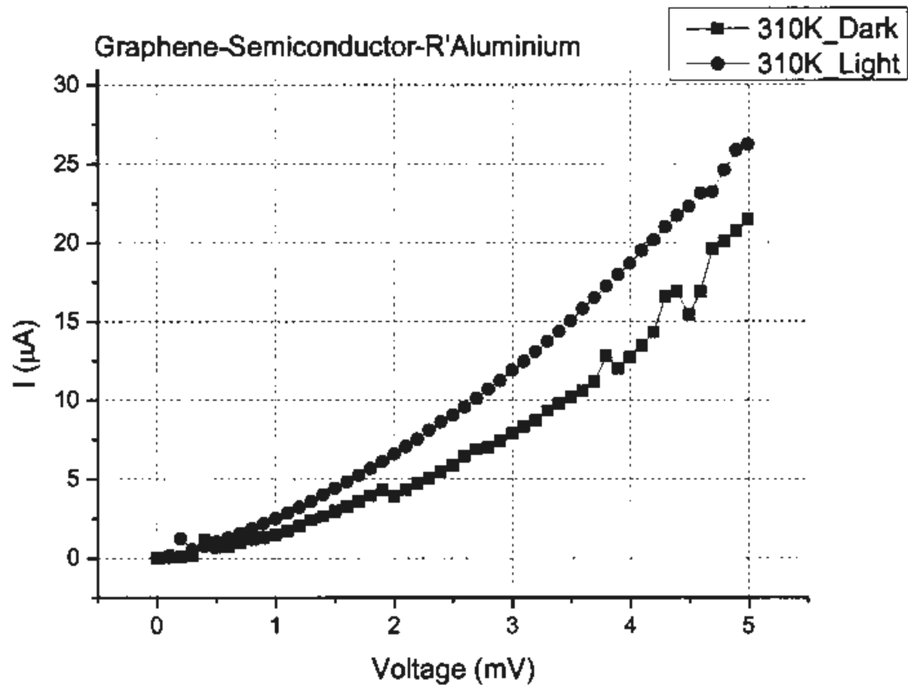

Fig. 5.17: I - V dark and light scan on the temperature 310 k for the device fabricated using the routine 2

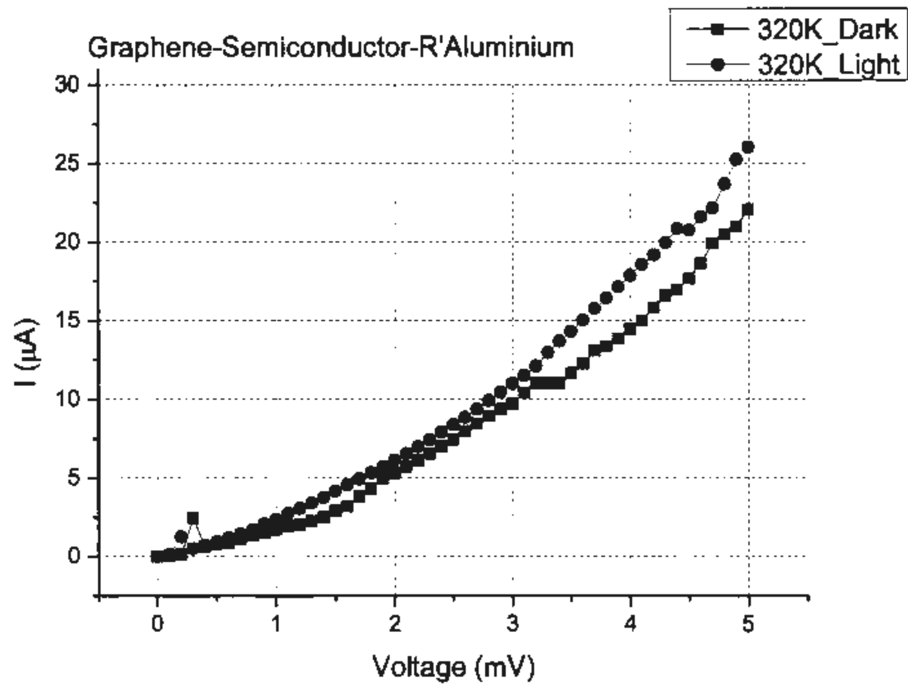

Fig. 5.18: I - V dark and light scan on the temperature 320 k for the device fabricated using the routine 2

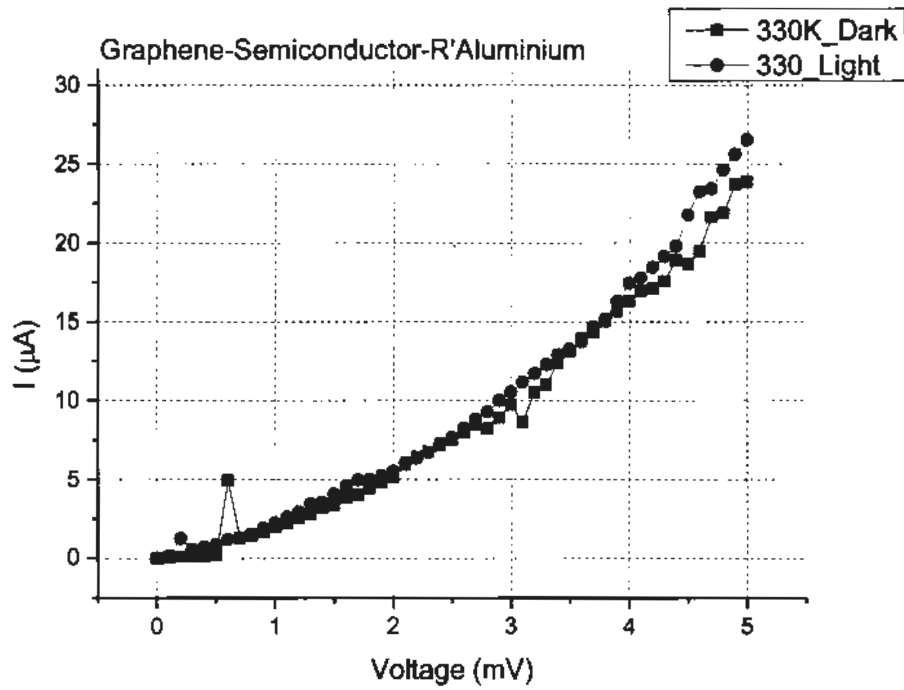

Fig. 5.19: I - V dark and light scan on the temperature 330 k for the device fabricated using the routine 2

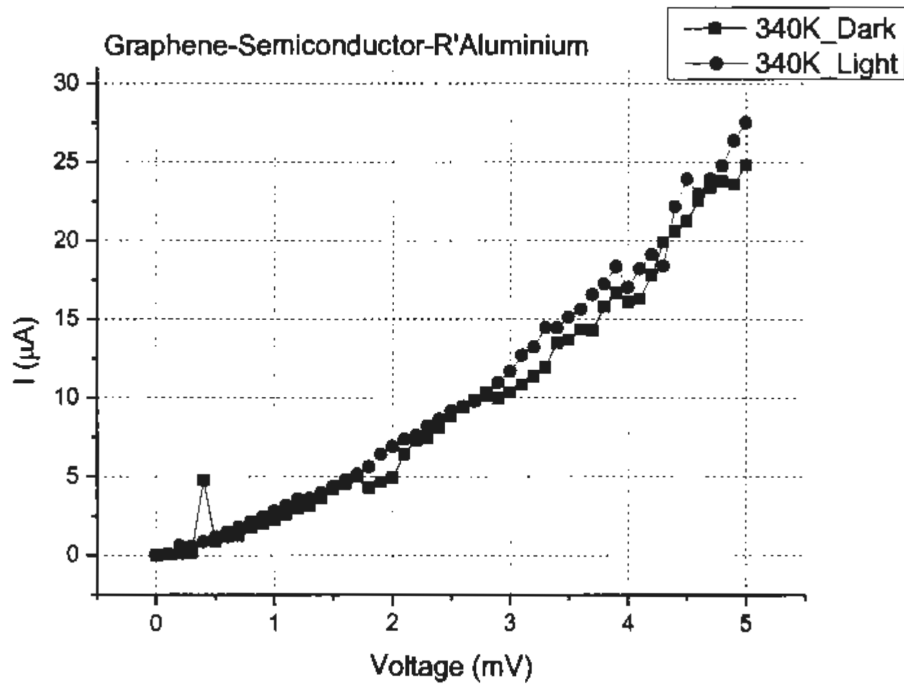

Fig. 5.20: I - V dark and light scan on the temperature 340 k for the device fabricated using the routine 2

The graphs show that the difference between the I-V measurements when the light is introduced to the device to the readings taken in the dark is minimal. Over 320k

temperature, the difference becomes almost zero and the curve of dark rides the curve of light. This almost negligible change in the device I-V curves needed detailed analysis with possible reasoning pointing towards the impact of the electrode growth quality on to the device measurements. Other measurements were also taken so that we can substantiate our imposed possibility of electrode quality on to the device functionality.

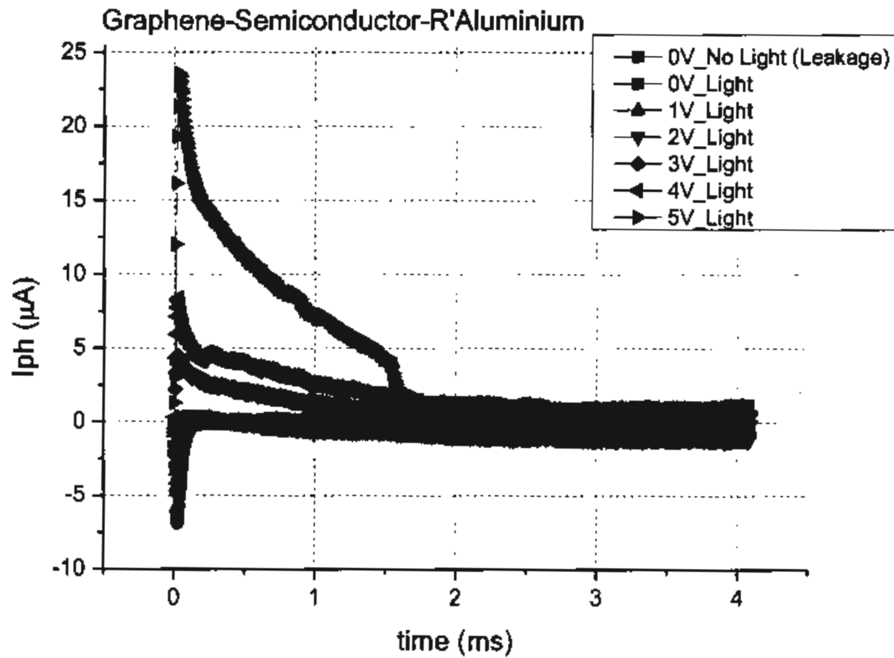

Fig. 5.21: Photo-stimulated current scan w.r.t time on multiple constant applied voltages on the device prepared by the Routine 2

The Photo – stimulated scan of current with time reveal that the device does bold some current for some time before dropping it down to zero. The voltages provided to the device are actually the amount of light that will generate the equivalent voltage of 1volt. The device show good current readings for 5v, however that current is loosed by the device very quickly. For the rest of the cases the current is not that high.

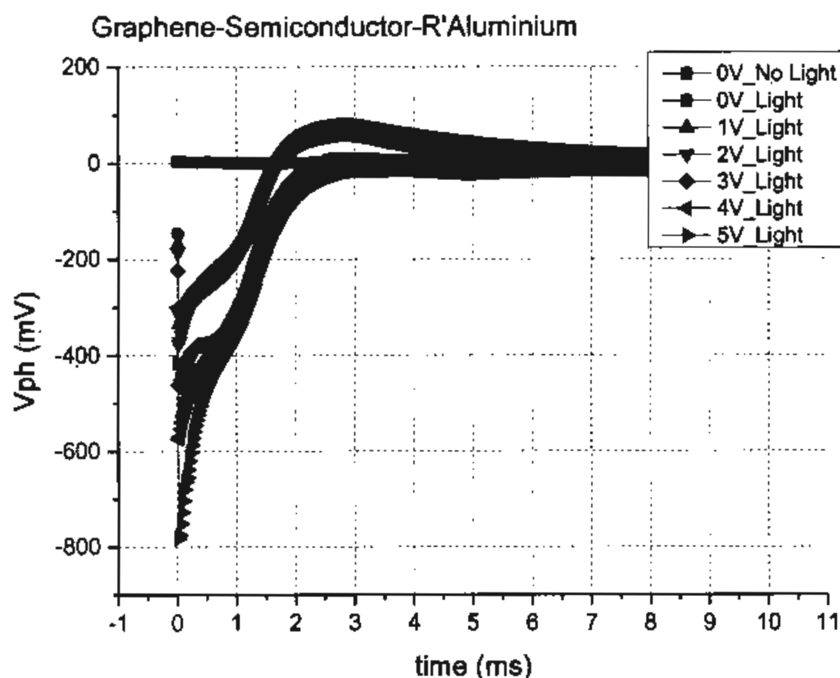

Fig. 5.22: Photo-stimulated voltage scan w.r.t time on multiple constant applied voltages on the device prepared by Routine 2

Figure 5.22 shows photo-stimulated voltage of the device fabricated by using the routine 2 the device shows rather a capacitive behaviour, storing the charge for some time before nullifying it to zero. However the range of the voltage is very small with the order of magnitude of 10^{-2} volts. This small of charge will most probably be consumed by the device internal leakages. The next measurement graph show exactly that.

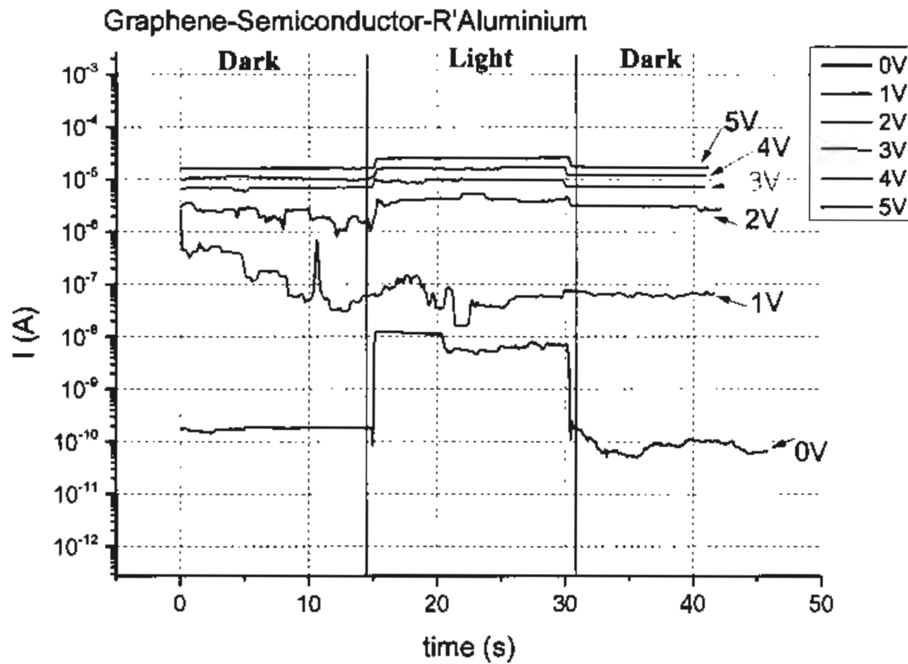

Fig. 5.23: Dark and Light Electric current measurements w.r.t time for the device fabricated using the routine 2

The curves of the graph shows the current consumed by the device when no light is exposed to the device and the case when exposed. The exposure time of light 15 second. The Graph show very less current in 0 volt condition, ranging in 10^{-8} to 10^{-10} A. This means that the device is consuming energy when no biased is applied. This consumption of energy by the device is the result of internal leakages not good for a detector operation.

5.3 Result and analysis of device graphene/Ni/Al MSM (Routine 3)

The device prepared through this routine had a structure similar to that made in the routine 2, but this device had the Aluminium electrode been made homogeneous. The detailed routine can be seen in the chapter 3. For the growth of the aluminium electrode the machine Atomistic layer deposition System is used. The replacement of Graphene\Ni electrode with Aluminium in this routine is done to get the desired

measurements for such potential device structure. The initial Hall Effect measurements are shown in the table below:

Table 5.2: Hall Effect measurements of the device fabricated using the routine 2

Sample	Metal Thickness	Rs (ohm/sq)	Rho (ohm-cm)	Con (1/ohm-cm)	Ns (/cm^2)	Ns (/cm^3)	μs (cm^2/Vs)
Graphene Aluminu m MSM	401.23nm :300nm/5 00μm Si	1.90 E+03	9.51 E+01	1.07 E-02	-7.29 E+12	-1.46 E+14	5.10 E+02

The sheet resistance of the device matrix is found out to be 1.9 E+03. This value of the resistance points towards channel formation inside the device. This is crucial to know as the channel formation inside the device means that the device itself is now formed and working. The detailed measurements are shown below:

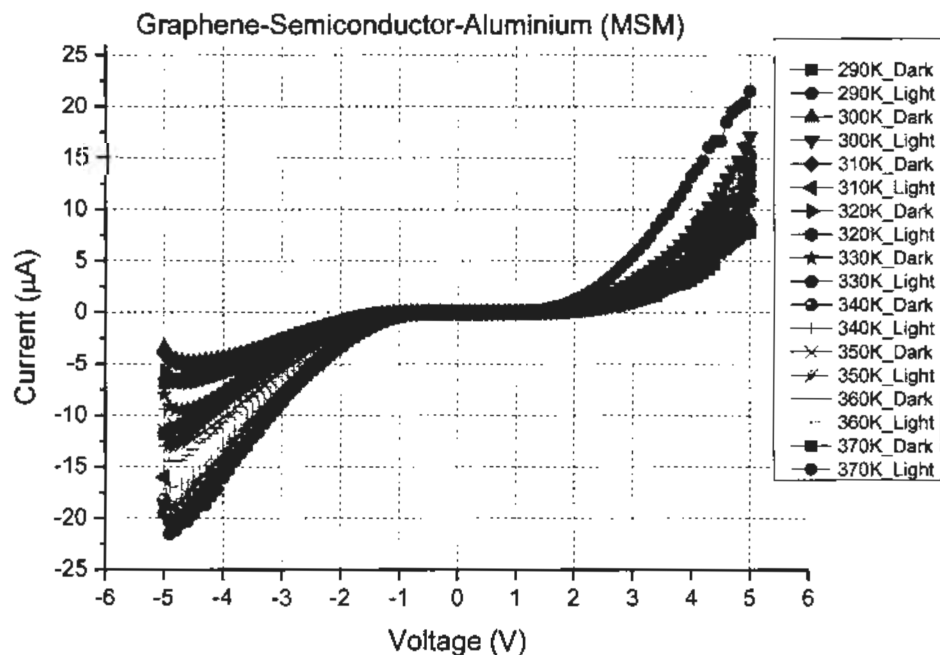

Fig. 5.24: Dark and Light I-V scans of the sample fabricated using the routine 3 at different temperatures

A complete I-V scan is shown in the figure 5.24. Both the forward and the reversed biased behaviour of the detector is recorded. This was implied in this case just to confirm the non schottky characteristics of the device. And since both the forward and

the reversed biased behaviour show exactly the same cure topology, the device under study is not a scbottky detector.

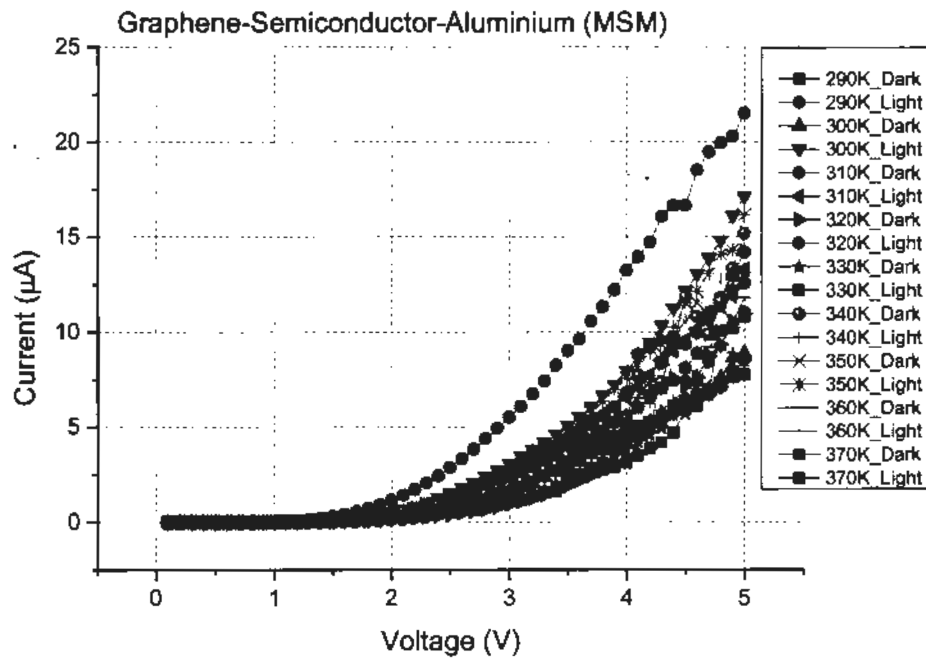

Fig. 5.25: I-V Dark and Light Curves of MSM device Prepared form Routine 3 at different temperatures

The forward biased behaviour is shown in the figure 5.25. I-V readings taken at multiple temperature in light and dark environment shows the device detection capability. Changing temperature also reveal the device functionality change in the form of output parameters. These parameter gives the clear picture as to the device possible integration in to a workable system. I-V curves of this device show promising results, with the maximum delta/difference compared to the rest of the cases. Figure 5.25 is exposed in the following graphs for clear picture:

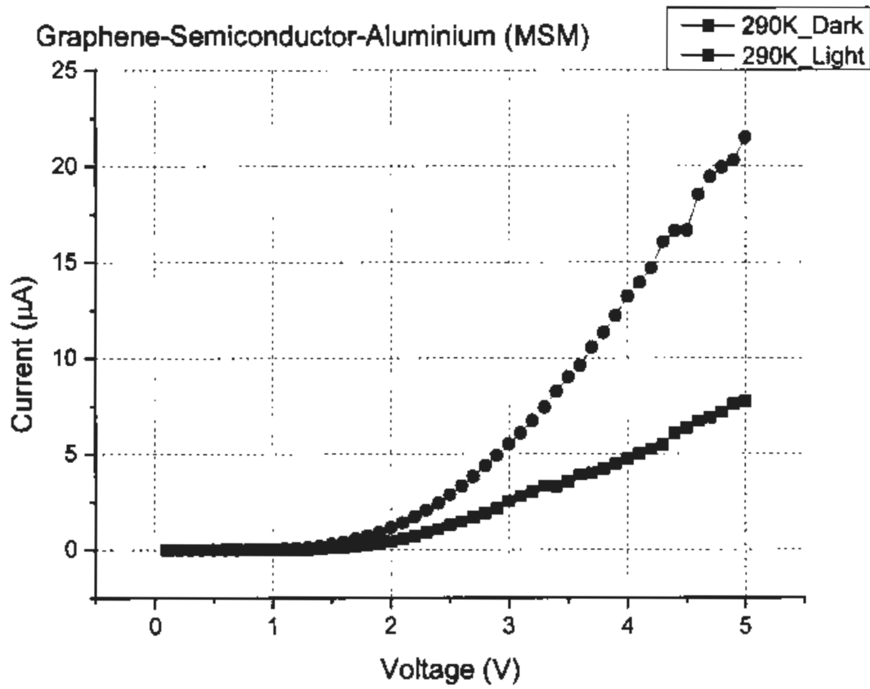

Fig. 5.26: I - V dark and light scan on the temperature 290 k for the device fabricated using the routine 3

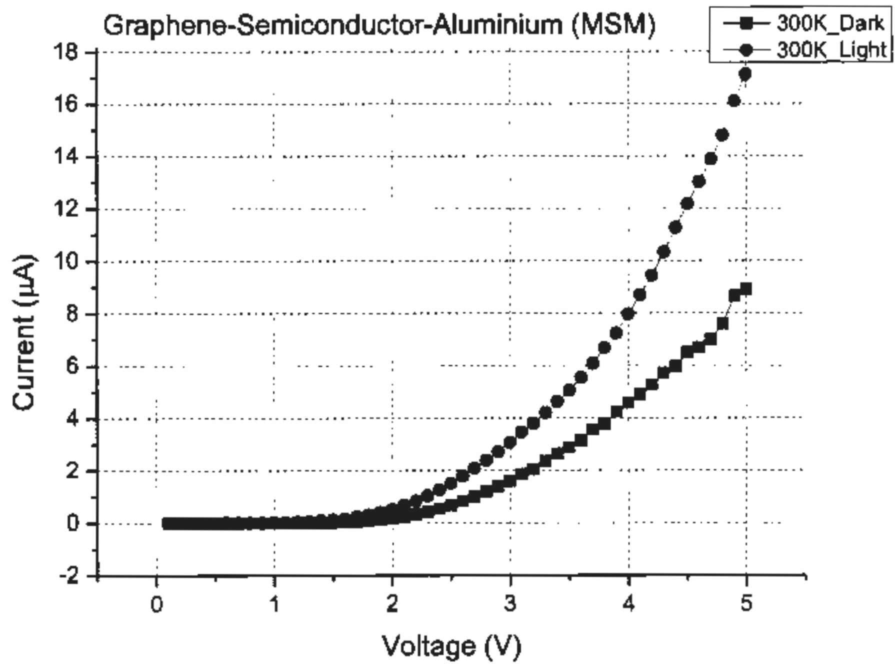

Fig. 5.27: I - V dark and light scan on the temperature 300 k for the device fabricated using the routine 3

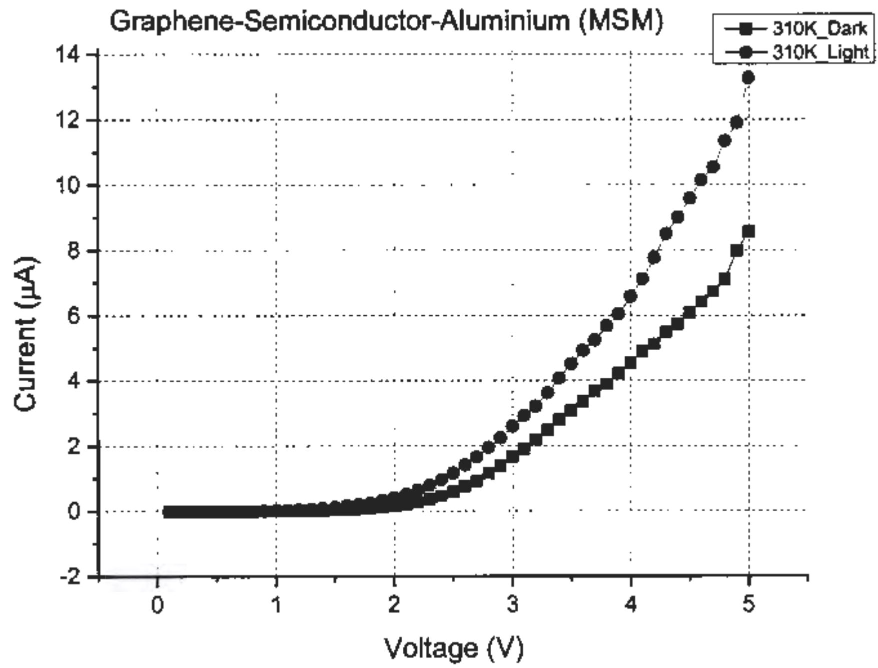

Fig. 5.28: I - V dark and light scan on the temperature 310 k for the device fabricated using the routine 3

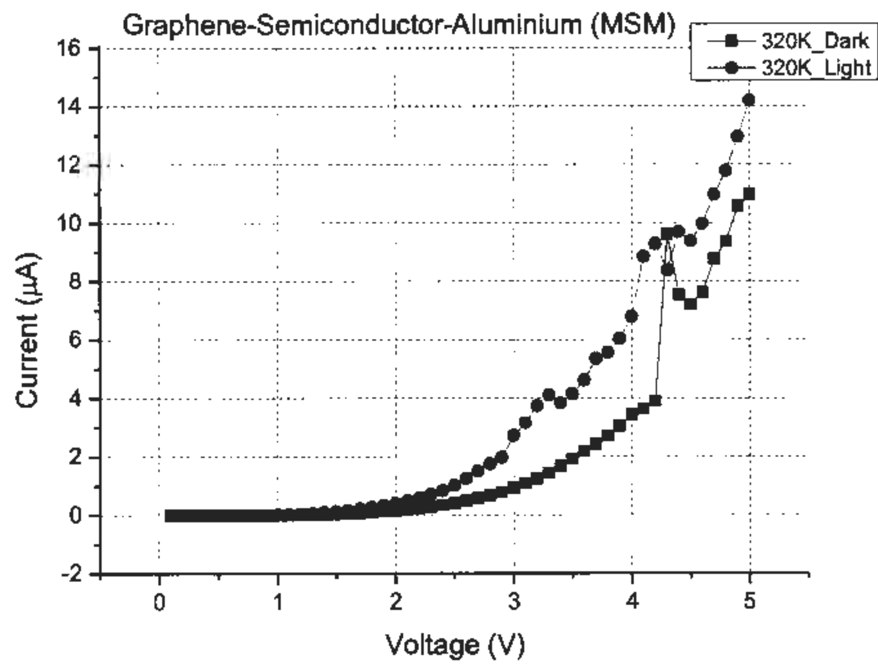

Fig. 5.29: I - V dark and light scan on the temperature 320 k for the device fabricated using the routine 3

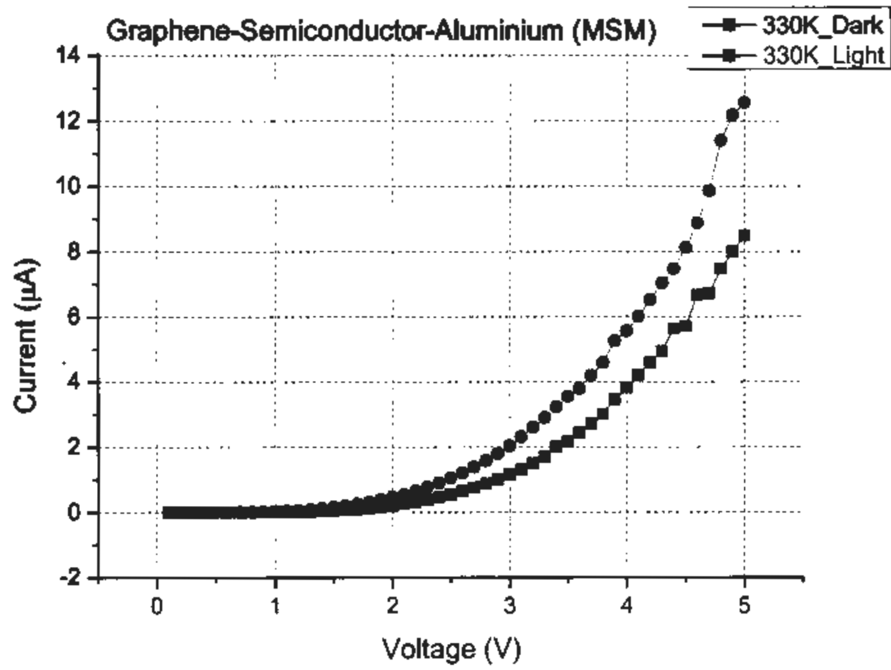

Fig. 5.30: I - V dark and light scan on the temperature 330 k for the device fabricated using the routine 3

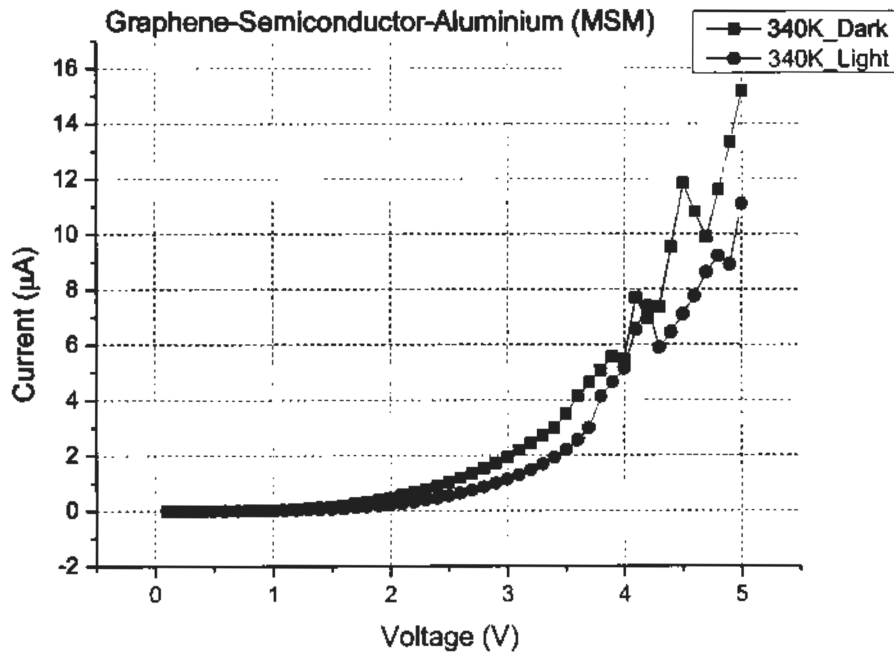

Fig. 5.31: I - V dark and light scan on the temperature 340 k for the device fabricated using the routine 3

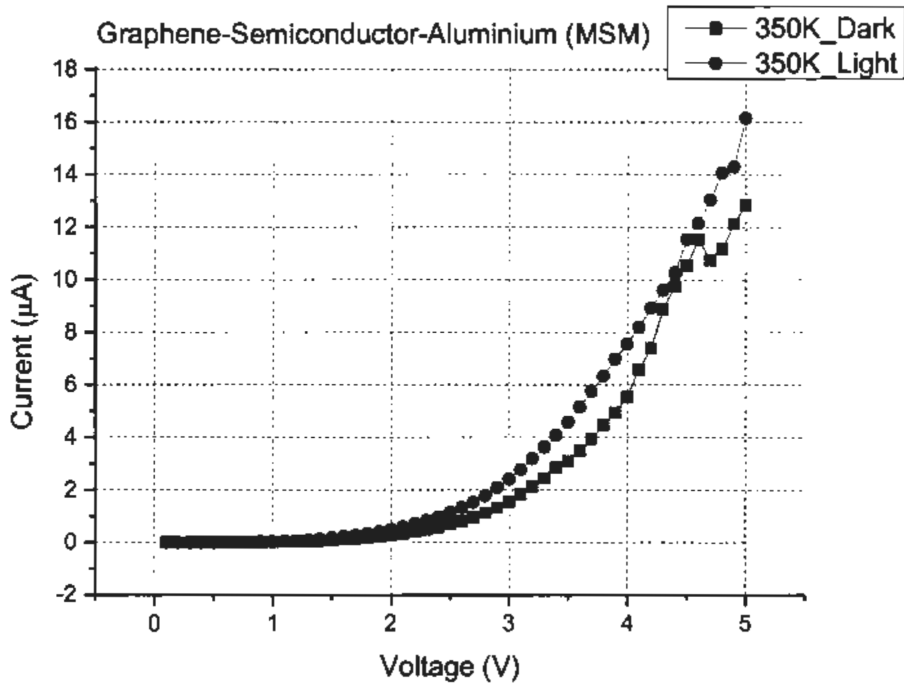

Fig. 5.32: I - V dark and light scan on the temperature 350 k for the device fabricated using the routine 3

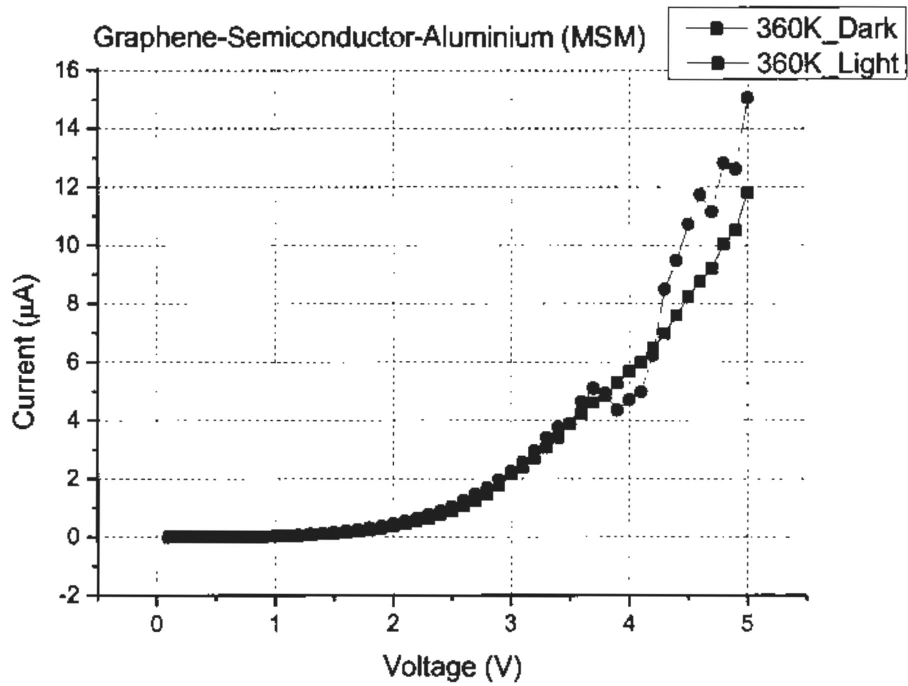

Fig. 5.33: I - V dark and light scan on the temperature 360 k for the device fabricated using the routine 3

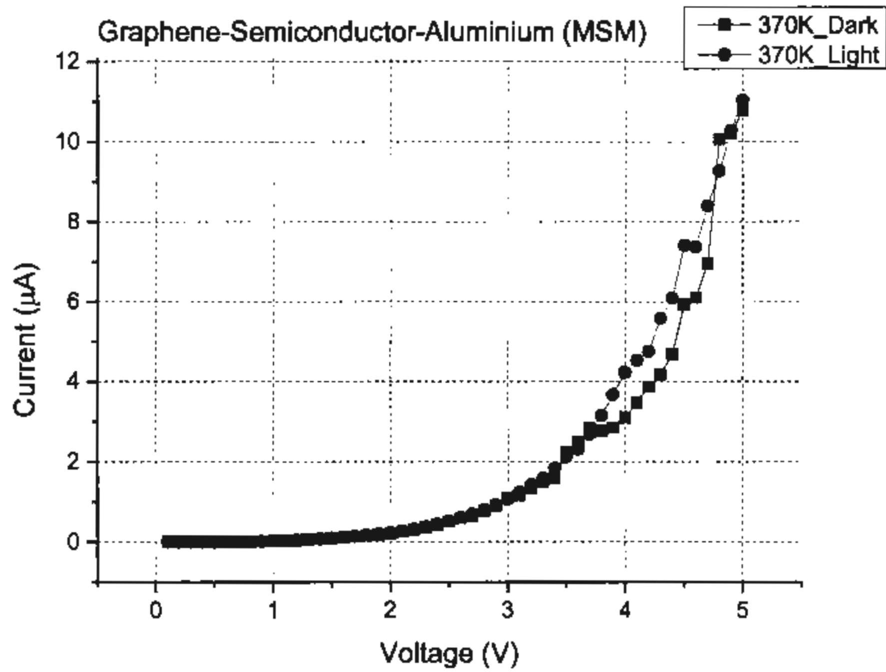

Fig. 5.34: I - V dark and light scan on the temperature 370 k for the device fabricated using the routine 3

The curves mentioned above shows that as the temperature is increased the device detection capability diminish and also at the lower voltage the difference is not so prominent. For the case of temperature 290k the delta difference between the dark and the light is found out to he the greatest among the rest of the cases for the voltage of 3v and above. The current ranges to the top at 5v with the value of 0.23 mA.

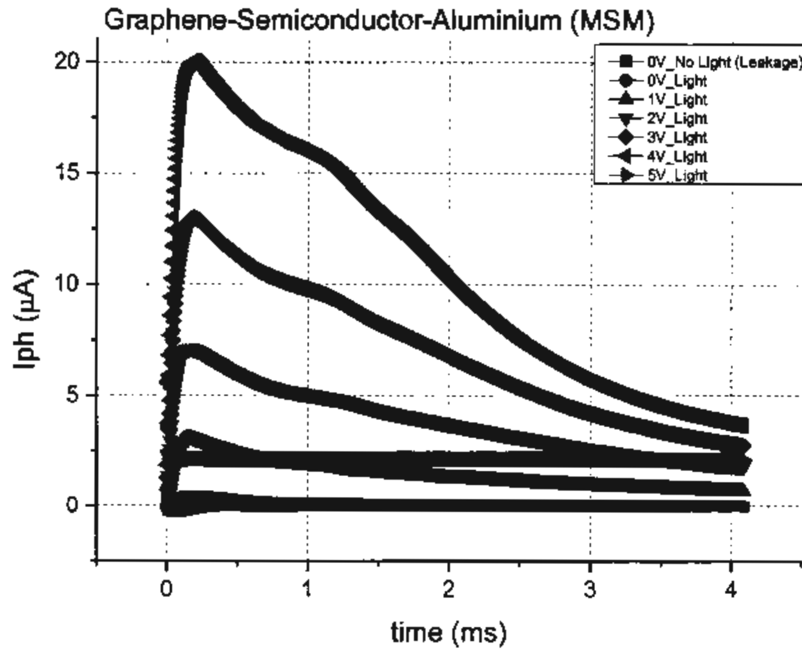

Fig. 5.35: Photo-stimulated current scan w.r.t time on multiple constant applied voltages on the device prepared by the Routine 3

The graph in the figure 5.35 show the light stimulated current scan of the device when exposed to the light. The readings are showing that the device is holding the charge for quite a longer period of time and also the range of the current produced is also quite large in magnitude. This may yield the possibility of use of this device in the application where the detector is required to store the charge for read out electronics [56 - 68]. To substantiate our answer voltage scan is also taken in the figure below:

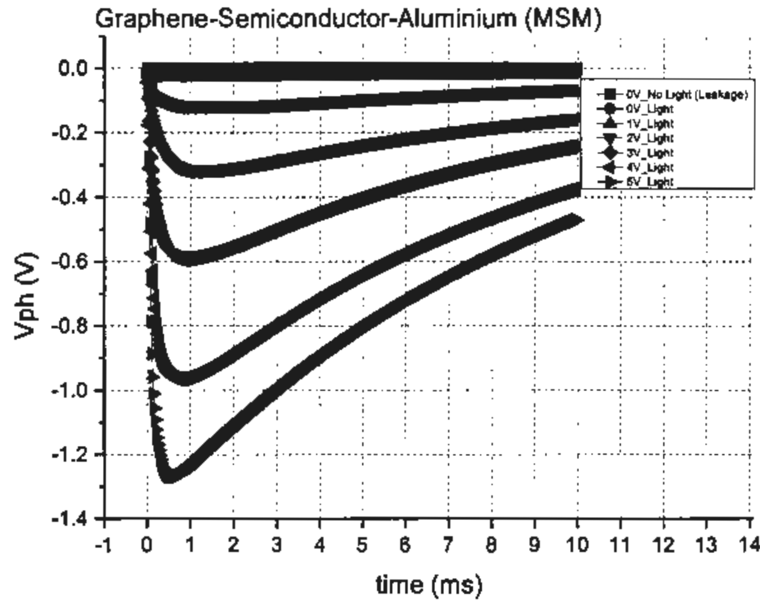

Fig. 5.36: Photo-stimulated voltage scan w.r.t time on multiple constant applied voltages on the device prepared by Routine 3

Photo-stimulated voltage scan is taken on multiple incident light intensities in the figure 5.36. The curves show that photo-stimulated voltage increase with increase in the applied light respect to time. The maximum value that is achieved is closed to $1.3V_{ph}$

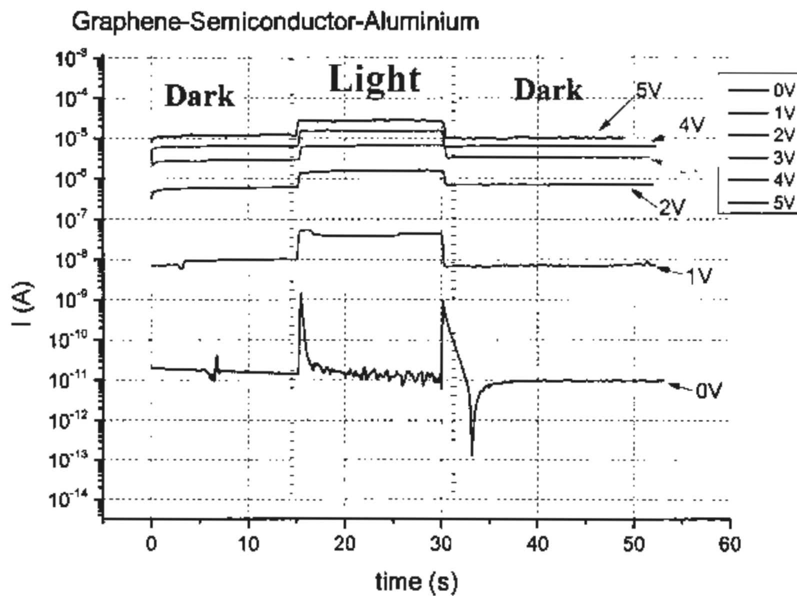

Fig. 5.37: Dark and Light Electric current measurements w.r.t time for the device fabricated using the routine 3

Figure 5.37 is the behaviour of the device when exposed to the longer period of light (15 seconds), as done in the previous cases. The graph show improvement in the device behaviour especially on the case of 0v. In this case when the device is exposed to light the device shows a spike in the current generated but then comes to rest position. This particular behaviour is favourable to the case of 0v and also does point out towards the less leakages inside the device. Ideally when no voltage is applied the light incident on the device should not induce any current change in it. This can be seen here, making this specific device better than the rest of the discussed cases.

5.4 Result and analysis of device All Aluminium MSM (Routine 4)

The device fabricated using the routine 4 is all Aluminium electrode Metal Semiconductor Metal structure. The electrodes are grown keeping in mind the quality of the film grown. The process protocols are devised to achieve a uniform layer of Aluminium of thickness 300nm on both the electrodes. The initial measurements were taken on the nano chip reliability grade Hall Effect system are as follows:

Table 5.3: Hall effect results of All Aluminium Metal Semiconductor Metal Structure

Sample	Metal Thickness	Rs (ohm/sq)	Rho (ohm-cm)	Con (1/ohm-cm)	Ns ($/cm^2$)	Ns ($/cm^3$)	µs (cm^2/Vs)
Aluminum MSM	300nm:300 nm/500µm Si	1.72 E+04	8.62 E+02	1.17 E-03	-1.01 E+12	-2.03 E+13	4.01 E+02

The sheet resistance is found out to be 1.72 E+04 ohm/sq which is only possible when the device has a workable channel. This structure is fabricated keeping in view of the use of Aluminium in the semiconductor industry. Also we need to get the idea about the potential of all aluminium MSM with respect to the rest of the cases.

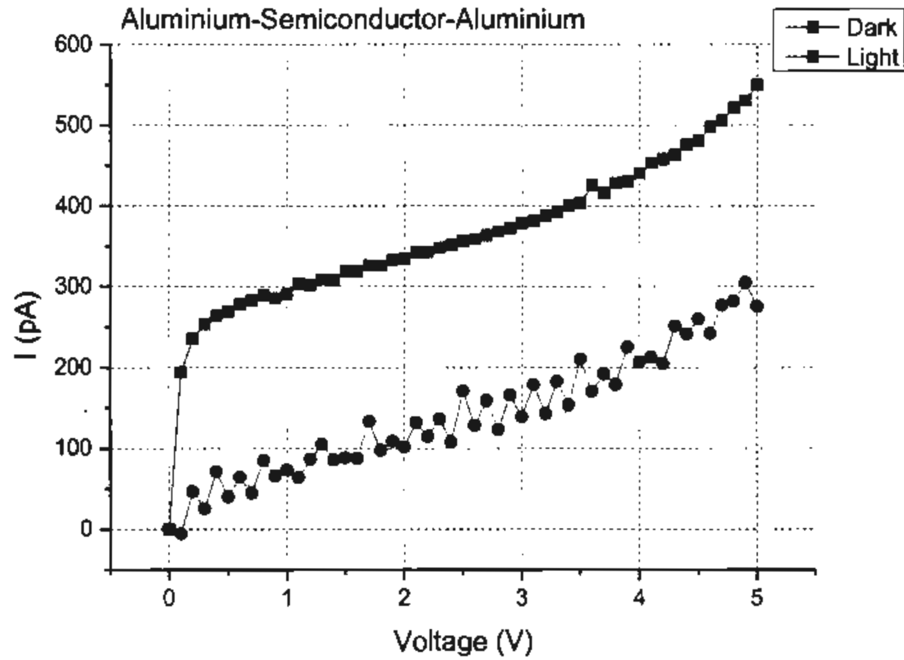

Fig. 5.38: Dark and Light I-V scans of the sample fabricated using the routine 4

The graph shown in the figure 5.38 is the dark and the light characteristics of the device fabricated using the routine 4. This all Aluminium MSM device matrix show some want of a reverse behaviour. Meaning when the device is exposed to the light its I-V curves shifts even lower then the device dark curve. Also the range of the current is in pA which is very lowered as compared to the previous cases. This much less of the current will make it very difficult to control such device.

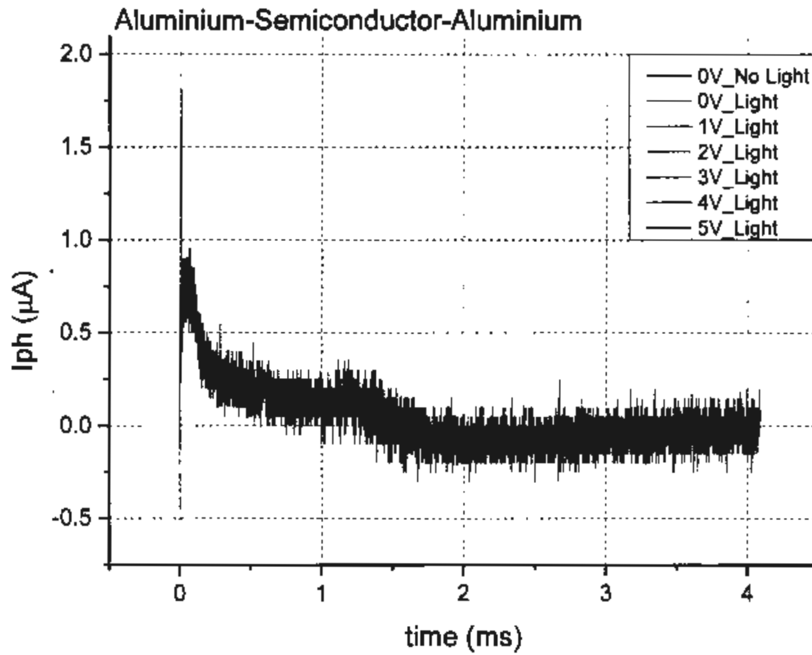

Fig. 5.39: Photo-stimulated current scan w.r.t time on multiple constant applied light intensities on the device prepared by the Routine 4

The photo-stimulated current scan with respect to time is shown here in the figure 5.39 above. This can be seen in the graph that even with different applied intensities of light the current generated by the device is somewhat of same magnitude. This points towards the fact that the device does not get affected much by the incident light or in other word the detection done by the device is not so prominent.

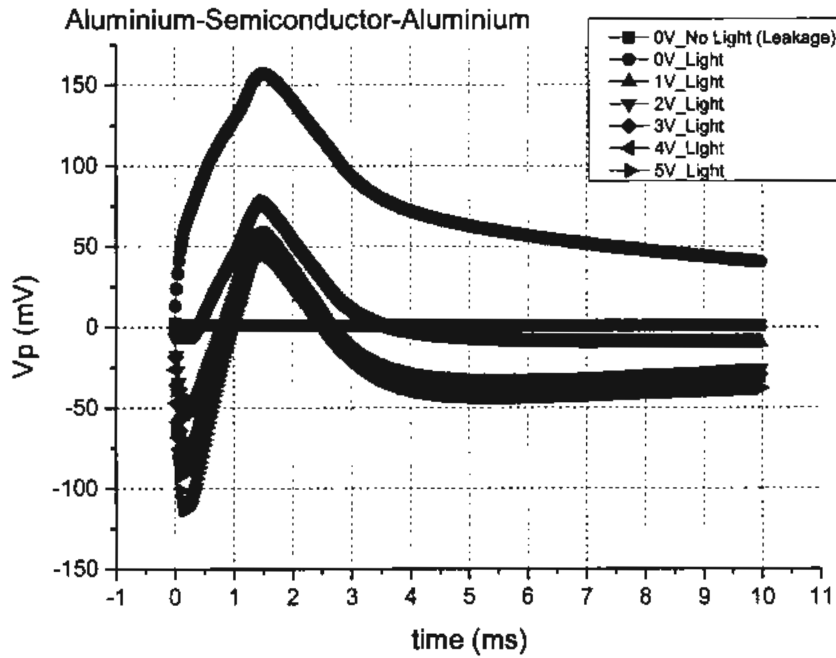

Fig. 5.40: Photo-stimulated voltage scan w.r.t time on multiple constant applied light intensities on the device prepared by Routine 4

In figure 5.40 on 0 applied light the device gives a good voltage response. This voltage is not the photo stimulated as the device is not exposed to any light yet. As soon as the device is exposed to the light the voltage drops and on 5v the value is minimum. This is also seen in the I-V Dark and light measurements of this specific device where applied light reduces the value of the current. The initial rise in the voltage value may be the device intrinsic behaviour to the incoming light.

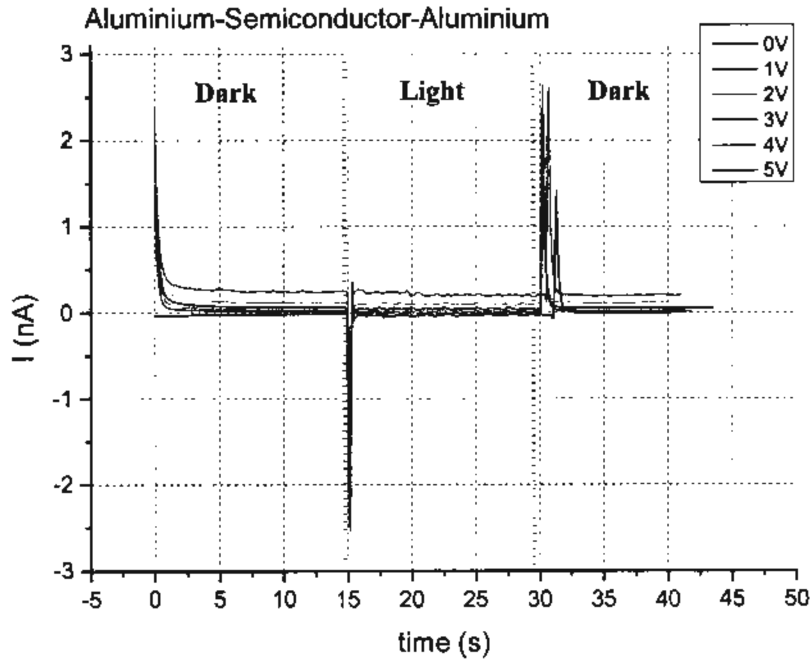

Fig. 5.41: Dark and Light Electric current measurements w.r.t time for the device fabricated using the routine 4

In the graph above the all-aluminium MSM device transient response to the light and dark environment is shown. This can be seen that when the light is incident on to the device the current produced is very small. And after the initial sudden spike the system returns back to the initial condition. This means that the device does not able to produce enough current from the incident light also the leakage inside the device is diminishing the current that is produced by the light. This much low of the current production and the leakage inside the device makes this device not suitable for conventional elcetronics, as this specific device will be very hard to control.

5.5 Comparison of the fabricated devices

Out of the four devices prepared the devices fabricated using the routine 1 and routine 3 gives the best results in their respective operational domain. The device fabricated using the routine 1 was graphene/Ni electrode based MSM structure and the device fabricated using the routine 3 was graphene/Ni and Aluminium electrode based device matrix. The results are compared here for better understanding:

Table 5.4: Comparative Hall effect results of the devices fabricated

Sample	Routine	Metal Thickness	Rs (ohm/sq)	Rho (ohm-cm)	Con (1/ohm-cm)	Ns (/cm^2)	Ns (/cm^3)	μs (cm^2/Vs)
All Aluminum MSM	Routine 4	**300nm:300 nm/500μm Si**	1.72 E+04	8.62 E+02	1.17 E-03	-1.01 E+12	-2.03 E+13	4.01 E+02
Graphene/ Ni MSM	Routine 1	**401.23nm: 401.23nm/ 500μm Si**	2.61 E+03	1.30 E+02	7.67 E-03	-3.32 E+13	-6.63 E+14	7.24 E+01
Graphene Aluminum MSM	Routine 3	**401.23nm: 300nm/500 μm Si**	1.90 E+03	9.51 E+01	1.07 E-02	-7.29 E+12	-1.46 E+14	5.10 E+02

Hall Effect parameters of 3 devices fabricated using 3 different routines are displayed in the table 5.4 above. The 4th device fabricated using routine 2 (see chapter 3 for more details) is not discussed here because that device show the least acceptable results for the comparison and the detail reasoning for that is already explained in this chapter. From the table it can be seen that the sheet resistance is maximum for the device fabricated using routine 4 and for the rest of the devices the value is almost similar. However the carrier concentration of graphene/Ni MSM and Graphene/Aluminium MSM is also greater than the All-Aluminium MSM. The rest of the results are compared below.

In the following graphs the abbreviations "ASA, GSA, GSG, GSrA" means "All Aluminium MSM device (Routine 4), Graphene/Ni/Aluminium MSM device (Routine 3), Graphene/Ni MSM device (Routine 1) and Graphene/Ni/Rough Aluminium MSM device (Routine 2) " respectively

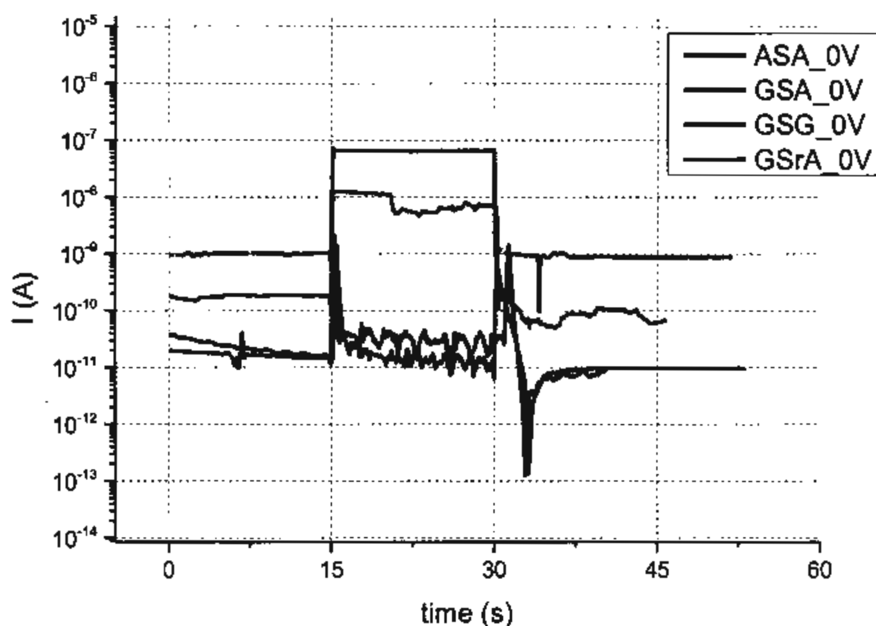

Fig. 5.42: Dark and Light transient behaviour comparison of the devices at 0v

From the graph above at 0v condition the behaviour of GSA device seems the best of all, as at this condition ideally no current should flow from the device even when the device is exposed to the light. A sudden spike is observed in the device current when the transient is changed from dark to light and back to dark again. On the other hand the GSG device shows huge increase in the current at 0v condition and also maintains this current over the region of applied light. The rest of the devices gives uneven or rather noise response to this condition.

At 1v condition the GSA device and GSG device both show increase in the generated current, however GSA device show greater delta in the current from dark to light then the GSG device. Even though the ranges of current achieved by GSG device on 1v applied bias is better than the GSA device but due to very little delta difference between dark and light currents makes this device very difficult to use for potential read out

electronics. The rest of the devices show uneven behaviour not suitable for working detector. The detailed graph is shown below:

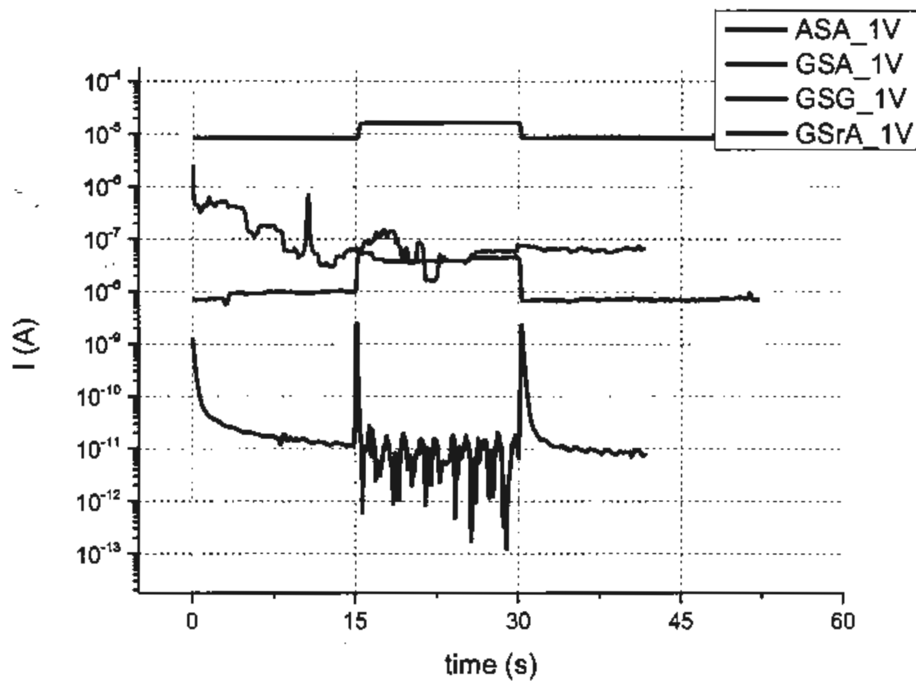

Fig. 5.43: Dark and Light transient behaviour comparison of the devices at 1v

At 2v condition the transients of the device GSG and GSA are closing up with GSA device showing increase in the ranges of the current but the delta difference of GSA get reduced and on the contrary the GSG device shows increase in the delta value. The rest of the devices still show uneven transient behaviour as shown below:

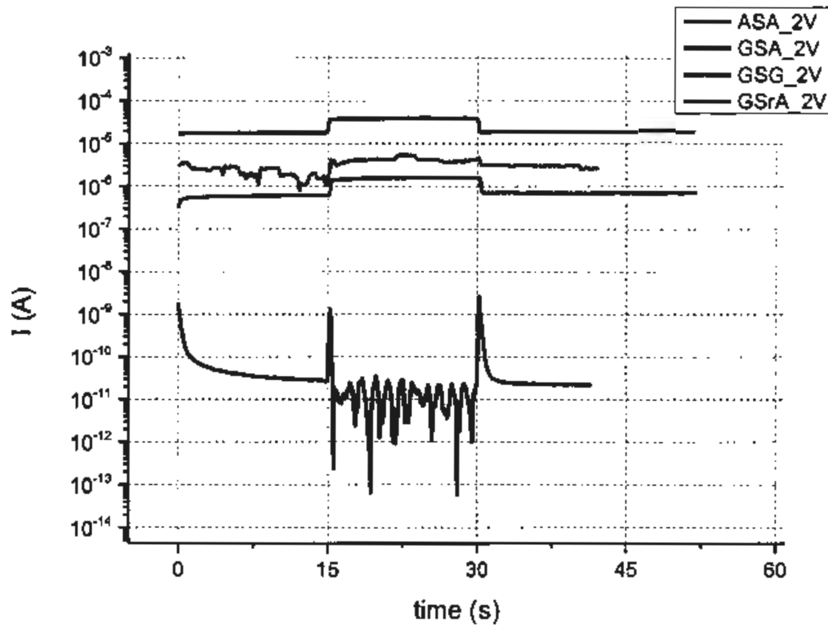

Fig. 5.44: Dark and Light transient behaviour comparison of the devices at 2v

At the 3v condition GSA and GSG device both sbow the increase in the value of currents and noticeable increase in delta as well compared to 2v condition above. The GSrA device show very negligible increase in the transient delta and ASA device shows almost zero transient. The detailed comparison is given in the graph below:

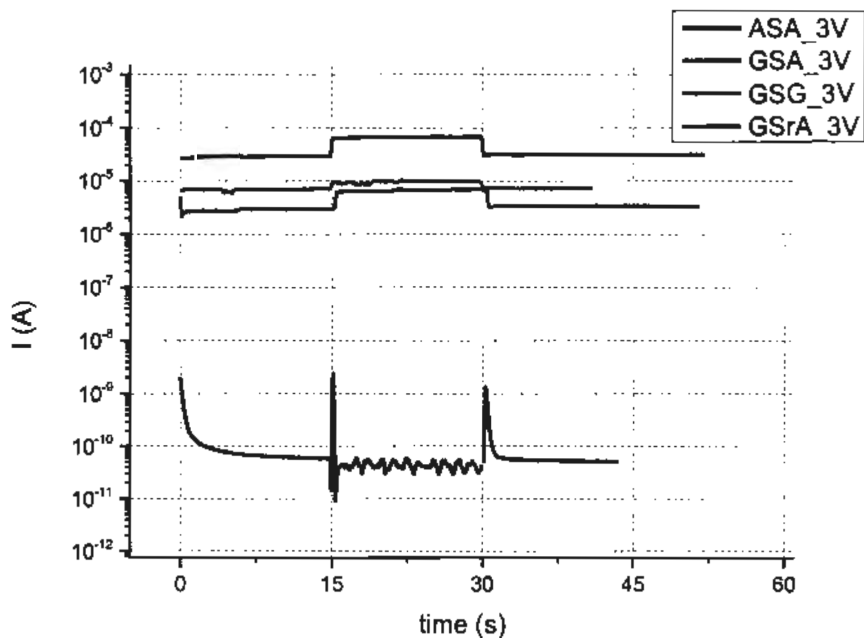

Fig. 5.45: Dark and Light transient behaviour comparison of the devices at 3v

At 4v condition the current increases for both devices GSG and GSA however the GSA device show larger increase in the current ranges than the GSG device at this condition GSrA device also seems to show the transient behaviour with very little delta. The ASA device show almost zero change. This can be seen in the figure 5.46 below:

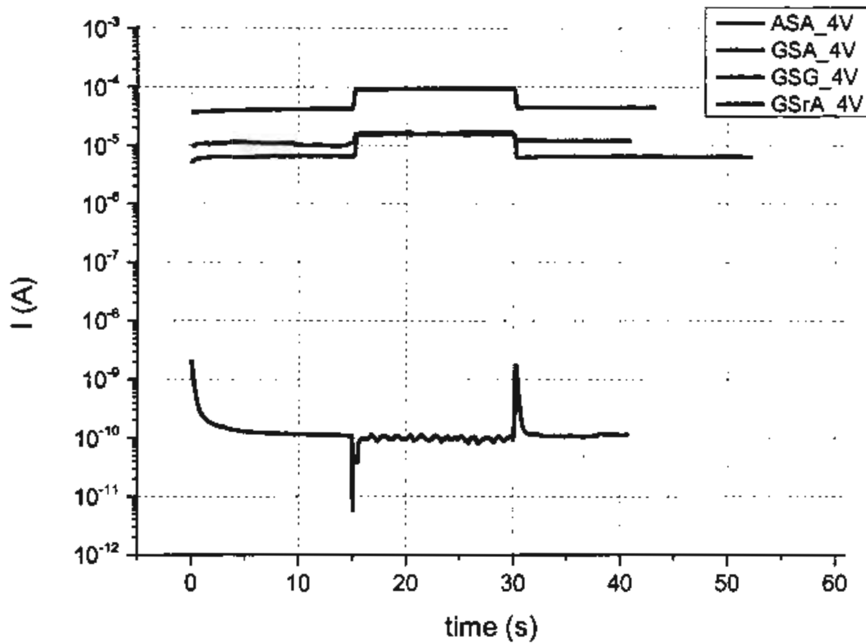

Fig. 5.46: Dark and Light transient behaviour comparison of the devices at 4v

At 5 v applied voltage condition the GSA device current increases even more, showing transient very close to the GSG device. Also the delta difference between light and dark also increases for GSA device. The GSG device does show some increase in the current value but the change is small. At this voltage GSrA device also starts to show the transient change from dark to light conditions, with increase in the delta difference as well. The graph is shown below:

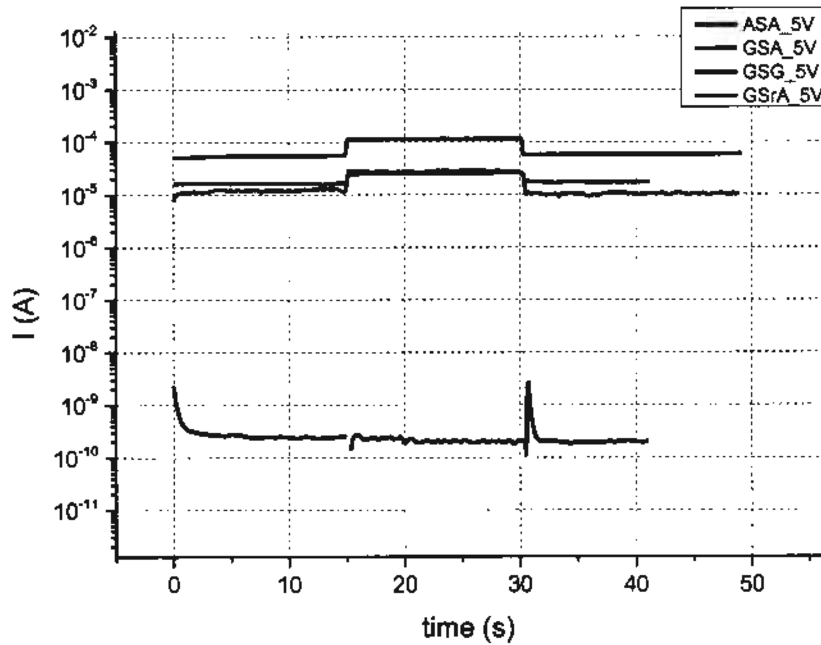

Fig. 5.47: Dark and Light transient behaviour comparison of the devices at 5v

From the comparison drawn above it is clear that two devices GSA and GSG show better results out of the four fabricated. Each device show different behaviour when put through the experimentation. To summarize the GSA device show better performance of storing the charge for the longer time frame but shows less current ranges compared to GSG device. The GSG device show fast switching performance but does not retain the charge for longer period of time.

From the perspective of leakage GSA device show the least current losses among the rest. This single parameter led to the conclusion that GSA device is better among the rest and will be compared with already reported devices in the market to see where it stack.

Two reported devices are taken for comparison with our GSA device [56, 80]. Both devices are schottky junction devices. A single MSM unit cell is fabricated in these studies same as ours. Both devices used graphene in some capacity to enhance the performance of their respective MSM structure. Same I-V curves are reported by these

two studies taken at room temperature. When our device results are compared with the device reported in reference [58, 80] we find out at 1v the current achieved by these respective devices are 10^{-9} A [58] and 10^{-6} A [80]. At the same conditions the current achieved by our fabricated device is 20 x 10^{-6} A. For the device reported in the reference [58] the data is taken on multiple temperatures as well. We have done the same for our device as well. At 300k our device is achieving the current in the ranges of 10^{-6} however the device reported in reference [58] is reported to achieve only 10^{-8} range of current. At 340k the reported device is achieving the current in the range of 10^{-7} but our fabricated device is achieving 14x 10^{-6} A current, which is still higher than the reported device. At 370k the current of the reported device touches the range of 10^{-6} A same as our device however at this temperature our devices dark and light characteristics overlap meaning the detection is almost gone.

Chapter 6

Conclusion and Future Work

In this study four Metal Semiconductor Metal Unit structures were fabricated and studied. The idea was to see the possibility of using graphene to fabricate a workable MSM structure for future electronics. Four different devices are fabricated. The four devices fabricated in this thesis used four different routines of process protocol and material selectivity. The fabricated devices were then tested for comparison with each other in terms of leakage, output voltage and current. The transient behaviour was also studied to quantify our judgement upon the quality of the device. The main purpose of this thesis is to assess the use of graphene in the metal semiconductor metal structural matrix and its potential outcomes resulting in its use in the next generation electronics. The structure MSM was chosen for study due to its ease of design and less fabrication steps. Based on the results the key findings are as follows:

1) Graphene Induced MSM can be make using easier method such as mechanical engraving however the quality of the film is compromised.
2) All Graphene MSM structure did show the detection phenomenon but the structure has a lot of leakage issues.
3) The All graphene MSM show better switching capability among the rest of the devices with good output current ranges.
4) In order to reduce the leakage Graphene/Ni MSM must use other materials like Al (in our case) in combination with Graphene/Ni matrix.

5) The quality of the electrodes grown effect the output of the sensors very promptly. This is observed in the case where rough Al electrode was purposely grown on to the device surface.
6) The devices fabricated here are the unit cell. The real time device will be fabricated using the array of such devices on single pedestal. This way there may be the possibility that the devices output parameter may improve.

Future Work

The study presented here has lot of potential of improvement. The Metal Semiconductor Metal structure has huge application in the optical industry. The structure flexibility of design and ease of manufacturing makes it one of the most important device matrix for future application. ITRS has introduced the heterogeneous integration for the assembling of future electronics. This approach requires multi-disciplinary devices to be integrated on a single high end platform. MSM structure can really play its part on the input end of such complex designs. Four devices are fabricated here using four different fabrication routines. Each with different electrical characteristics. These devices were tested electrically so that a comparison can be raised.

The study of the fabricated devices reveal that that more detailed work in the future can be done to improve such devices output parameters. Multiple imaging technologies can be used to see the quality of the film and the atomic arrangement of the devices. Raman scan can be done on the devices to see their respective parameter shifts. Detailed Electrode study can be done so that the graphene present in the device can be utilized to perform multiple task when introduced to external environment. A whole study of the effect of thermal budget on the fabricated devices can be performed. The future of MSM structures totally rely on the clear assessment and the available flexibility in the

design selection and the material integration. These notions will ensure the use of such structure in the future industry driven hybrid electronics.

References:

[1] M. Mayberry, Pushing Past the Frontiers Of Technology, nist, USA, 2016.

[2] H. Iwai, "Future of nano CMOS technology", Microelectronics Technology and Devices, Brazil, 2013.

[3] Y Song, H. Zhou, Q. Xu, J. Luo, H. Yin, J. Yan and H. Zhong, "Mobility Enhancement Technology for Scaling of CMOS Devices: Overview and Status", Journal of Electronic Materials, Springer Link, 2011.

[4] T. Lee, "The Hardware Enablers for the Internet of Things – Part II (More than Moore)", IEEE internet of things, IEEE, 2015.

[5] M. Bohr, "The evolution of scaling from the homogeneous era to the heterogeneous era", International Electron Devices Meeting (IEDM), IEEE, Washington, USA, 2011.

[6] F. F. Aghdam and H. Liao, "Reliability study on high-k bi-layer dielectrics", Reliability and Maintainability Symposium, Orlando, USA, 2017.

[7] S. Deleonibus, "Looking into the future of Nanoelcetronics in the Diversification Efficient Era", Science China Information Sciences, Springer Link, 2016.

[8] R. C. Johnson, "Intel Shows Life Beyond CMOS", International Symposium on Physical Design, USA, 2017.

[9] F. F. Masouleh, N. Das, "Application of Metal-Semiconductor-Metal Photodetector in High-Speed Optical Communication Systems," Advances in Optical Communication, InTech, 2014, **1**, pp. 87 – 114.

[10] B. Y. Zheng, Y. Wang, P. Nordlander, N. J. Halas, "color-selective and CMOS-compatible photo detection based on aluminum plasmonics", Advanced Material, 2014, **26**, pp. 6318 – 6323.

[11] C. Lin and C. W. Liu, "Metal-Insulator-Semiconductor Photodetectors", Sensors, 2010, **10**, pp. 8797 – 8826.

[12] S. M. Sze, D. J. Coleman and Jr. A. Loya, "Current transport in metal-semiconductor-metal (MSM) structures", Solid-State Electronics, Elsevier, 1971, **14**, pp. 1209 – 1218.

[13] J.-L. Reverchon, M. Mosca, N. Grandjean, F. Omnes, F. Semond, J.-Y. Duboz and L. Hirsch, "UV Metal Semiconductor Metal Detectors", UV Solid-State Light Emitters and Detectors, Springer link, 2004.

[14] V. E. Babicheva, R. Malureanu and A. V. Lavrinenko " Finite-thickness metal-semiconductor-metal waveguide as plasmonic modulator", AIP Conference Proceedings, USA, 2012.

[15] Z. Hassan, Y. C. Lee, S. S. Ng, F. K. Yam, Y. Liu, Z. Rang, M. Z. Kauser, P. P. Ruden and M. I. Nathan, "AlGaN metal-semiconductor-metal structure for pressure sensing applications", physica status solidi (c), 2006, **3**, pp. 2287 – 2290.

[16] A. Vijayakumar, R. M. Todi and K. B. Sundaram, "Amorphous-SiCBN-Based Metal–Semiconductor–Metal Photodetector for High-Temperature Applications", IEEE Electron Device Letters, IEEE, **28**, pp. 713 – 715.

[17] P. R. Wallace, "The Band Theory of Graphite," Physical Review, 1947, **71**, pp. 622 – 634.

[18] G. Ruess and V. vogt, “Höchstlamellarer Kohlenstoff aus Graphitoxyhydroxyd.” Monatshefte für Chemie und verwandte Teile anderer Wissenschaften, 1948, **78**, pp. 222 – 242.

[19] A. Geim and P. Kim, “carbon wonderland”, Scientific American, 2008, **298**, pp. 90 – 97.

[20] K.S. Novoselov, A.K. Geim and S.V. Morozoven, “electric field effect in atomically thin carbon”, Science, 2004, **306**, pp. 666 – 669.

[21] K.S. Novoselvo, L. Colombo and P.R. Gellert, “A road-map for graphene”, Nature, 2012, **490**, pp. 192 – 200.

[22] A. Zurutuza and C. Marinelli, “Challenges and opportunities in graphene commercialization”, Nature Nanotechnology, 2014, **9**, pp. 730 – 734.

[23] D. A. Boyd, W. H. Lin, C. C. Hsu, M. L. Teague, C. C. Chen, Y. Y. Lo and W. Y. Chan, “Single-step deposition of high-mobility graphene at reduced temperatures”, Nature communication, 2015, **6**, p. 6620.

[24] F. Schwierz, “Graphene transistors”, Nature Nanotechnology, 2010, **5**, pp. 487 – 496.

[25] K. Bhupendra, Sharma and J. H. Ahn, “Graphene based field effect transistors: Efforts made towards flexible electronics”, Solid-State Electronics, 2013, **89**, pp. 177 – 188.

[26] X. Wang, X. Jiang, T. Wang, J. Shi, M. Liu, Q. Zeng, Z. Cheng and X. Qiu, “Electrically Configurable Graphene Field-Effect Transistors with a Graded-Potential Gate”, Nano Letters, 2015, **5**, pp. 3212 – 3216.

[27] K. M. F. Shahil and A. A. Balandin, "Thermal properties of graphene and multilayer graphene: Applications in thermal interface materials", Solid State Communications, Elsevier, 2012, **152**, pp. 1331 – 1340.

[28] L. Lancellotti, T. Polichetti, F. Ricciardella, O. Tarih, S. Gnanapragasam, S. Daliento and G. D. Francia, "Graphene applications in Schottky barrier solar cells", Thin Solid Films, Elsevier, 2012, **522**, pp. 390 – 394.

[29] Q. Ke and J. Wang, "Graphene-based materials for super capacitor electrodes – A review", Journal of Materiomics, Elsevier, 2016, **2**, pp. 37 – 54.

[30] E. O. Polat, O. Balcı and C. Kocabas, "Graphene based flexible electrochromic devices", Scientific Reports, 2014, **4**, p. 6484.

[31] J. A. Carballo, W. T. J. Chan, P. A. Gargini, A. B. Kahng and S. Nath, "ITRS 2.0: Toward a re-framing of the Semiconductor Technology Roadmap", 32nd IEEE International Conference on Computer Design, Seoul, South Korea, 2014.

[32] W. Chen, "Heterogeneous Integra-on Roadmap", HIR Roadmap Workshop, IEEE Electronic Packaging Society, 2017.

[33] A. Karar, C. L. Tan, K. Alameh and Y. T. Lee, "Nano-patterned High-responsivity GaAs metal semiconductor metal photodetector", High Capacity Optical Networks and Enabling Technologies, 2011, **1**, pp. 30 – 33.

[34] S. V. Averine and N. V. Alkeev, "Impulse response of the metal-semiconductor-metal photodetector", 6th International Conference on Ultra-wide band and Ultrashort Impulse Signals, IEEE, 2012, **1**, pp. 55 – 57.

[35] F. Xie, H. Lu, D. Chen, X. Ji, F. Yan, R. Zhang, Y. Zheng, L. Li, and J. Zhou, "Ultra-low dark current AlGaN-based solar-blind metal–semiconductor–metal photodetectors for high-temperature applications", IEEE Sensors Journal, IEEE, 2012, **12**, pp. 2086 – 2090.

[36] S. Singh, "Al doped ZnO based metal–semiconductor–metal and metal–insulator–semiconductor–insulator–metal UV sensors", Optik - International Journal for Light and Electron Optics, 2016, **127**, pp. 3523 – 3526.

[37] A. M. Selmana and Z. Hassana, "Fabrication and characterization of metal–semiconductor–metal ultraviolet photodetector based on rutile TiO2 nanorod", Materials Research Bulletin, 2016, **73**, pp. 29 – 37.

[38] S. V. Averin, P. I. Kuznetsov, V. A. Zhitov, L. Yu. Zakharov, V. M. Kotov and N. V. Alkeev, "Electrically tunable spectral responsivity in metal–semiconductor–metal photodetectors based on low-dimensional ZnCdS/ZnMgS/GaP, ZnCdS/ZnS/GaP heterostructures", Solid-State Electronics, Elsevier, 2015, **114**, pp. 135 – 140.

[39] M. E. Besseghi, A. Aissat and D. Decoster, "Simulation of the Metal-Semiconductor-Metal photodetector based on InGaAs for the photodetection at the wavelength 1.55 μm", Optik - International Journal for Light and Electron Optics, Elsevier, 2014, **125**, pp. 2543 – 2546.

[40] A. D. Zebentouta, A. K. Aissat, Z. Bensaad, M. Zegaoui, A. Pagies and D. Decoster, "GaAs metal–semiconductor–metal Schottky microwave optical switches", Optics & Laser Technology, Elsevier, 2013, **47**, pp. 1 – 3.

[41] V. E. Babicheva, I. V. Kulkova, R. Malureanu, K. Yvind and A. V. Lavrinenko, “Plasmonic modulator based on gain-assisted metal–semiconductor–metal waveguide”, Photonics and Nanostructures - Fundamentals and Applications, 2012, **10**, pp. 389 – 399.

[42] A. M. Selman and Z. Hassan, “Growth and characterization of rutile TiO2 nanorods on various substrates with fabricated fast-response metal–semiconductor–metal UV detector based on Si substrate”, Superlattices and Microstructures, Elsevier, 2015, **83**, pp. 549 – 564.

[43] N. Xu, B. Huang, J. Li and B. Wang, “Semiconductor–metal and metal–semiconductor transitions in twisting graphene nanoribbons”, Solid State Communications, Elsevier, 2015, **202**, pp. 39 – 42.

[44] Y. H. Ng, A. Iwase, N. J. Bell, A. Kudo and R. Amal, “Semiconductor/reduced graphene oxide nanocomposites derived from photocatalytic reactions”, Catalysis Today, Elsevier, 2011, **164**, pp. 353 – 357.

[45] X. Ma, M. Li and J. He, “CMOS-compatible integrated spectrometer based on echelle diffraction grating and MSM photodetector array”, IEEE Photonics Journal, IEEE, 2013, **5**, p. 13448241.

[46] D. Geum, S. H. Shin, S. Hong and J. Jang, “Metal-semiconductor–metal varactors based on InAlN/GaN heterostructure with cutoff frequency of 308 GHz”, Electron Device Letters, Elsevier, 2015, **36**, pp. 306 – 308.

[47] X. Li, M. B. Jordan, T. Ayari, S. Sundaram, Y. E. Gmili, S. Alam, M. Alam, G. Patriarche, P. L. Voss, J. P. Salvestrini and A. Ougazzaden, “Flexible metal-semiconductor-metal device prototype on wafer-scale thick boron nitride layers grown by MOVPE”, Scientific Reports, 2017, **7**, p. 786.

[48] V. E. Babicheva, R. M. Andrei and V. Lavrinenko, "Plasmonic finite-thickness metal–semiconductor–metal waveguide as ultra-compact modulator", Photonics and Nanostructures - Fundamentals and Applications, Elsevier, 2013, **11**, pp. 323 – 334.

[49] S. Cheirsirikul, S. Jesen and C. Hruanun, "MSM Diamond UV detector", IEEE International Conference on Nano/Micro Engineered and Molecular Systems, Kaohsiung, Taiwan, 2011.

[50] S. Singh and S. H. Park, "Fabrication and properties of ZnO nanorods based MSM UV detectors on silicon substrates", Optik - International Journal for Light and Electron Optics, Elsevier, 2017, **137**, pp. 96 – 100.

[51] J. D. Hwang and Y. C. Chang, "Enhancing the Ultraviolet/Visible Rejection Ratio of MgxZn1−xO Metal-Semiconductor-Metal Photodetectors Using Oxygen-Plasma Treatment", IEEE Transactions on Electron Devices, IEEE, 2017, **64**, pp. 3234 – 3238.

[52] M. Suja, S. B. Bashar, L. Su and J. Liu, "Realization of deep ultraviolet random lasing in MgZnO metal-semiconductor-metal devices", Photonics Conference, IEEE, Waikoloa, USA, 2016.

[53] Y. Ding, H. Hu, H. Ou, L. K. Oxenløwe and K. Yvind, "Effective carrier sweepout in a silicon waveguide by a metal-semiconductor-metal structure", Conference on Lasers and Electro-Optics, IEEE, San Jose, USA, 2015.

[54] B. Zhang, J. Wang, X. Li, C. Jin, H. Jiang and M. Yu, "Effects of depletion region in GaN-based metal-semiconductor-metal planar inter-digitated varactor", IEEE International Conference on Electron Devices and Solid-State Circuits, IEEE, Chengdu, China, 2014.

[55] X. X. Gong, G. T. Fei, W. B. Fu, B. N. Zhong, X. D. Gao and L. D. Zhang, "Metal-semiconductor-metal infrared photodetector based on PbTe nanowires with fast response and recovery time", Applied Surface Science, Elsevier, 2017, **404**, pp. 7 – 11.

[56] Y. An, A. Behnam, E. Pop and A. Ural, "Metal-semiconductor-metal photodetectors based on graphene/p-type silicon Schottky junctions", Applied Physics Letters, 2013, **102**, p. 013110.

[57] M. Kumara, Y. Noha, K. Polat, A. K. Okyay and D. Lee, "Metal–semiconductor–metal UV photodetector based on Ga doped ZnO/graphene interface", Solid State Communications, Elsevier, 2015, **224**, pp. 37 – 40.

[58] C. J. Lee, S. B. Kang, H. G. Cha, C. H. Won, S. K. Hong, B. J. Cho, H. Park, J. H. Lee and S. H. Hahm, "GaN metal–semiconductor–metal UV sensor with multi-layer graphene as Schottky electrodes", Japanese Journal of Applied Physics, IOP Science, 2015, **54**, p. 06FF08.

[59] J. Hicks, A. Tejeda, A. Taleb-Ibrahimi, M. S. Nevius, F. Wang, K. Shepperd, J. Palmer, F. Bertran, P. Le Fèvre, J. Kunc, W. A. de Heer, C. Berger and E. H. Conrad, "A wide-bandgap metal–semiconductor–metal nanostructure made entirely from graphene", Nature Physics, 2013, **9**, pp. 49–54.

[60] S. Rathi, I. Lee, D. Lim, J. Wang, Y. Ochiai, N. Aoki, K. Watanabe, T. Taniguchi, G. H. Lee, Y. J. Yu, P. Kim and G. H. Kim, "Tunable Electrical and Optical Characteristics in Monolayer Graphene and Few-Layer MoS_2 Heterostructure Devices", Nano Letters, 2015, **15** , pp. 5017 – 5024.

[61] W. Y. Kong, G. A. Wu, K. Y. Wang, T. F. Zhang, Y. F. Zou, D. D. Wang and L. B. Luo, "Graphene-β-Ga2O3 Heterojunction for Highly

Sensitive Deep UV Photodetector Application", Advanced Materials, 2016, **28**, pp. 10725 – 1073.

[62] F. X. Liang, J. Z. Wang, Y. Wang, Y. Lin, L. Liang, Y. Gao and L. B. Luo, "Single-layer graphene/titanium oxide cubic nanorods array/FTO heterojunction for sensitive ultraviolet light detection", Applied Surface Science, Elsevier, 2017, **426**, pp. 391 – 398.

[63] D. Zhang, F. Jing, F. Gao, L. Shen, D. Sun, J. Zhou, Y. Chen and S. Ruan, "Enhanced performance of a TiO_2 ultraviolet detector modified with graphene oxide", RSC Advances, 2015, **5**, pp. 83795 – 83800.

[64] F. Yang , H. Cong, K. Yu, L. Zhou, N. Wang, Z. Liu, C. Li, Q. Wang, and B. Cheng, "Ultrathin Broadband Germanium–Graphene Hybrid Photodetector with High Performance", ACS Applied Material and Interfaces, 2017, **9**, pp 13422 – 13429.

[65] I. K. Moon, B. Ki, S. Yoon, J. Choi and J. Oh, "Lateral photovoltaic effect in flexible free-standing reduced graphene oxide film for self-powered position-sensitive detection", Scientific Reports, 2016, **6**, p. 33525.

[66] J. H. Seol, S. B. Kang, C. J. Lee, C. H. Won, H. Park, J. H. Lee and S. H. Hahm, "Graphene/Al_2O_3/AlGaN/GaN Schottky MISIM Diode for Sensing Double UV Bands", IEEE Sensors Journal, IEEE, 2016, 16, pp. 6903 – 6907.

[67] H. C. Chiamori, R. Miller, A. Suria, N. Broad and D. G. Senesky, "Irradiation effects of graphene-enhanced gallium nitride (GaN) metal-semiconductor-metal (MSM) ultraviolet photodetectors", Sensors for Extreme Harsh Environments II, SPIE, 2015, 9491, p. 7.

[68] X. Wang and X. Gan, "Graphene integrated photodetectors and opto-electronic devices — a review", Chinese Physics B, IOP Science, 2017, **26,** p. 34203.

[69] T. Duffar, "Crystal Growth Processes Based on Capillarity: Czochralski, Floating Zone, Shaping and Crucible Techniques", Wiley, 2010.

[70] G. Ouimet, D. L. Rath, S. L. Cohen, E. E. Fisch, G. W. Gale, "Defect reduction and cost savings through re-inventing RCA cleans", Advanced Semiconductor Manufacturing Conference and Workshop, IEEE, Cambridge, USA, 1996.

[71] H. U. Kim and S. W. Rhee, "Electrical Properties of Bulk Silicon Dioxide and SiO_2/Si Interface Formed by Tetraethylorthosilicate-Ozone Chemical Vapor Deposition", Journal of The Electrochemical Society, 2000, **147**, pp. 1473 – 1476.

[72] J. H. Park and T. S. Sudarshan, "Chemical Vapor Deposition", ASM International, Ohio, USA, 2001.

[73] Strem Chemicals, "Applications of Metal Diketonate Precursors for CVD and ALD", AZO NANO, 2013.

[74] Jong-Hee Park, T. S. Sudarshan, "Chemical Vapor Deposition", ASM International, Ohio, USA, 2001.

[75] P. Trinsoutrot, H. Vergnes and B. Caussat, "Three dimensional graphene synthesis on nickel foam by chemical vapor deposition from ethylene", Materials Science and Engineering: B, Elsevier, 2014, **179,** pp. 12 – 16.

[76] M. S. Lee and K. J. Lee, "Separation of iron and nickel from a spent FeCl3 etching solution by solvent extraction", Hydrometallurgy, Elsevier, 2005, 80, pp. 163 – 169.